This is to certify that the

dissertation entitled

Suspension Bridge Response to Spatially

Varying Ground Motion

presented by

Ahmad Radi Hawwari

has been accepted towards fulfillment
of the requirements for

Doctor of Philosophy degree in Civil Engineering

R S Harichandran

Major professor

Date May 19, 1992

SUSPENSION BRIDGE RESPONSE TO SPATIALLY VARYING GROUND MOTION

BY

Ahmad Radi Hawwari

A DISSERTATION

submitted to

Michigan State University
in partial fullfilment of the requirements
for the degree of

DOCTOR OF PHILOSOPHY

Department of Civil and Environmental Engineering

1992

ABSTRACT

SUSPENSION BRIDGE RESPONSE TO SPATIALLY VARYING GROUND MOTION

By

Ahmad Radi Hawwari

The stochastic lateral responses of the Golden Gate suspension bridge, which has a center span length of 4,200 feet and a side span length of 1,125 feet was investigated. A two dimensional finite element model of the bridge was used. A space-time earthquake ground motion model that accounts for both coherency decay and seismic wave propagation was used to specify the support motions. The double-filter spectrum fitted to an artificial accelerogram similar to the El Centro earthquake was used.

Linear stationary random vibration analysis was used to compute the bridge responses. Three models of excitations were considered at the supports: (1) correlated ground motion model accounting for both wave propagation and coherency decay; (2) identical support motion; (3) delayed excitation caused by wave propagation. Transient response analysis was also performed to determine whether the suspension bridge will attain its stationary response during typical durations of strong shaking (10 to 20 seconds). The effects of shear deformation on the natural frequencies and mode shapes, and their corresponding effect on the linear stationary random vibration responses was investigated. Inclusion of

shear deformation drastically lowers the frequencies of a group of modes, resulting in smaller moment and shear responses, but slightly higher displacement responses.

Results indicate that the use of identical excitations significantly over-estimates the responses at some locations and under-estimates the responses at others, the relative deviation being more severe for the longer center span. The use of delayed excitations gives acceptable results for the side span, but shows greater deviations for the center span in which the moment and shear are sometimes significantly under-estimated. The increase in the apparent wave velocity causes progressively higher responses at some locations of the span and progressively lower responses at others. Results of transient analyses indicate that for common ground motion durations, the assumption of stationarity may grossly over-estimate the side span responses. The transient displacement response of the center span can overshoot the stationary response considerably, but the moment and shear responses gradually approach their stationary values in about 40 seconds.

To my parents

Salha and Radi Hawwari

for their love, confidence, devotion,

and sacrifice

Acknowledgments

I am gratefully indebted to my thesis advisor, Dr. Ronald Harichandran, for his invaluable guidance throughout the course of this research.

I would like to express my gratitude to all members in my Ph.D. guidance committee, Dr. Robert Wen, Dr. Parvis Soroushian, Dr. William Sledd, and Dr. John Masterson.

I would also like to give special thanks to the loved ones in my family for their continuous love, understanding, and encouragement.

TABLE OF CONTENTS

LIST OF TABLES

LIST OF FIGURES

LIST OF SYMBOLS

$[A]$, A_{il} = matrix of static displacement due to unit re strained displacements and its elements;

$[C]$ = overall damping matrix;

Cov (u_{s_i}, u_{d_i}) = covariance between static and dynamic displacements;

$C_{FF}, C_{FR}, C_{RF}, C_{RR}$ = partitions of the damping matrix;

$\{D_{eg}\}_i$, $\{D_{em}\}_i$ = global and local member end -displacements corresponding to the ith mode;

DOF = acronym for degree-of-freedom;

E_{si} = modulus of elasticity corresponding to the ith deck;

f = linear frequency;

$e(t)$ = temporal modulating function;

$\{f\}_i$ = element end forces corresponding to the ith mode shape;

G_j = generalizedmodal excitation;

g = gravitational acceleration;

H_w = horizontal component of cable tension;

$h(x_i)$ = length of hanger corresponding to ith span;

$H_j(w), H_j(-w)$ = modal frequency response function for mode j and its conjugate;

$h_j(t)$ = impulse function due to an impulse excitation $G_j = \delta(t)$;

I_{jk} = nodal covariances contributing to the overall dynamic response;

J_{si} = area moment of inertia of the deck;

$[K]$ = overall stiffness matrix;

$K_{FF}, K_{FR}, K_{RF}, K_{RR}$ = partitions of the overall stiffness matrix;

$[K_{se}]_e$, $[K_{sg}]_e$, $[K_{ce}]_e$, $[K_{cg}]_e$ = subelement matrices corresponding to elastic stiffness of deck, gravitational stiffness of deck, elastic stiffness of cables, and gravitational stiffness of cables;

L = length of element;

$[M]$ = overall consistent mass matrix;

$M_{FF}, M_{FR}, M_{RF}, M_{RR}$ = partitions of mass matrix;

$[m_s]_e, [m_c]_e$ = subelement consistent mass matrices corresponding to deck and cables, respectively;

$\overline{m}_c, \overline{m}_{si}$ = mass of two cables per unit length of the span, and mass of the deck per unit length of the ith span;

n = number of free **DOF**;

$[P]$ = static end force matrix;

P_{ij} = the ith element end force due to a unit displacement along the jth restrained **DOF**;

r = number of restrained **DOF**;

Re[ ] = real part of argument;

$R_{u_{F_i}}(\tau), R_{u_{s_i}}(\tau), R_{u_{d_i}}(\tau)$ = autocorrelation functions of the ith element of $\{u_F\}$, $\{u_s\}$, and $\{u_d\}$;

$R_{u_{s_i}u_{d_i}}(\tau)$ = cross autocorrelation function of the ith element of $\{u_s\}$ and the ith element of $\{u_d\}$;

$R_{\ddot{u}_{Rl}\ddot{u}_{Rm}}(\tau)$ = cross autocorrelation of the nodal force excitations at l^{th} and m^{th} element of $\{u_d\}$;

SDF = acronym for degree(s)-of-freedom;

$S_{u_{F_i}}(\omega), S_{u_{s_i}}(\omega), S_{u_{d_i}}(\omega)$ = **SDF**'s of the ith element of $\{u_F\}$, $\{u_s\}$, and $\{u_d\}$;

$S_{u_{s_i}u_{d_i}}(\omega)$ = cross **SDF**'s of the ith element of $\{u_s\}$ and the ith element of $\{u_d\}$;

$S_{\ddot{u}_{Rl}\ddot{u}_{Rm}}(\omega)$ = cross **SDF** of the nodal force excitations at l^{th} and m^{th} elements of $\{u_F\}$;

$S_{\ddot{u}}(\omega)$ = point auto **SDF** of the ground acceleration;

$S_{\ddot{u}_A\ddot{u}_B}(\omega)$ = cross **SDF** between the acceleration of two locations A and B;

$T_c(t), T_s(t))$ = kinetic energies caused by the lateral vibrational displacements w_c and w_s, respectively;

$\{\ddot{u}\}, \{\dot{u}\}, \{u\}$ = vectors of nodal accelerations, velocities, and displacements;

$\{u_F\}, \{u_R\}$ = free and restrained **DOF** vectors;

$\{u_s\}$, $\{u_d\}$ = pseudo-static and dynamic components of $\{u_F\}$;

$u_j(t)$ = bridge element nodal displacement;

$V_c(t)$, $V_s(t)$ = potential energy of laterally vibrating cable and deck, respectively;

$V_{se}(t)$, $V(t)_{sg}$ = elastic potential and gravitational potential energy of deck;

V = apparent wave propagation velocity in the direction AB;

w_c, w_s = displacement components of cable and deck along z axes, respectively;

$\bar{w}_c$, $\bar{w}_{si}$ = dead weight of the two cables per unit length and deck per unit length of the i[ti] span, respectively;

Y_j = generalized modal displacement;

$z(t)$ = stationary random process;

$\{\Gamma_j\}$ = vector of participation factor for mode j;

$\delta(t)$ = Dirac delta function;

ε = machine precision;

η = performance index;

θ_i = angle of rotation of the deck with respect to the vertical plane passing through the deflected position of the cable (at section x_i);

ν_c, ν_s = upward displacements of the cables and deck;

ν = separation between locations A and B;

$\xi_1(\bar{x})$, $\xi_2(\bar{x})$ = normalized coordinates;

ξ_j = ratio of critical damping;

$\rho(\nu, f)$ = coherency function;

$\sigma^2_{u_{F_i}}$, $\sigma^2_{u_{s_i}}$, $\sigma^2_{u_{d_i}}$ = variance of the ith element of $\{u_F\}$, $\{u_s\}$, and $\{u_d\}$;

$\sigma^2_{f_i}$ = variance of the ith element end force;

$\sigma^2_{s_i}$ = variance of the ith static element end force;

τ = time delay in seconds;

φ_i = angle of rotation of the cable plane (at section x_i);

ϕ = shear deformation parameter;

$[\Psi]$ = matrix of mode shapes;

$\{\psi_j\}$ = mode shape corresponding to natural frequency ω_j;

ψ_{ij} = elements of mode shape matrix;

ω_g, ξ_g, ω_f, ξ_f = parameters of the Clough-Penzien SDF;

subscripts

F, FF = quantity corresponding to free displacement;

FR, RF = quantity corresponding to free and restrained displacement or vice versa;

R, RR = quantity corresponding to restrained displacement;

e = quantity corresponding to element;

superscripts

$\dot{}$ = first partial derivative with respect to time;

$\ddot{}$ = second partial derivative with respect to time;

$*$ = complex conjugate;

T = matrix transpose;

1. General Introduction and Background

1.1 Literature Review

Lifeline structures, such as pipelines, bridges and communication transmission systems, are important infrastructures of cities and urban communities. The functional reliability of these lifelines after an earthquake, is therefore essential to the safety and health of society.

Lifelines differ from conventional 'point' structures in that they extend for long distances along or close to the ground surface, and tend to have long periods of vibration (e.g., long-span suspension bridges). If the base dimensions of the structure are small relative to the vibration wavelength in the soil, the assumption that the wavelengths of earthquake ground waves are long compared to the structural dimensions is acceptable. For example, if the velocity of the wave propagation is 6,000 ft/sec, a sinusoidal wave of 3.0 Hz frequency will have a wave length of 2,000 ft, and a building with a base dimension of 100 ft will be subjected to essentially the same motions over its entire length. On the other hand, a long-span suspension bridge, which might have a length of several thousand feet, obviously would be subjected to drastically different motions at its foundations.

In classical deterministic analysis, a recorded time history at one point is used as the input motion, and the differential motion between two points is estimated by considering a delay in the arrival of the seismic wave between the points. This deterministic approach is capable of realistically describing the response of conventional structures subjected to earthquakes, but is restrictive for long-span suspension bridges because it neglects the loss of coherence between support excitations.

In the stochastic approach, the spatial variation of seismic ground motion is modelled as a random process with a given power spectral density, and the spatial variation is described by a correlation function and a phase shift. Recorded earthquake data from seismograph arrays are used to estimate the power spectral density and the correlation function.

In recent years, the earthquake response of suspension bridges has been studied using a frequency-domain random vibration approach to take into account not only the differences in ground motion inputs, but also the correlation among the various input motions (Rubin and Abdel-Ghaffar 1983, Abdel-Ghaffar and Strigfellow 1984, Abdel-Ghaffar and Rubin 1983 and 1982). It was found that the transmission time can have a significant effect on the response.

In a study on pipeline response to spatially variable ground motions, Zerva, et. al. (1988) concluded that the differential ground motion is of major importance. Whereas perfectly correlated support motion will yield zero differential displacements and forces between the pipe systems, partially correlated support motion can give high differential displacements.

In a study of the response of one- and two-span beams to spatially varying seismic excitation Harichandran and Wang (1988), concluded that it is important to consider the spatial variation of earthquake ground motion in the analysis of structures, especially for long statically indeterminate ones. They found that:

1. Both wave propagation and spatial correlation effects can be significant, but for cases where the apparent wave propagation velocity is large compared to the structural length the latter effect is more important.
2. For indeterminate structures, the pseudo-static stress is very significant especially for stiff structures, and neglecting this can result in a significant error.
3. Fully correlated support motions do not excite anti-symmetric modes which are excited by general support motions, and therefore in a few cases the former can result in a lower dynamic displacement than the latter.

The effects of spatially varying ground motion on the response of deck arch bridges was studied by Sweidan (1990), and the following conclusions were made:

1. The most important component of the response of arch bridges is the dynamic response (as opposed to the pseudo-static response).
2. The most important effect of the differential support excitation is the substantial increase in arch axial forces and bending moments.
3. The seismic wave velocity has a very important effect on the response of long structures.
4. The arch bridges studied by Sweidan attained stationary response during a strong ground motion of five seconds or more.

In a conclusion, all of the studies mentioned above indicate the importance of the effect of spatial variation of earthquake ground motion on the response of long structures.

1.2 Purpose and Scope

This research is concerned with the effects of spatially varying ground motion on the lateral response of an actual long span suspension bridge. The study was conducted on the Golden Gate Bridge in California with a 4,200 feet center span and 1,125 feet side spans. Two dimensional finite element model which accounts for the cable's uplift developed by Abdel-Ghaffar (1976) is used, with the corrections made by Castellani and Felloti (1986). A ground motion model proposed by Harichandran and Vanmarcke (1986) is used, where the model accounts for the correlation between the accelerations at two different points in the form of a coherency function. The effects of spatial variation in the excitation was studied in detail using linear stationary random vibration analysis. The transient response of the suspension bridge, was also performed to determine whether the suspension bridge will reach its stationary response during typical durations of strong shaking (10 to 20 seconds). The effects of shear deformation on the natural frequencies and mode shapes, and their corresponding effect on the linear stationary random vibration analysis of the bridge also investigated.

The bridge modeling and theoretical formulation is presented in Chapters 2 and 3. Chapter 2 is concerned with the finite element modeling to formulate the equations of motion and its finite element solution. Chapter 3 presents the derivation of the response components using linear random vibration theory and, the approach used to study the transient response. The ground motion model is also discussed in Chapter 3. The results from the analyses are presented in Chapter 4. A rigorous analysis of the response components and the response due to different ground motion models is investigated. The effects of apparent wave velocities and the relative modal contributions of the responses are investigated and discussed in details. Results from the transient response of the suspension bridge are presented. The effect of shear deformation on the response is discussed and presented. Finally, Chapter 5 summarize the main conclusions and contributions of this research and suggests possible direction for future research.

2. Free Lateral Vibration of Suspension Bridges

Analysis of suspension bridges subjected to lateral dynamic loads were developed by Moisseif, et. al. (1933), Silverman (1957), Selberg (1958), Hirai, et. al. (1960), Konishi,et. al. (1965), and Ito (1966), before the discovery of digital computers; and by Abdel-Ghaffar (1978), and Sigbjonsson, et. al. (1981), in recent times.

The contribution of the first group of researchers is mainly confined to solving, in an approximate way, the system of equations governing the dynamic equilibrium, and to finding a closed form solution for the first natural frequency of vibration. Ito, however, disagrees with his precursors by including, as a restoring force for the cable, the effect of the cable's uplift which accompanies the lateral displacement. This effect is also the cause of disagreement between the analysis of Abdel-Ghaffar, who includes it, and that of Sigbjornsson and Hjorth-Hansen, who neglect it. The importance of this effect on the period of the first natural mode is limited to a few percent for short span bridges, for which the predominant restoring action is the pendulum effect exerted by the suspended deck (which is the same in both approaches). Greater influence is expected for long bridges (say with a span of 2,000 ft or more).

In this work, the model developed by Abdel-Ghaffar is adopted in formulating of the equations of motion. The incorrect sign in the expression of the strain energy of the cables discussed by Castellani and Felotti (1986), is followed through carefully through the formulation of the equations of motion and the finite element modeling.

In this study, the Golden Gate Bridge is used as a typical example.

2.1 Description of the Bridge

The Golden Gate Bridge which lies across the entrance to San Francisco Bay and joins the northern and southern peninsulas was built in 1937. The main span is 4,200 feet, the largest ever constructed at the time. Each of the side spans is 1,125 feet long and is suspended from the main cables. The width of the roadway is 90 feet, and provides six traffic lanes and two sidewalks. The roadway initially consisted of a slab, a floor system, two stiffening trusses, and a lateral bracing system. The lateral bracing was in the plane of the top chords of the stiffening trusses (Strauss 1937). Since 1937 the bridge was subjected to several strong wind storms. After the storm of December 1st, 1951 a decision was made to stiffen the lateral bracing system. Lateral bracing in the plane of the bottom chords of the stiffening trusses were added. The addition of the bottom laterals made a closed box of the floor system for resisting torsion, greatly increasing the torsional rigidity of the roadway (Paine 1970).The general layout and the principal dimensions of the bridge are given in Figure 2.1, and the lateral structural properties of the Golden Gate Bridge are summerized in Table 2.1. For more description and the complete details of the structural components of the bridge see Strauss (1937) and Paine (1970).

2.2 Basic Assumptions for Analysis

1. The vibration amplitude around the equilibrium position is small, so that nonlinear terms in the differential equation of equilibrium can be neglected. As a consequence, lateral displacements are uncoupled from torsional motion.
2. The bending stiffness of the cables is neglected.
3. It is assumed that the hangers are pin-ended struts, and inextensible.
4. In modeling the bridge as a 2-D structure the two main cables are assumed to move in tandem as if they were connected by horizontal struts.
5. The ends of the cables are taken to be fixed.
6. As a corollary to the assumption in step 1, the increment of the horizontal component of cable tension $H(t)$, due to lateral vibration is small in comparison with the initial dead-load horizontal component of cable tension H_w.

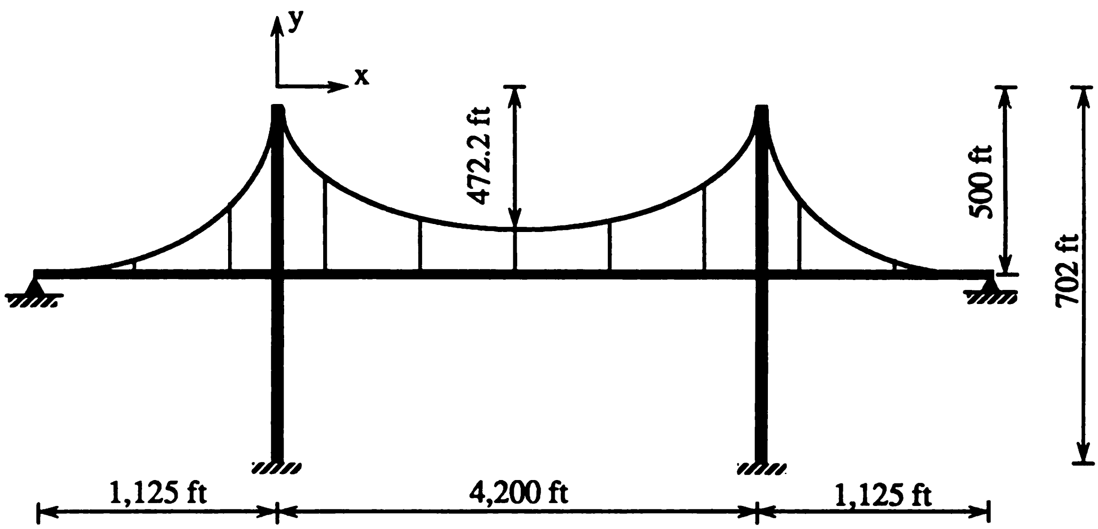

Figure 2.1 : Definition diagram of the Golden Gate Bridge

Table 2.1 : Structural properties related to the lateral vibration of the Golden Gate Bridge.

	Parameter	Center Span	Side Span
	Span length	L_2=4,200 ft	L_1=L_2= 1,125 ft
	Span width	b = 90 ft	b = 90 ft
Deck	weight	$\overline{W}_{s2}$ = 16.02 k/ft	$\overline{W}_{s(1,3)}$=16.42 k/ft
	Modulus	E_{s2} = 29,000 ksi	$E_{s1,s3}$=29,000 ksi
Properties	Moment of inertia	J_{s2} = 7,639.58 ft^4	$J_{s1,s3}$ =7,639.58 ft^4
	Shear deformation parameter	266.3	118.36
	Modulus	E_c= 29,000 ksi	
Cable	Cross sectional area	A_c = 831.9 in^2	
	Length	L_E = 7698 ft	
Properties	Horiz. component of tension	H_w = 53467 kips	
	Weight	$\overline{W}_c$ = 6.68 k/ft	

7. All stresses in the bridge remain within the elastic limit and therefore obey Hooke's law.

8. The initial curvature of the stiffening structure is considered small in comparison with the cable curvature and is therefore neglected.

9. The Golden Gate bridge was studied by Baron, et. al. (1976). The first nine transverse modes were obtained by means of the 3-dimensional model. The period of vibration of the first mode was found to be 20.23 seconds, no transverse modes of the towers were obtained in the calculations of the structure as a whole. It is observed that the towers act as rigid frames in the transverse direction and their periods of vibration are considerably smaller than those of the deck and cables. Therefore, the tower-piers are assumed to move as rigid bodies under ground motion excitation.

2.3 Derivation of the Equations of Motion

The derivation of the governing differential equations of lateral vibration of the cable and deck system is carried out in a general form by using Hamilton's variational principle. The resulting equations are linearized and reduced to a standard form through use of the previously stated simplifying assumptions. The exhaustive derivation was done by Abdel-Ghaffar (1976 and 1978). Applying the sign correction mentioned by Castellani and Felotti (1986), a summary of the corrected energy equations and the final form of equations of motion are briefly described.

The coordinate systems and vibrational displacements are described diagrammatically in Figure 2.2. By considering Figure 2.2, the upward displacements v_c and v_s of the cables and deck, respectively, may be expressed as

$$v_c(x_i, t) = -y_c(x_i)\,[1 - \cos\varphi_i] \quad , i=1,2,3 \tag{2.1}$$

and

$$v_s(x_i, t) = -y_c(x_i)\,(1 - \cos\varphi_i) - h(x_i)\,(1 - \cos\theta_i) \quad , i=1,2,3 \tag{2.2}$$

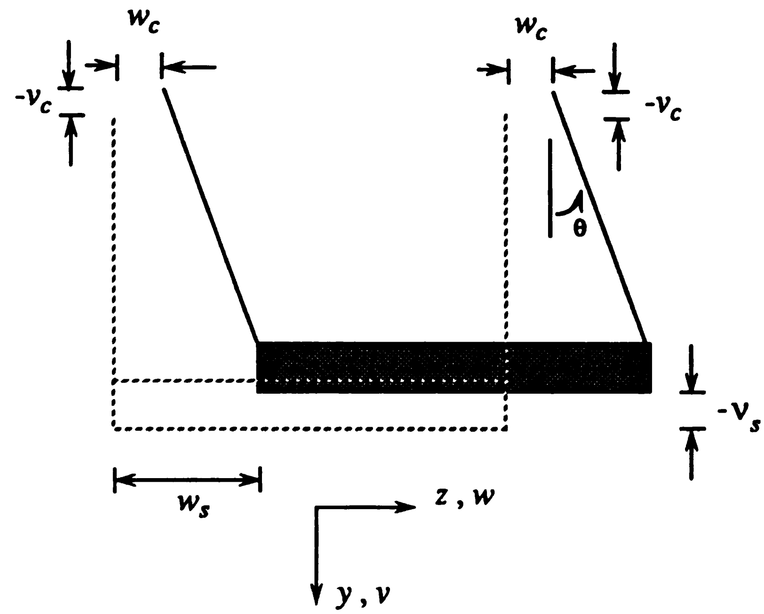

a) Lateral (bending) deformation

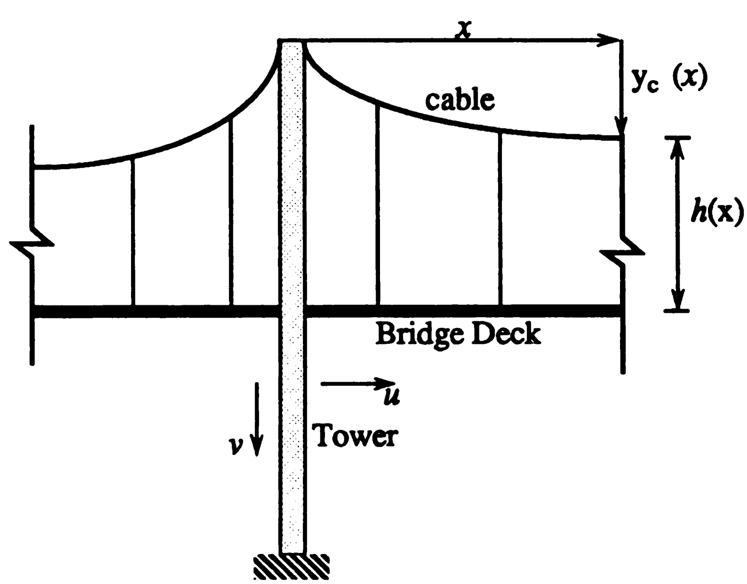

b) Coordinate system

Figure 2.2 : Laterally vibrating suspension bridge

in which φ_i is the angle of rotation of the cable plane (at section x_i) with respect to the vertical plane passing through the tower top; and θ_i is the angle of rotation of the deck with respect to the vertical plane passing through the deflected position of the cable at section x_i

Since w_c and w_s are very small quantities compared with y_c and h, we may write

$$v_c \approx -\frac{w_c^2}{2y_c} \tag{2.3}$$

$$v_s \approx \frac{-w_c^2}{2y_c} - \frac{(w_s - w_c)^2}{2h} \tag{2.4}$$

where w_c , w_s , y_c , h are described in Figure 2.2.

The potential energy of the laterally vibrating cable, $V_c(t)$, is comprised of two parts: the strain energy $V_{ce}(t)$ and the gravitational potential energy $V_{cg}(t)$. Thus, the total potential energy of the cable is expressed as

$$V_c(t) = V_{ce}(t) + V_{cg}(t) \tag{2.5}$$

The linear strain energy expression of the two cables can be formed as

$$V_{ce}(t) = \sum_{i=1}^{3} 2H_w \left(\frac{1}{2} \int_0^{l_i} \left(\frac{\partial w_c}{\partial w_i} \right)^2 dx_i - \frac{1}{2} \left(\frac{\overline{w}_c + \overline{w}_{si}}{H_w} \right) \int_0^{l_i} \left(\frac{w_c^2}{2y_c} \right) dx_i \right) \tag{2.6}$$

where H_w = horizontal component of cable tension.

$\overline{w}_c$ = dead weight of the two cables per unit length of the span.

$\overline{w}_{si}$ = dead weight of deck per unit length of the ith span.

The expression for the gravitational potential energy $V_{cg}(t)$ of the two cables due to the upward deflection v_c which occurs together with their lateral movement w_c can be written as

$$V_{cg}(t) = -\sum_{i=1}^{3} \int_{0}^{l_i} \bar{w}_c \left(\frac{w_c^2(x_i, t)}{2y_c(x_i)} \right) dx_i \qquad (2.7)$$

The potential energy of the laterally vibrating deck $V_s(t)$ also consists of two parts: (1) the elastic potential energy (i.e, the strain energy) $V_{se}(t)$ due to the effects of bending moments, shear forces and normal forces; and (2) the gravitational potential energy $V_{sg}(t)$ due to upward movement.

The energy stored in the deck due to bending can be written as

$$V_{se}(t) = \frac{1}{2} \sum_{i=1}^{3} \int_{0}^{l_i} E_{si} J_{si} \left(\frac{\partial^2}{\partial x_i^2} (w_s(x_i, t)) \right)^2 dx_i \qquad (2.8)$$

where E_{si} = modulus of elasticity of the deck in the ith span.

J_{si} = area moment of inertia of the deck about its vertical axis y_i in the ith span.

The gravitational energy $V_{sg}(t)$ of the deck due to upward displacement v_s is

$$V_{sg}(t) = -\frac{1}{2} \sum_{i=1}^{3} \int_{0}^{l_i} \bar{w}_{si} \left(\frac{w_c^2(x_i, t)}{y_c x_i} + \frac{(w_s(x_i, t) - w_c x_i, t)^2}{h x_i} \right) dx_i \qquad (2.9)$$

The kinetic energies caused by the lateral vibrational displacements w_c and w_s of the two cables and of the deck, respectively, are expressed as

$$T_c(t) = \frac{1}{2} \sum_{i=1}^{3} \int_{0}^{l_i} \bar{m}_c \left(\frac{\partial w_c(x_i, t)}{\partial t} \right)^2 dx_i \qquad (2.10)$$

and

$$T_s(t) = \frac{1}{2}\sum_{i=1}^{3}\int_0^{l_i} \bar{m}_{si}\left(\frac{\partial w_s(x_i,t)}{\partial t}\right)^2 dx_i \tag{2.11}$$

in which $\bar{m}_c = \bar{w}_c/g$ is the mass of the two cables per unit length of the span, $\bar{m}_{si} = \bar{w}_{si}/g$ is the mass of the deck per unit length of the i^{th} span; and g is the acceleration due to gravity.

The kinetic energies caused by vertical movements, v_c and v_s, of the cables and the deck, respectively, are given by

$$\tilde{T}_c(t) = -\frac{1}{2}\sum_{i=1}^{3}\int_0^{l_i} \bar{m}_c\left(\frac{\partial}{\partial t}\left(\frac{w_c^2}{2y_c}\right)\right)^2 dx_i \tag{2.12}$$

and

$$\tilde{T}_s(t) = -\frac{1}{2}\sum_{i=1}^{3}\int_0^{l_i} \bar{m}_c\left(\frac{\partial}{\partial t}\left(\frac{w_c^2}{2y_c} + \frac{(w_s - w_c)^2}{2h}\right)\right)^2 dx_i \tag{2.13}$$

Hamilton's principle is used to derive the linearized equations of motion (Abdel-Ghaffar 1976). The equations of motion are found to be

$$\bar{m}_c\frac{\partial^2 w_c}{\partial t^2} - 2H_w\frac{\partial^2 w_c}{\partial x_i^2} - \bar{w}_{si}\left(\frac{w_s - w_c}{h}\right) = 0\text{ , i=1,2,3} \tag{2.14}$$

for the cable; and

$$\bar{m}_{si}\frac{\partial^2 w_s}{\partial t^2} + \frac{\partial^2}{\partial x_i^2}\left(E_{si}J_{si}\frac{\partial^2 w_s}{\partial x_i^2}\right) + \bar{w}_{si}\left(\frac{w_s - w_c}{h}\right) = 0\text{ , i=1,2,3} \tag{2.15}$$

for the deck.

2.4 Finite Element Formulation of Lateral Vibration

The method of analysis based on the finite element technique takes into account the characteristics of both the cable and deck. The cable is idealized by a set of string elements, while the deck is idealized by a set of beam elements. The two types of elements, connected by rigid hangers, form the bridge element. The stiffness and inertia properties for each set of elements are derived and assembled to obtain the gross assemblage characteristics. The description of the bridge element and the finite element discretization of the bridge side span and center span are described diagrammatically in Figure 2.3 to Figure 2.5. The node numbering scheme used for the bridge side and center spans is illustrated in Figure 2.6, and Figure 2.7.

The interpolation functions associated with the two degrees of freedom of the nodal point in the deck subelement are taken to be cubic Hermitian polynomials. The lateral vibration of the suspended-structure can now be expressed in terms of the bridge element nodal displacements $u_j(t)$, $j = 1,2,3,4,5$, and 6, as

$$w_{se}(\xi_1, \xi_2;t) = \left[\xi_1^2 (3-2\xi_1) \;\; -L\xi_1^2\xi_2 \;\; 0 \;\; \xi_2^2 \; (3-2\xi_2) \;\; -L\xi_1\xi_2^2 \;\; 0 \right]_e \{u(t)\}_e \quad (2.16)$$

or

$$w_{se}(\xi_1, \xi_2;t) = \{f_s(\xi_1, \xi_2)\}_e^T \{u(t)\}_e \quad (2.17)$$

where e is a subscript indicating element, L is the length of element, and ξ_1, ξ_2 are the normalized coordinates defined as

$$\xi_1(\bar{x}) = (1-\frac{\bar{x}}{L}) \text{ and } \xi_2(\bar{x}) = \frac{\bar{x}}{L} \quad (2.18)$$

The interpolation function associated with the one degree of freedom of the cable nodal point is taken to be linear. Thus, the cable lateral displacement can be expressed in terms of the six nodal displacements of the bridge element, as

$$w_{ce}(\xi_1, \xi_2;t) = \left[0 \;\; 0 \;\; \xi_1 \;\; 0 \;\; 0 \;\; \xi_2\right]_e \{u(t)\}_e \quad (2.19)$$

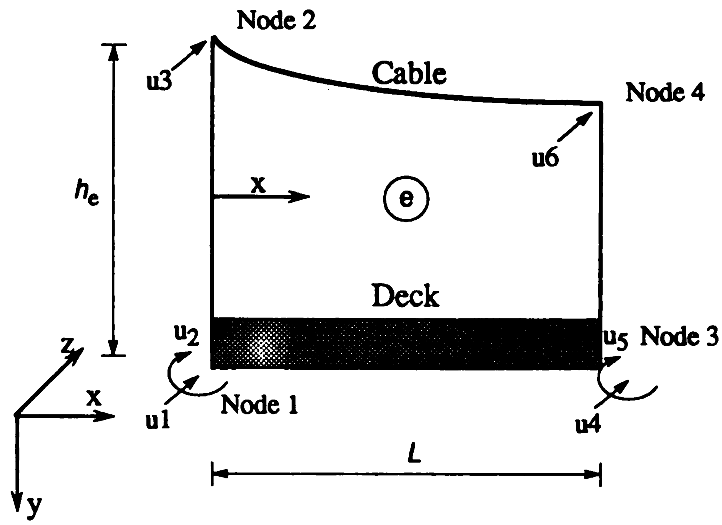

Figure 2.3 : Finite element and nodal displacements

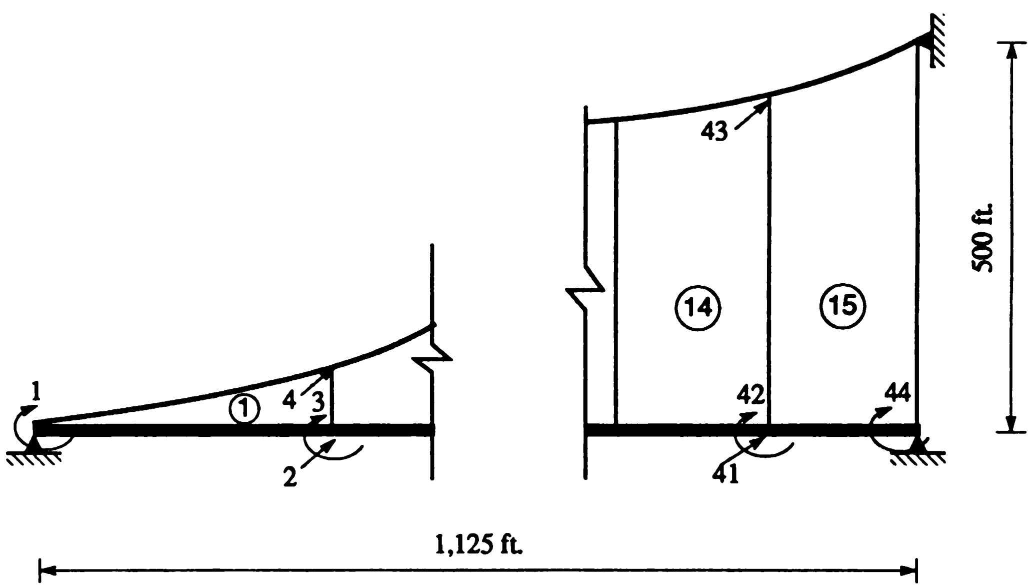

Figure 2.4 : Finite element discretization of the side span

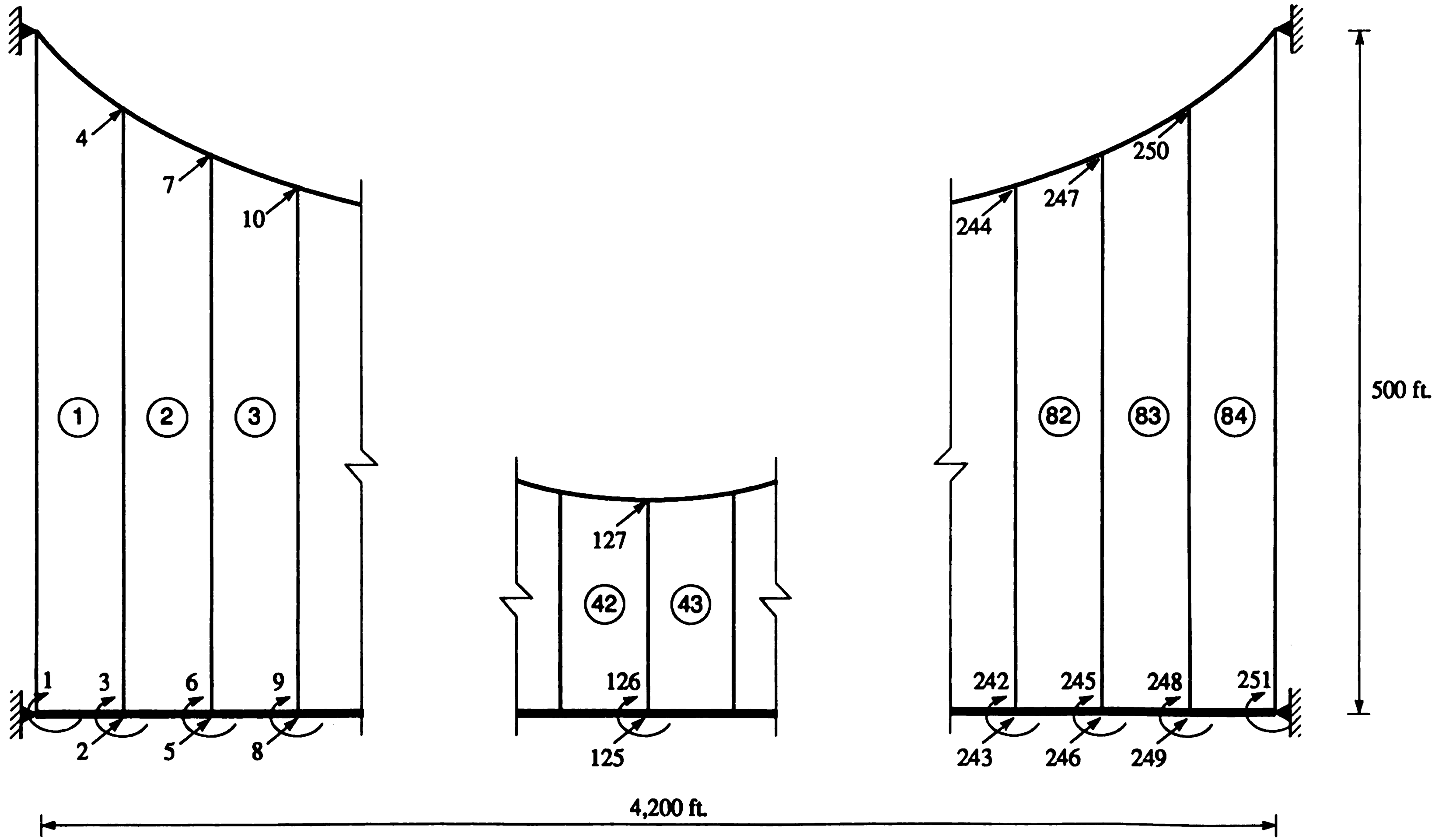

Figure 2.5 : Finite element discretization of the center span

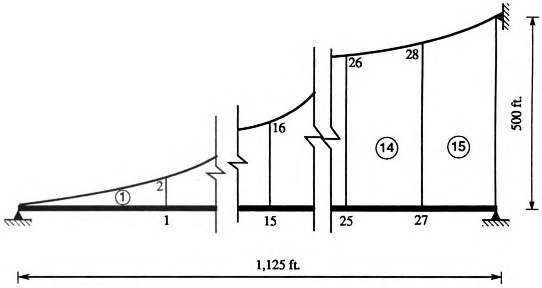

Figure 2.6 : Node numbering scheme for side span

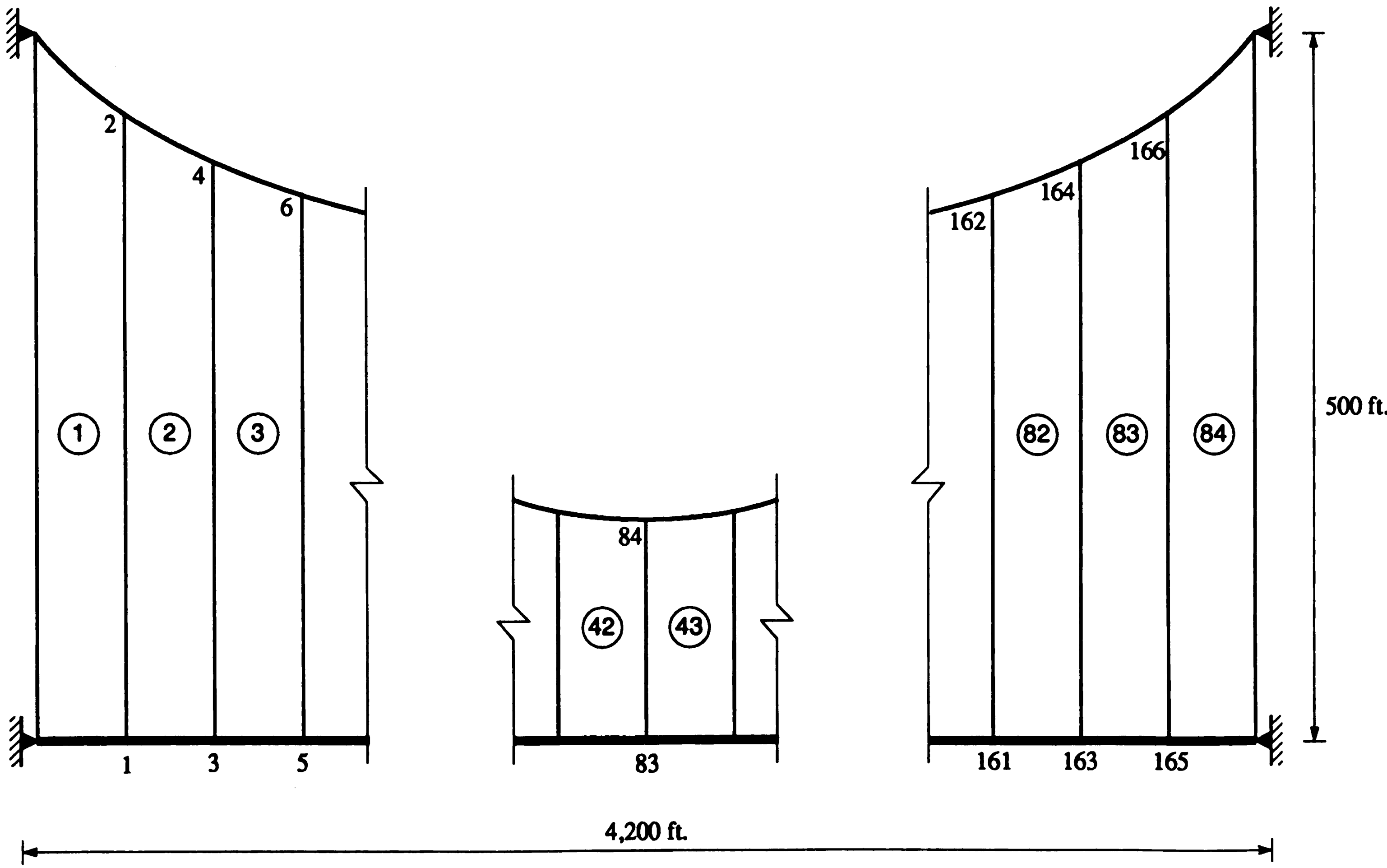

Figure 2.7 : Node numbering scheme for center span

or

$$w_{ce}(\xi_1, \xi_2; t) = \{f_c(\xi_1, \xi_2)\}_e^T \{u(t)\}_e \tag{2.20}$$

The application of equations (2.17) and (2.20) in equation (2.8) yields the elastic stiffness matrix of the deck:

$$[k_{se}]_e = \int_o^L E_{se} J_{se} \{f''_s\}_e \{f''_s\}_e^T d\bar{x} \tag{2.21}$$

$$[k_{se}]_e = \frac{E_{se} J_{se}}{L^3} \begin{bmatrix} 12 & -6L & 0 & -12 & -6L & 0 \\ -6L & 4L^2 & 0 & 6L & 2L^2 & 0 \\ 0 & 0 & 0 & 0 & 0 & 0 \\ -12 & 6L & 0 & 12 & 6L & 0 \\ -6L & 2L^2 & 0 & 6L & 4L^2 & 0 \\ 0 & 0 & 0 & 0 & 0 & 0 \end{bmatrix} \tag{2.22}$$

If shear deformation is included in the deck, the elastic stiffness matrix becomes (Przemieniecki 1968)

$$[k_{se}]_e = \frac{E_{se} J_{se}}{L^3 (1+\phi)} \begin{bmatrix} 12 & -6L & 0 & -12 & -6L & 0 \\ -6L & (4+\phi)L^2 & 0 & 6 & (2-\phi)L^2 & 0 \\ 0 & 0 & 0 & 0 & 0 & 0 \\ -12 & 6 & 0 & 12 & 6L & 0 \\ -6L & (2-\phi)L^2 & 0 & 6L & (4+\phi)L^2 & 0 \\ 0 & 0 & 0 & 0 & 0 & 0 \end{bmatrix} \tag{2.23}$$

where ϕ is the shear deformation parameter.

The use of equations (2.17) and (2.20) in equation (2.9) yields the gravitational stiffness matrix of the deck:

$$[k_{sg}]_e = \frac{\bar{w}_{se}L}{420h_e}\begin{bmatrix} 156 & 22L & -147 & 54 & -13L & -63 \\ 22L & 4L^2 & -21L & 13L & -3L^2 & -14L \\ -147 & -21L & 140\left(1+\frac{h_e}{y_e}\right) & -63 & 14L & 70\left(1+\frac{h_e}{y_e}\right) \\ 54 & 13L & -63 & 156 & -22L & -147 \\ -13L & -3L^2 & 14L & -22L & 4L^2 & -21L \\ -63 & -14L & 70\left(1+\frac{h_e}{y_e}\right) & -147 & -21L & 140\left(1+\frac{h_e}{y_e}\right) \end{bmatrix} \tag{2.24}$$

where $\bar{w}_{se}$ is the weight of the deck subelement per unit length.

Similarly, using equations (2.17) and (2.20) in the equation (2.5) yields the elastic stiffness matrix of cables:

$$[k_{ce}]_e = \frac{2H_w}{L}\begin{bmatrix} 0 & 0 & 0 & 0 & 0 & 0 \\ 0 & 0 & 0 & 0 & 0 & 0 \\ 0 & 0 & 1 & 0 & 0 & -1 \\ 0 & 0 & 0 & 0 & 0 & 0 \\ 0 & 0 & 0 & 0 & 0 & 0 \\ 0 & 0 & -1 & 0 & 0 & 1 \end{bmatrix} - \left(\frac{\bar{w}_{se}+\bar{w}_{ce}}{6y_e}\right)\begin{bmatrix} 0 & 0 & 0 & 0 & 0 & 0 \\ 0 & 0 & 0 & 0 & 0 & 0 \\ 0 & 0 & 2 & 0 & 0 & 1 \\ 0 & 0 & 0 & 0 & 0 & 0 \\ 0 & 0 & 0 & 0 & 0 & 0 \\ 0 & 0 & 1 & 0 & 0 & 2 \end{bmatrix} \tag{2.25}$$

The gravitational stiffness matrix of cables is formed by applying equations (2.17) and (2.20) in equation (2.7):

$$[k_{cg}]_e = \frac{\bar{w}_{ce}L}{6y_e}\begin{bmatrix} 0 & 0 & 0 & 0 & 0 & 0 \\ 0 & 0 & 0 & 0 & 0 & 0 \\ 0 & 0 & 2 & 0 & 0 & 1 \\ 0 & 0 & 0 & 0 & 0 & 0 \\ 0 & 0 & 0 & 0 & 0 & 0 \\ 0 & 0 & 1 & 0 & 0 & 2 \end{bmatrix} \tag{2.26}$$

The use of equations (2.17) and (2.20) in equation (2.11) yields the consistent mass matrix of the deck:

$$[m_s]_e = \frac{\overline{m}_{se}L}{420}\begin{bmatrix} 156 & -22L & 0 & 54 & 13L & 0 \\ -22L & 4L^2 & 0 & -13L & -3L^2 & 0 \\ 0 & 0 & 0 & 0 & 0 & 0 \\ 54 & -13L & 0 & 156 & 22L & 0 \\ 13L & -3L^2 & 0 & 22L & 4L^2 & 0 \\ 0 & 0 & 0 & 0 & 0 & 0 \end{bmatrix} \tag{2.27}$$

If shear deformation in the deck is accounted for, then the following consistent mass matrix (Przemieniecki 1968) is obtained:

$$[m_s]_e = [m_{s1}] \tag{2.28}$$

where $[m_{s1}]$ is given by Figures 2.8.

Finally, using equations (2.17) and (2.20) in equation (2.10) yields the mass matrix of the cable:

$$[m_c]_e = \frac{\overline{m}_{ce}L}{6}\begin{bmatrix} 0 & 0 & 0 & 0 & 0 & 0 \\ 0 & 0 & 0 & 0 & 0 & 0 \\ 0 & 0 & 2 & 0 & 0 & 1 \\ 0 & 0 & 0 & 0 & 0 & 0 \\ 0 & 0 & 0 & 0 & 0 & 0 \\ 0 & 0 & 1 & 0 & 0 & 2 \end{bmatrix} \tag{2.36}$$

The various matrices corresponding to the overall structure are assembled from the element matrices in the standard way. The following structure matrices are assembled:

1. The elastic stiffness matrix of the deck $[K_{SE}]$ from the element matrices $[k_{se}]_e$.
2. The gravitational stiffness matrix of the deck $[K_{SG}]$ from the element matrices $[k_{sg}]_e$.
3. The elastic stiffness matrix of the cables $[K_{CE}]$ from the element matrices $[k_{ce}]_e$.

$$[m_{s1}] = \frac{\bar{m}_{se}L}{(1+\phi)^2}\begin{bmatrix} (\frac{13}{35}+\frac{7\phi}{10}+\frac{\phi^2}{3}) & -(\frac{11}{210}+\frac{11\phi}{120}+\frac{\phi^2}{24})L & 0 & (\frac{9}{70}+\frac{3\phi}{10}+\frac{\phi^2}{6}) & (\frac{13}{420}+\frac{3\phi}{40}+\frac{\phi^2}{24})L & 0 \\ -(\frac{11}{210}+\frac{11\phi}{120}+\frac{\phi^2}{24}) & (\frac{1}{105}+\frac{\phi}{60}+\frac{\phi^2}{120})L^2 & 0 & -(\frac{13}{420}+\frac{3\phi}{40}+\frac{\phi^2}{24})L & -(\frac{1}{140}+\frac{\phi}{60}+\frac{\phi^2}{120})L^2 & 0 \\ 0 & 0 & 0 & 0 & 0 & 0 \\ (\frac{9}{70}+\frac{3\phi}{10}+\frac{\phi^2}{6}) & -(\frac{13}{420}+\frac{3\phi}{40}+\frac{\phi^2}{24})L & 0 & (\frac{13}{35}+\frac{7\phi}{10}+\frac{\phi^2}{3}) & (\frac{11}{210}+\frac{11\phi}{120}+\frac{\phi^2}{24})L & 0 \\ (\frac{13}{420}+\frac{3\phi}{40}+\frac{\phi^2}{24})L & -(\frac{1}{140}+\frac{\phi}{60}+\frac{\phi^2}{120})L^2 & 0 & (\frac{11}{210}+\frac{11\phi}{120}+\frac{\phi^2}{24})L & (\frac{1}{105}+\frac{\phi}{60}+\frac{\phi^2}{120})L^2 & 0 \\ 0 & 0 & 0 & 0 & 0 & 0 \end{bmatrix}$$

Figure 2.8 : Consistent mass matrix when shear deformation is included

4. The gravitational stiffness matrix of the cables $[K_{CG}]$ from the element matrices $[k_{sg}]_e$.
5. The mass matrix of the deck $[M_S]$ from the element matrices $[m_s]_e$.
6. The mass matrix of the cables $[M_c]$ from element matrices $[m_c]_e$.

The free vibration equations of the bridge are

$$[M]\,\{\ddot{u}\} + [K]\,\{u\} = \{0\} \tag{2.37}$$

in which

$$[M] = [M_S] + [M_C] \tag{2.38}$$

and

$$[K] = [K_{SE}] + [K_{SG}] + [K_{CE}] + [K_{CG}] \tag{2.39}$$

3. Random Vibration Analysis

The damped equations of motion of the bridge can be written as

$$[M]\ \{\ddot{u}\} + [C]\ \{\dot{u}\} + [K]\ \{u\} = \{0\} \tag{3.1}$$

where $[M]$ is the overall consistent mass matrix of equation (2.39), $[C]$ is the damping matrix, $[K]$ is the overall stiffness matrix of equation (2.40), and $\{\ddot{u}\}$, $\{\dot{u}\}$, and $\{u\}$ are vectors of nodal accelerations, velocities, and displacements. Equation (3.1) represents the equations of motion for all nodal displacements, regardless of whether they are free or restrained.

Equation (3.1), can be rearranged and partitioned as follow:

$$\begin{bmatrix} M_{FF} & M_{FR} \\ M_{RF} & M_{RR} \end{bmatrix} \begin{bmatrix} \{\ddot{u}_F\} \\ \{\ddot{u}_R\} \end{bmatrix} + \begin{bmatrix} C_{FF} & C_{FR} \\ C_{RF} & C_{RR} \end{bmatrix} \begin{bmatrix} \{\dot{u}_F\} \\ \{\dot{u}_R\} \end{bmatrix} + \begin{bmatrix} K_{FF} & K_{FR} \\ K_{RF} & K_{RR} \end{bmatrix} \begin{bmatrix} \{u_F\} \\ \{u_R\} \end{bmatrix} = \begin{bmatrix} \{0\} \\ \{0\} \end{bmatrix} \tag{3.2}$$

The subscript F refers to free nodal displacements, while the subscript R denotes restrained nodal displacements.

The free nodal displacement vector $\{u_F\}$ can be decomposed into pseudo-static and dynamic parts, $\{u_s\}$ and $\{u_d\}$, respectively:

$$\{u_F\} = \{u_s\} + \{u_d\} \tag{3.3}$$

The pseudo-static displacements are obtained from the support displacements. The static equilibrium equations, with no external loading are:

$$[K_{FF}]\ \{u_F\} + [K_{FR}]\ \{u_R\} = \{0\} \tag{3.4}$$

$\{u_s\}$ are the free displacements from the above equation due to prescribed displacements $\{u_R\}$ and is therefore given by

$$\{u_s\} = -[K_{FF}]^{-1}\ [K_{FR}]\ \{u_R\} \tag{3.5}$$

Equation (3.5) represents the instantaneous free displacements of the structure due to support movement $\{u_R\}$ at time t. Substituting equation (3.5) into equation (3.2), and assuming stiffness proportional damping (for which $[C] = \alpha\ [K]$) yields (Harichandran and Wang 1988)

$$([K_{FF}]\{\ddot{u}_d\} + [C_{FF}]\{\dot{u}_d\} + [K_{FF}]\{u_d\}) \approx ([M_{FF}][K_{FF}]^{-1}[K_{FR}] - [M_{FR}])\{\ddot{u}_R\} \tag{3.6}$$

in which the term $([C_{FF}]\ [K_{FF}]\ [K_{FR}] - [C_{FR}])\ \{\dot{u}_R\}$ is dropped. Equation(3.6) is also approximately true for any light damping.

3.1 Modal Analysis

The free vibration equations of motion are

$$[M_{FF}]\ \{\ddot{u}_d\} + [K_{FF}]\ \{u_d\}\ =\ \{0\} \tag{3.7}$$

For free vibrations of the undamped structure, we seek solutions of equation (3.7) in the form

$$\{\ddot{u}_d\}\ =\ [\Psi]\ \{Y\}\, e^{i\omega t} \tag{3.8}$$

in which $[\Psi]\ =\ \left[\{\psi_1\}\ \{\psi_2\}\ -\ -\ -\ \{\psi_n\}\right]$ is the matrix of mode shapes, and $\{Y\}$ are a set of generalized coordinates. Substituting equation (3.8) in equation (3.7) yields the generalized eigenvalue problem

$$([K_{FF}] - [\mathrm{diag}(\omega^2)]\ [M_{FF}])\ [\Psi]\ =\ [0] \tag{3.9}$$

The solution of these equations yield the natural frequencies of vibration ω_j, and the mode shapes, $\{\psi_j\}$, of the structure. Substituting

$$\{u_d\}\ =\ [\Psi]\ \{Y\} \tag{3.10}$$

into equation (3.6), premultiplying by $[\Psi]^T$ and assuming that mode shapes are orthogonal to the damping matrix (classical damping), results in the uncoupled modal equtions

$$\ddot{Y}_j + 2\xi_j\omega_j\dot{Y}_j + \omega_j^2 Y_j = G_j \text{ , } j=1,2,3,\ldots\ldots\ldots,n \tag{3.11}$$

where

$$G_j = \frac{\{\psi_j\}^T[\,[M_{FF}]\,[K_{FF}]^{-1}[K_{FR}] - [M_{FR}]\,]}{M_j}\{\ddot{u}_R\} = \{\Gamma_j\}^T\{\ddot{u}_R\} \tag{3.12}$$

$$\{\Gamma_j\} = \frac{[\,[M_{FF}]\,[K_{FF}]^{-1}[K_{FR}] - [M_{FR}]\,]^T\{\psi_j\}}{M_j} \tag{3.13}$$

$$M_j = \{\psi_j\}^T[M_{FF}]\,\{\psi_j\} \tag{3.14}$$

In practice it is common to assume modal damping ratios ξ_j rather than to assemble the matrix $[C]$ in equation (3.1). It is convenient to collect the excitations $G_j(t)$ into a vector $\{G(t)\}$ and the modal participation factors $\{\Gamma_j\}$ into a matrix

$$[\Gamma] = \left[\{\Gamma_1\}\ \{\Gamma_2\}\ -\ -\ -\ \{\Gamma_n\}\right] \tag{3.15}$$

in which case equation (3.12) may be written as

$$\{G\} = [\Gamma]^T\{\ddot{u}_R\} \tag{3.16}$$

The modal participation factor matrix $[\Gamma]$ is of size $r \times n$, where r is the number of restrained degrees-of-freedom and n is the number of mode shapes considered in the analysis.

3.2 Random Vibration Theory

The autocorrelation function of the i^{th} free displacement is defined as

$$R_{u_{F_i}}(\tau) = E\{u_{F_i}(\tau)\,u_{F_i}(t+\tau)\} \tag{3.17}$$

Using equation (3.3) in equation (3.17), we obtain the following expression

$$R_{u_{F_i}}(\tau) = R_{u_{d_i}}(\tau) + R_{u_{d_i}u_{s_i}}(\tau) + R_{u_{s_i}u_{d_i}}(\tau) + R_{u_{s_i}}(\tau) \tag{3.18}$$

where $R_{u_{d_i}}$, $R_{u_{s_i}}$, and $R_{u_{d_i}u_{s_i}}$ are the autocorrelations of the dynamic displacement component, the static displacement component, and the cross correlation between the dynamic and static component, respectively.

For stationary response

$$R_{u_{d_i}u_{s_i}}(\tau) = R_{u_{s_i}u_{d_i}}(-\tau) \tag{3.19}$$

The Fourier Transform of equation (3.18) yields the spectral density function of the ith free displacement

$$S_{u_{F_i}}(\omega) = S_{u_{d_i}}(\omega) + S_{u_{d_i}u_{s_i}}(\omega) + S_{u_{s_i}u_{d_i}}(\omega) + S_{u_{s_i}}(\omega) \tag{3.20}$$

For stationary response

$$S_{u_{d_i}u_{s_i}}(\omega) = S^{*}{}_{u_{s_i}u_{d_i}}(\omega) \tag{3.21}$$

where the asterisk denotes the complex conjugate.

The variance of the ith free displacement can be obtained by integrating equation (3.20)

$$\begin{aligned} \sigma^2_{u_{F_i}} &= \int_{-\infty}^{\infty} S_{u_{d_i}}(\omega)\, d\omega + \int_{-\infty}^{\infty} S_{u_{s_i}}(\omega)\, d\omega + 2\mathrm{Re}\left[\int_{-\infty}^{\infty} S_{u_{s_i}u_{d_i}}(\omega)\, d\omega\right] \\ \sigma^2_{u_{F_i}} &= \sigma^2_{u_{d_i}} + \sigma^2_{u_{s_i}} + 2\mathrm{Cov}\,(u_{s_i}, u_{d_i}) \end{aligned} \tag{3.22}$$

where Re[ ] denotes the real part of the argument, $\sigma^2_{u_{s_i}}$ and $\sigma^2_{u_{d_i}}$ are the variances of the pseudo-static and dynamic ith displacement, and Cov (u_{s_i}, u_{d_i}) is the covariance between the static and dynamic displacements.

3.2.1 Variance of Dynamic Displacements

Applying the definition of the autocorrelation function in equation (3.17) to the ith dynamic displacement, and using equation (3.10) we obtain

$$R_{u_{d_i}}(\tau) = \sum_{j=1}^{n}\sum_{k=1}^{n}\Psi_{ij}\Psi_{ik}E\{Y_j(t)Y_k(t+\tau)\} \tag{3.23}$$

where the index n is equal to the number of mode shapes considered in the analysis.

The equation of motion expressed by equation (3.10) can be solved using Duhamel's integral as

$$Y_j(t) = \int_{-\infty}^{\infty} G_j(t-\theta)\,h_j(\theta)\,d\theta \tag{3.24}$$

where $h_j(t)$ is the impulse response function for mode j and $h_j(t)$ is the response function due to an impulse excitation $G_j = \delta(t)$, where $\delta(t)$ is the Dirac delta function.

Substituting equation (3.24) into equation (3.23), yields

$$R_{u_{d_i}}(\tau) = \sum_{j=1}^{n}\sum_{k=1}^{n}\Psi_{ij}\Psi_{ik}E\left\{\int_{-\infty}^{\infty} G_j(t-\theta_1)\,h_j(\theta_1)\,d\theta_1\int_{-\infty}^{\infty} G_k(t+\tau-\theta_2)\,h_k(\theta_2)\,d\theta_2\right\} \tag{3.25}$$

Equation (3.25) shows that the impulse response does not depend on the time lag τ, thus it can be written as

$$R_{u_{d_i}}(\tau) = \sum_{j=1}^{n}\sum_{k=1}^{n}\Psi_{ij}\Psi_{ik}\int_{-\infty}^{\infty}\int_{-\infty}^{\infty} h_j(\theta_1)\,h_k(\theta_2)\,E\{G_j(t-\theta_1)\,G_k(t+\tau-\theta_2)\}\,d\theta_1 d\theta_2 \tag{3.26}$$

substituting equation (3.12) into equation (3.26) yields

$$R_{u_{d_i}}(\tau) = \sum_{j=1}^{n}\sum_{k=1}^{n}\sum_{l=1}^{r}\sum_{m=1}^{r}\Psi_{ij}\Psi_{ik}\Gamma_{lj}\Gamma_{mk}\int_{-\infty}^{\infty}\int_{-\infty}^{\infty} R_{\ddot{u}_{Rl}\ddot{u}_{Rm}}(\tau-\theta_2+\theta_1)\,h_j(\theta_1)\,h_k(\theta_2)\,d\theta_1 d\theta_2 \tag{3.27}$$

The Fourier Transform of the above equation yields the spectral density function of the ith dynamic displacement :

$$S_{u_{d_i}}(\omega) = \frac{1}{2\pi}\sum_{j=1}^{n}\sum_{k=1}^{n}\sum_{l=1}^{r}\sum_{m=1}^{r}\psi_{ij}\psi_{ik}\Gamma_{lj}\Gamma_{mk}\int_{-\infty}^{\infty}\int_{-\infty}^{\infty}\int_{-\infty}^{\infty}R_{\ddot{u}_{Rl}\ddot{u}_{Rm}}(\tau-\theta_2+\theta_1)\,h_j(\theta_1)\,h_k(\theta_2)\,e^{-i\omega\tau}d\theta_1 d\theta_2 d\tau \tag{3.28}$$

The impulse function $h_j(\theta)$ is related to the frequency response function $H_j(\omega)$ through

$$h_j(\theta) = \frac{1}{2\pi}\int_{-\infty}^{\infty}H_j(\omega)\,e^{i\omega\theta}d\theta \tag{3.29}$$

using equation (3.29) and a change of variables to $(\tau-\theta_2+\theta_1)$ in equation (3.29) yields

$$S_{u_{d_i}}(\omega) = \sum_{j=1}^{n}\sum_{k=1}^{n}\sum_{l=1}^{r}\sum_{m=1}^{r}\psi_{ij}\psi_{ik}\Gamma_{lj}\Gamma_{mk}H_j(-\omega)\,H_k(\omega)\,S_{\ddot{u}_{Rl}\ddot{u}_{Rm}}(\omega) \tag{3.30}$$

Integrating equation (3.30) yields the variance of the free dynamic response $u_{d_i}(t)$:

$$\begin{aligned}\sigma^2_{u_{d_i}} &= \sum_{j=1}^{n}\sum_{k=1}^{n}\sum_{l=1}^{r}\sum_{m=1}^{r}\psi_{ij}\psi_{ik}\Gamma_{lj}\Gamma_{mk}\int_{-\infty}^{\infty}H_j(-\omega)\,H_k(\omega)\,S_{\ddot{u}_{Rl}\ddot{u}_{Rm}}(\omega)\,d\omega \\ &= \sum_{j=1}^{n}\sum_{k=1}^{n}\psi_{ij}\psi_{ik}I_{jk}\end{aligned} \tag{3.31}$$

where $H_j(\omega)$ may be obtained directly from equation (3.11), and has the form

$$H_j(\omega) = \frac{1}{(\omega_j^2-\omega^2)+2i\xi_j\omega_j\omega} \tag{3.32}$$

and

$$I_{jk} = \sum_{l=1}^{r}\sum_{m=1}^{r}\Gamma_{lj}\Gamma_{mk}\int_{-\infty}^{\infty}H_j(-\omega)\,H_k(\omega)\,S_{\ddot{u}_{Rl}\ddot{u}_{Rm}}(\omega)\,d\omega \tag{3.33}$$

are the nodal covariances contributing to the overall dynamic response.

3.2.2 Variance of Pseudo-Static Displacements

The static displacements of the free nodes due to static support motion is expressed by equation (3.5), and can be rewritten in a compact form as

$$\{u_s\} = [A]\{u_R\} \tag{3.34}$$

where $[A] = -[K_{FF}]^{-1}[K_{FR}]$

[A] represents an $n \times r$ matrix, where each column in it represents the static displacements of the free nodes due to a unit displacement of the corresponding support, while all other support displacements are zero.

Applying the autocorrelation function to the ith pseudo-static displacement and using the summation expansion of equation (3.33) yields

$$R_{u_{s_i}}(\tau) = \sum_{l=1}^{r}\sum_{m=1}^{r} A_{il}A_{im}R_{u_{Rl}u_{Rm}}(\tau) \tag{3.35}$$

and the spectral density function of the pseudo-static displacement is obtained through the Fourier transform of equation (3.34)

$$S_{u_{s_i}}(\omega) = \sum_{l=1}^{r}\sum_{m=1}^{r} A_{il}A_{im}S_{u_{Rl}u_{Rm}}(\omega) \tag{3.36}$$

Equation (3.35) can be expressed in terms of the spectral density function of acceleration as

$$S_{u_{s_i}}(\omega) = \sum_{l=1}^{r}\sum_{m=1}^{r} A_{il}A_{im}\frac{1}{\omega^4}S_{\ddot{u}_{Rl}\ddot{u}_{Rm}}(\omega) \tag{3.37}$$

The variance of the ith pseudo-static displacement is then

$$\sigma^2_{u_{s_i}} = \sum_{l=1}^{r}\sum_{m=1}^{r} A_{il}A_{im}\int_{-\infty}^{\infty}\frac{1}{\omega^4}S_{\ddot{u}_{Rl}\ddot{u}_{Rm}}(\omega)\,d\omega \tag{3.38}$$

3.2.3 Covariance between Pseudo-Static and Dynamic Displacements

The cross correlation between static and dynamic displacements is expressed in equation (3.18), using this expression and equations (3.10) and (3.34), we obtain

$$R_{u_{s_i}u_{d_i}}(\tau) = \sum_{l=1}^{r}\sum_{k=1}^{n} A_{il}\Psi_{ik}E\{u_{R_l}(t)\,Y_k(t+\tau)\} \tag{3.39}$$

Using Duhamel's integral (equation (3.24)), the relation between the impulse response function $h_j(\theta)$ and the frequency response function of equation (3.29), and applying a change of variable to equation (3.38), the spectral density function between the static and dynamic displacement can be obtained as (Harichandran and Wang 1988)

$$S_{u_{s_i}u_{d_i}}(\omega) = \sum_{l=1}^{r}\sum_{k=1}^{n}\sum_{m=1}^{r} A_{il}\Psi_{ik}\Gamma_{mk}H_k(\omega)\,S_{u_{Rl}\ddot{u}_{Rm}}(\omega) \tag{3.40}$$

Differentiating the cross correlation function $R_{u_{Rl}u_{Rm}}(\tau)$ twice, yields

$$R''_{u_{Rl}u_{Rm}}(\tau) = R_{u_{Rl}\ddot{u}_{Rm}}(\tau) \tag{3.41}$$

Differentiating the Fourier Transform relation between the autocorrelation function and the spectral density function, we obtain

$$R''_{u_{Rl}u_{Rm}}(\tau) = \int_{-\infty}^{\infty} -\omega^2 S_{u_{Rl}u_{Rm}}(\omega)\,e^{i\omega\tau}d\omega \tag{3.42}$$

From equation (3.40) and equation (3.41), it follows that

$$S_{u_{Rl}\ddot{u}_{Rm}}(\omega) = \frac{1}{2\pi}\int_{-\infty}^{\infty} R''_{u_{Rl}u_{rm}}(\tau)\,e^{-i\omega\tau}d\tau \tag{3.43}$$

or,

$$S_{u_{Rl}\ddot{u}_{Rm}}(\omega) = -\omega^2 S_{u_{Rl}u_{Rm}}(\omega) \tag{3.44}$$

Using the fact that

$$S_{u_{Rl}u_{Rm}}(\omega) = \frac{1}{\omega^4} S_{\ddot{u}_{Rl}\ddot{u}_{Rm}}(\omega) \tag{3.45}$$

and substituting in equation (3.43) yields

$$S_{u_{Rl}\ddot{u}_{Rm}}(\omega) = -\frac{1}{\omega^2} S_{\ddot{u}_{Rl}\ddot{u}_{Rm}}(\omega) \tag{3.46}$$

Substituting equation (3.45) into equation (3.39) and using equation (3.22) yields

$$\mathrm{Cov}\,(u_{s_i}, u_{d_i}) = \sum_{l=1}^{r} \sum_{k=1}^{n} \sum_{m=1}^{r} A_{il} \Psi_{ik} \Gamma_{mk} \int_{-\infty}^{\infty} -\frac{1}{\omega^2} H_k(\omega)\, S_{\ddot{u}_{Rl}\ddot{u}_{Rm}}(\omega)\, d\omega \tag{3.47}$$

The covariance has the property

$$\mathrm{Cov}\,(u_{d_i}, u_{s_i}) = \mathrm{Cov}\,(u_{s_i}, u_{d_i}) \tag{3.48}$$

3.2.4 Variance of Dynamic Element End Forces

From the solution of the eigenvalue problem we obtain mode shapes in the global coordinate system. For a general beam element with d.o.f. (j, k) at the left end, and (l, m) at the right end, the member end-displacements corresponding to the ith mode are

$$\{D_{eg}\}_i = \begin{bmatrix} \Psi_{ji} \\ \Psi_{ki} \\ \Psi_{li} \\ \Psi_{mi} \end{bmatrix} \tag{3.49}$$

If the beam element is inclined, then the member end-displacements in local coordinates can be obtained by

$$\{D_{em}\}_i = [T]\,\{D_{eg}\}_i \tag{3.50}$$

in which *[T]* is rotational transformation matrix.

The element end forces corresponding to the ith mode shape can be computed as

$$\{f\}_i = [k_e]\,\{D_{em}\}_i \tag{3.51}$$

where $[k_e]$ is the element stiffness matrix in local coordinates.

Performing this sequence of operations for all the eigenvectors, the resulting element end forces can be collected into a matrix $[F]$ in which the F_{ij} element is the ith element end force corresponding to the jth mode shape. Using the same procedure described in Section 3.2.1, it can be shown that the variance of the ith dynamic element end force is expressed as

$$\begin{aligned} \sigma_{f_i}^2 &= \sum_{j=1}^{n}\sum_{k=1}^{n}\sum_{l=1}^{r}\sum_{m=1}^{r} F_{ij}F_{ik}\Gamma_{lj}\Gamma_{mk}\int_{-\infty}^{\infty} H_j(-\omega)\,H_k(\omega)\,S_{\ddot{u}_{Rl}\ddot{u}_{Rm}}(\omega)\,d\omega \\ &= \sum_{j=1}^{n}\sum_{k=1}^{n} F_{ij}F_{ik}I_{jk} \end{aligned} \tag{3.52}$$

where I_{jk} is defined in equation (3.33).

3.2.5 Variance of Static Element End Forces

Similar to the dynamic element end forces, making use of equation (3.33), we can assemble a static element end force matrix $[P]$ in which P_{ij} is the ith element end force due to a unit displacement along the jth restrained degree of freedom. Using the same formulation described in Section 3.2.2, it can be shown that the variance of the ith static element end force is expressed as

$$\sigma_{s_i}^2 = \sum_{l=1}^{r}\sum_{m=1}^{r} P_{il}P_{im}\int_{-\infty}^{\infty}\frac{1}{\omega^4}S_{\ddot{u}_{Rl}\ddot{u}_{Rm}}(\omega)\,d\omega \tag{3.53}$$

3.2.6 Covariance of Pseudo-Static and Dynamic Element End Forces

Following the procedure described in Section 3.2.3, the covariance between the pseudo-static and dynamic element end forces can be shown to be

$$\mathrm{Cov}\,(s_i, f_i) = \sum_{l=1}^{r} \sum_{k=1}^{n} \sum_{m=1}^{r} P_{il} F_{ik} \Gamma_{mk} \int_{-\infty}^{\infty} \left(-\frac{1}{\omega^2}\right) H_k(\omega)\, S_{\ddot{u}_{Rl}\ddot{u}_{Rm}}(\omega)\, d\omega \tag{3.54}$$

3.3 Transient Response

The theory summarized in Sections 3.1 to 3.3 is valid for stationary seismic excitation. However, earthquake acceleration amplitudes are characterized by a finite build-up time, a period of uniform intensity and a period of decay. It follows that responses of quiescent systems to such excitation are non-stationary. For a single degree-of-freedom system with undamped circular natural frequency ω_n and damping ratio ξ, the rate at which the response grows to the stationary state depends on the value of $\xi\omega_n$ and the duration of strong shaking. However, for a multi-degree-of-freedom system, the rate at which the total response grows depends on $\xi_j\omega_j$ for each mode, and on how much the lower modes contribute to the overall response. If the lower modes with small $\xi_j\omega_j$ do not contribute significantly, then the total response may reach stationarity rather quickly. In this study of suspension bridge response, the first few modes have extremely low frequencies ω_j and therefore may not reach the stationary state within the earthquake duration. Therefore, it is of interest to study the transient response of suspension bridges, subjected to non-stationary seismic excitation.

In most earthquake engineering applications it is reasonable to represent the non-stationary excitation by an envelope-modulated stationary random process that may be expressed as a product of a stationary random process with a deterministic envelope modulating function as:

$$\ddot{u}(t) = e(t)\, z(t) \tag{3.55}$$

where $z(t)$ is a stationary random process, and $e(t)$ is a temporal modulating function.

The generalized displacement response for the j^{th} mode may be expressed as:

$$Y_j(t) = \int_0^t h_j(t-\tau)\, e(\tau)\, z(\tau)\, d\tau \tag{3.56}$$

where $h_j(t)$ is the impulse response function of the j^{th} mode. In frequency domain analysis, it is convenient to define a "time-dependent frequency response function" as

$$H_j(\omega, t) = \int_0^t h_j(t-\tau)\, e(\tau)\, e^{i\omega\tau} d\tau \tag{3.56}$$

The response variance at a given time t is evaluated by substituting the function $H_j(\omega, t)$ in place of the normal frequency response function $H_j(\omega)$ in the expressions obtained for the stationary response. However, it is very difficult to express $H_j(\omega, t)$ in closed form for arbitrary $e(t)$, and closed form expression have been derived only for a few functional forms of $e(t)$.

The purpose of this work is to study the effect of correlated support excitations, and not really to determine the absolute response variances. Thus the exact form used for $e(t)$ is not very crucial, and the use of a Heaviside modulating function is sufficient to assess the effect of transient responses.

For the Heaviside modulation, Lin (1963) derived the expression for $H_j(\omega, t)$ as

$$H_j(\omega, t) = H_j(\omega)\left[1 - e^{-\xi_j\omega_j t} e^{-i\omega t}\left(\cos\omega_{jd}t + \frac{(\xi_j\omega_j + i\omega)}{\omega_{jd}}\sin\omega_{jd}t\right)\right] \tag{3.57}$$

where $\omega_{jd} = \omega_j\sqrt{1-\xi_j^2}$, and $H_j(\omega)$ is shown in equation (3.32).

3.4 Ground Motion Model

A mathematical model for the acceleration cross spectrum of ground acceleration $S_{\ddot{u}_{Rl}\ddot{u}_{Rm}}(\omega)$, is needed for the random vibration analysis of structures.

The ground motion model proposed by Harichandran and Vanmarcke (1986), is used in this study. The model considers the spatial as well as the temporal variation of earthquake ground motion, and was based on the analysis of recordings made by the SMART-1 seismograph array in Lotung, Taiwan. In this model the cross spectral density function between the acceleration of two locations A and B is expressed as:

$$S_{\ddot{u}_A \ddot{u}_B} = S_{\ddot{u}}(\omega)\, \rho\left(\nu, \frac{\omega}{2\pi}\right) e^{\frac{-i\omega\nu}{V}} \tag{3.58}$$

where

$$\rho(\nu, f) = A e^{\frac{-2\nu}{\alpha\theta(f)}(1 - A + \alpha A)} + (1 - A)\, e^{\frac{-2\nu}{\theta(f)}(1 - A + \alpha A)} \tag{3.59}$$

$$\theta(f) = k\left[1 + \left(\frac{f}{f_o}\right)^b\right]^{-\frac{1}{2}} \tag{3.60}$$

and

ν = separation between locations A and B.

f = linear frequency.

V = apparent wave propagation velocity in the direction AB.

and $S_{\ddot{u}}(\omega)$ = point auto spectral density function of the ground acceleration.

A, α, k, f_o, and b are model parameters where typical values are shown in Table 3.1 (Harichandran 1991). The function $\rho(\nu, f)$ is known as the coherency function and equation (3.59) is one of the more suitable forms based on the analysis of events recorded by the SMART-1 array. In general the absolute value of coherency decreases with increasing frequency and increasing separation, as shown in Figure 3.1 for separations corresponding to the side and center span lengths of the Golden Gate bridge.

Table 3.1 : Ground Motion Model Parameter.

Model	Parameter	Ground Motion
Coherency function	ω_g	15.0
	β_g	0.55
	ω_f	3.0
	β_f	0.6
	S_o	0.1387
Double-filter autospectrum	A	0.636
	α	0.0186
	k	31200
	$f_o\,(Hz)$	1.51
	b	2.95

The functional form suggested by Clough and Penzien (1975) for the auto spectral density function is used in this study. This function is expressed as

$$S_{\ddot{u}}(\omega) = |H_1(\omega)|^2 |H_2(\omega)|^2 S_o \tag{3.61}$$

where $|H_1(\omega)|^2$ is the Kanai-Tajimi spectrum

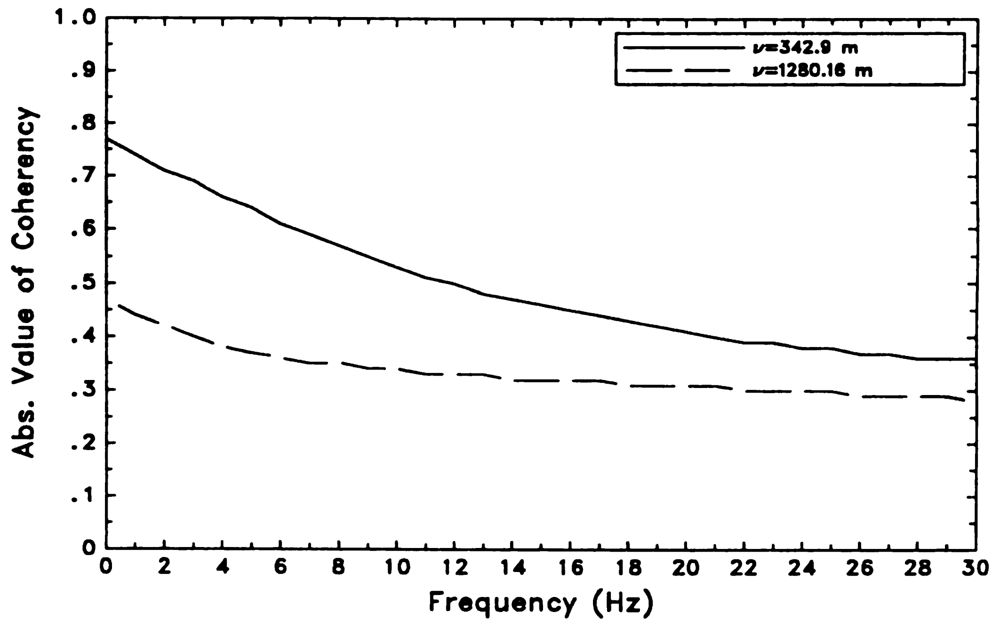

Figure 3.1 : Coherency function at two separations

$$|H_1(\omega)|^2 = \frac{(1 + 4\beta_g^2(\omega/\omega_g)^2)}{\left(1 - (\frac{\omega}{\omega_f})^2\right)^2 + 4\beta_f^2(\frac{\omega}{\omega_f})^2} \tag{3.62}$$

and

$$|H_2(\omega)|^2 = \frac{(\omega/\omega_f)^4}{\left(1 - (\frac{\omega}{\omega_f})^2\right)^2 + 4\beta_f^2(\frac{\omega}{\omega_f})^2} \tag{3.63}$$

in which the parameters ω_g, β_g, ω_f, and β_f, control the shape of the spectra, and S_o is an intensity parameter. These parameters can be estimated by fitting the function expressed in equation (3.61) to observed acceleration spectra. The auto spectral density function of the ground displacement is

$$S_u(\omega) = \frac{1}{\omega^4} S_{\ddot{u}}(\omega) \tag{3.64}$$

For studies requiring the spectrum of ground displacement, the Kanai-Tajimi spectrum becomes undefined as $\omega \rightarrow 0$ and the double-filter spectrum given by equation (3.61) overcomes this problem.

The double-filter spectrum was fitted to the artificial accelerogram of Type-B (Jennings, Housner, and Tsai, 1968). The Type-B accelerogram, is one of four types generated to model accelerograms corresponding to different earthquake magnitudes. Each of the artificial accelerogram is a section of a random process with a prescribed power spectral density, multiplied by an envelope function chosen to model the changing intensity at the beginning and end of real accelerograms. The Type-B motion has a duration of 50 seconds and is intended to model the shaking close to the fault in a magnitude 7 earthquake, similar to the El Centro earthquake of 1940 and the Taft, California, earthquake of 1952. The shape and intensity parameters of equations (3.59) to (3.61) were evaluated using a least squares fit to the spectrum estimated from an accelerogram. The band width of the smoothing window used for the spectral estimation was 0.5 Hz. The normalized autospectrum and the fitted model are plotted in Figure 3.2.

3.5 Computation Steps

A computer program was written to perform the analysis. The main segments of this program are summarized in the following steps:

1. The overall stiffness and consistent mass matrices were assembled from the element matrices using equations (2.38) and (2.39). These matrices are of order 48×48 for the side span and of 255×255 for the center span.
2. The partitioning of the overall mass and stiffness matrices were performed to obtain the $[K_{FF}]$, $[K_{FR}]$, $[M_{FF}]$, and $[M_{FR}]$, where the subscript F refers to free nodal displacements, while the subscript R denotes restrained displacements. The free

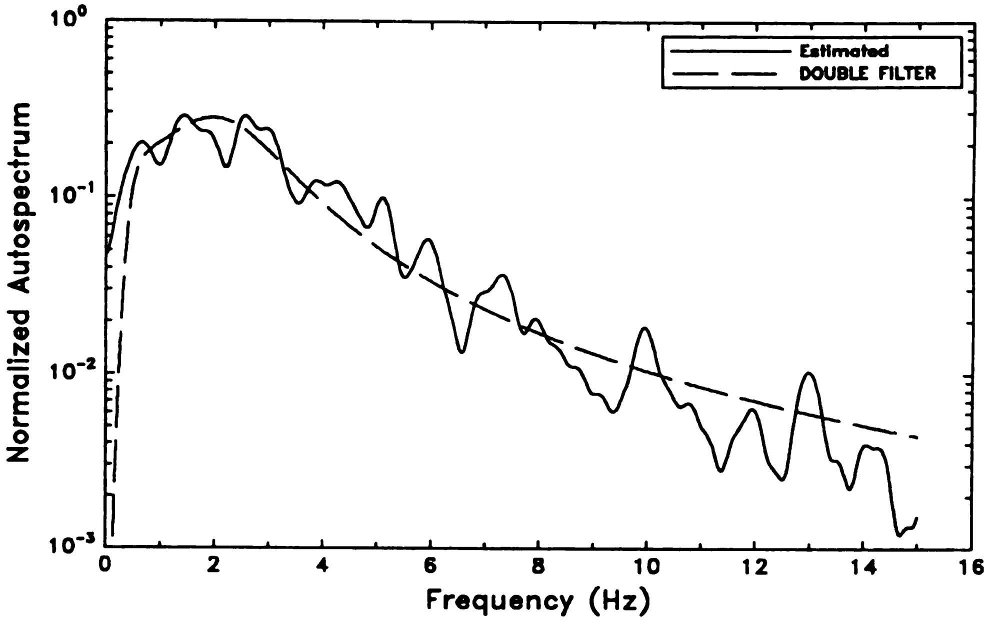

Figure 3.2 : Estimated and fitted autospectra for Type-B accelerogram

free matrices were of order 44 × 44 for the side span and of order 251 × 251 for the center span. The $[K_{FF}]$ and $[M_{FF}]$ matrices were banded and their half band width was equal to 6. Both $[M_{FF}]$ and $[K_{FF}]$ were positive definite symmetric matrices.

3. The matrix $[A]$ was established from the static displacements of the structure due to unit restrained displacements using equation (3.34). This matrix was of order 44 × 2 for the side span and of order 251 × 2 for the center span.

4. The generalized eigenvalue problem given by equation (3.9) was solved using the IMSL (1987) subroutine DGVCSP. This routine is designed to compute all of the

eigenvalues and eigenvectors of the real symmetric generalized eigenvalue problem, with symmetric positive definite $[M_{FF}]$. In this routine the Cholesky factorization $[M_{FF}] = [R]^T[R]$, with $[R]$ a triangular matrix, is used to convert equation (3.9) into the standard eigenvalue problem

$$([R]^{-T}[K_{FF}][R]^{-1})[R][\Psi] = [\mathrm{diag}(\omega^2)]([R][\Psi]) \tag{3.65}$$

The eigenvalues, $[\mathrm{diag}(\omega^2)]$ and eigenvectors $\{\bar{\psi}_i\}$ of $[R]^{-T}[K_{FF}][R]^{-1}$ are then computed. Equation (3.65) has the same eigenvalues as the original problem; and the eigenvectors of the original problem are found using $\{\psi_i\} = [R]^{-1}\{\bar{\psi}_i\}$. The eigenvectors are normalized such that a modified ∞-norm of each eigenvector is one.

The Cholosky factorization is computed by IMSL routine DLFTDS. The eigenvalues and eigenvectors of the real symmetric matrix $[R]^{-T}[K_{FF}][R]^{-1}$ are computesd as follow: first, accumulating orthogonal similarity transformations are used to reduce the matrix to an equivalent symmetric tridiagonal matrix; second, the implicit QL algorithm is used to compute the eigenvalues and eigenvectors of this tridiagonal matrix.

The performance index for the generalized real symmetric eigensystem of equation (3.9) is computed using IMSL routine DGPISP. In this routine a performance index η, is defined to be

$$\eta = \max_{1 \le j \le n} \frac{\| [K_{FF}]\{\psi_j\} - \omega_j^2 [M_{FF}]\{\psi_j\} \|_1}{\varepsilon(\|[K_{FF}]\|_1 + |\omega_j^2| \, \|[M_{FF}]\|_1) \, \|\{\psi_j\}\|_1} \tag{3.66}$$

where ε is the machine precision.

While the exact value of η is highly machine dependent, the performance of DEVCSF is considered excellent if $\eta < 1$ (which is the case for the side span

$\eta = 0.56$), good if $1 \le \eta \le 100$ (which is the case of the center span $\eta = 13.09$), and poor if $\eta > 100$.

5. Compute the participation factors matrix $[\Gamma]$ using equation (3.13).

6. Calculate the upper triangular part of the integration matrix of equation (3.33) and store the values in a one dimensional array of order $\frac{n(n+1)}{2}r^2$, where n is the number of modes considered and r is the number of nodal excitation points.

7. Calculate the integrals $\int_{-\infty}^{\infty} \frac{1}{\omega^4} S_{\ddot{u}_{Rl}\ddot{u}_{Rm}}(\omega)\, d\omega$ and store the values in a two dimensional $r \times r$ array.

8. Calculate the integrals $\int_{-\infty}^{\infty} \frac{1}{\omega^2} H_k(\omega)\, S_{\ddot{u}_{Rl}\ddot{u}_{Rm}}(\omega)\, d\omega$ and store the values in a three dimensional array of order $n \times r \times r$.

9. Calculate the dynamic and static displacement variances, and the covariances between dynamic and static responses using equations (3.31), (3.38), and (3.47), respectively.

10. Calculate the element end forces corresponding to the i$^{\text{th}}$ mode shape using equation (3.51), and collect the resulting element end forces into a matrix $[F]$ in which the F_{ij} element is the i$^{\text{th}}$ element end force corresponding to the j$^{\text{th}}$ mode shape.

11. Calculate the force responses (dynamic, static, and cross covariances) using equations (3.52), (3.53), and (3.54) respectively.

4. Numerical Results and Analysis

4.1 Free Vibration Analysis

The study of the Golden Gate Bridge was divided into two parts, the side span and the center span of the bridge. The side span of 1,125 feet length was subdivided into 15 elements, each of length 75 feet. The center span of 4,200 feet was subdivided into 84 elements each of length 50 feet (see Figure 2.3 and 2.4). All mode shapes and frequencies were extracted for the side and center spans using the IMSL library (see step 5 of section 3.5). A summarized description of the first eighteen frequencies and mode shapes of the side and center spans are presented in Table 4.1 and 4.2, respectively. The first nine mode shapes of the side span are shown in Figure 4.1, while the first eighteen mode shapes of the center span are shown in Figures 4.2 and 4.3.

It can be seen from Figure 4.1 that in the first two modes there is a coupled motion between the cables and the deck, the cables and the deck are moving in phase for the first mode, while in the second mode they are moving 180^0 out of phase. The first and second mode represent one fourth wave lateral motion of the cables and the deck, respectively. The third mode is a half-wave cable mode with hardly any participation from the deck, while the fifth mode is a half-wave deck mode with hardly any participation from the cables. The fourth mode represents a full-wave lateral motion of the cables. The smoothness of the higher mode shapes is degraded due to the coarseness of the discretization. For smoother shapes at higher frequencies one should consider increasing the number of elements per span length.

The first eighteen mode shapes of the center span are shown in Figures 4.2 and 4.3. Many of the modes reflect coupled lateral motion between the cables and the deck. Modes 1, 2, 5, and 7 are examples of in phase lateral motion between cables and deck, while modes

Table 4.1 : Golden Gate Bridge side span natural frequencies and periods of lateral vibration.

Mode #	Frequency (Hz)	Period (sec)	Primary contributer	Type of mode
1	0.3133	3.1918	deck & cables	symmetric
2	0.3435	2.9112	deck & cables	symmetric
3	0.6561	1.5242	cables	anti-symm.
4	0.9841	1.0162	cables	symmetric
5	1.2450	0.8032	deck	anti-symm.
6	1.3235	0.7556	cables	anti-symm.
7	1.6769	0.5963	cables	symmetric
8	2.0484	0.4882	cables	anti-symm.
9	2.4404	0.4098	cables	symmetric
10	2.7965	0.3576	deck	symmetric
11	2.8546	0.3503	cables	anti-symm.
12	3.2890	0.3040	cables	symmetric
13	3.7368	0.2676	cables	anti-symm.
14	4.1837	0.2390	cables	symmetric
15	4.6034	0.2172	cables	anti-symm.
16	4.9564	0.2018	cables	symmetric
17	4.9711	0.2012	deck	anti-symm.
18	5.1953	0.1925	cables	anti-symm.

Table 4.2 : Golden Gate Bridge center span natural frequencies and periods of lateral vibration.

Mode #	Frequency (Hz)	Period (sec)	Primary contributer	Type of mode
1	0.0480	20.8514	deck & cables	symmetric
2	0.1079	9.2708	deck & cables	anti-symm.
3	0.1985	5.0387	deck & cables	symmetric
4	0.2189	4.5676	cables	anti-symm.
5	0.2238	4.4681	deck & cables	symmetric
6	0.3249	3.0775	cables	symmetric
7	0.3537	2.8273	deck & cables	anti-symm.
8	0.3910	2.5577	deck & cables	anti-symm.
9	0.4548	2.1986	cables	symmetric
10	0.5357	1.8667	cables	anti-symm.
11	0.5732	1.7447	deck	symmetric
12	0.6205	1.6115	cables	symmetric
13	0.7026	1.4233	cables	anti-symm.
14	0.7877	1.2695	cables	symmetric
15	0.8184	1.2220	deck	anti-symm.
16	0.8732	1.1452	cables	anti-symm.
17	0.9590	1.0427	cables	symmetric
18	1.0455	0.9564	cables	anti-symm.

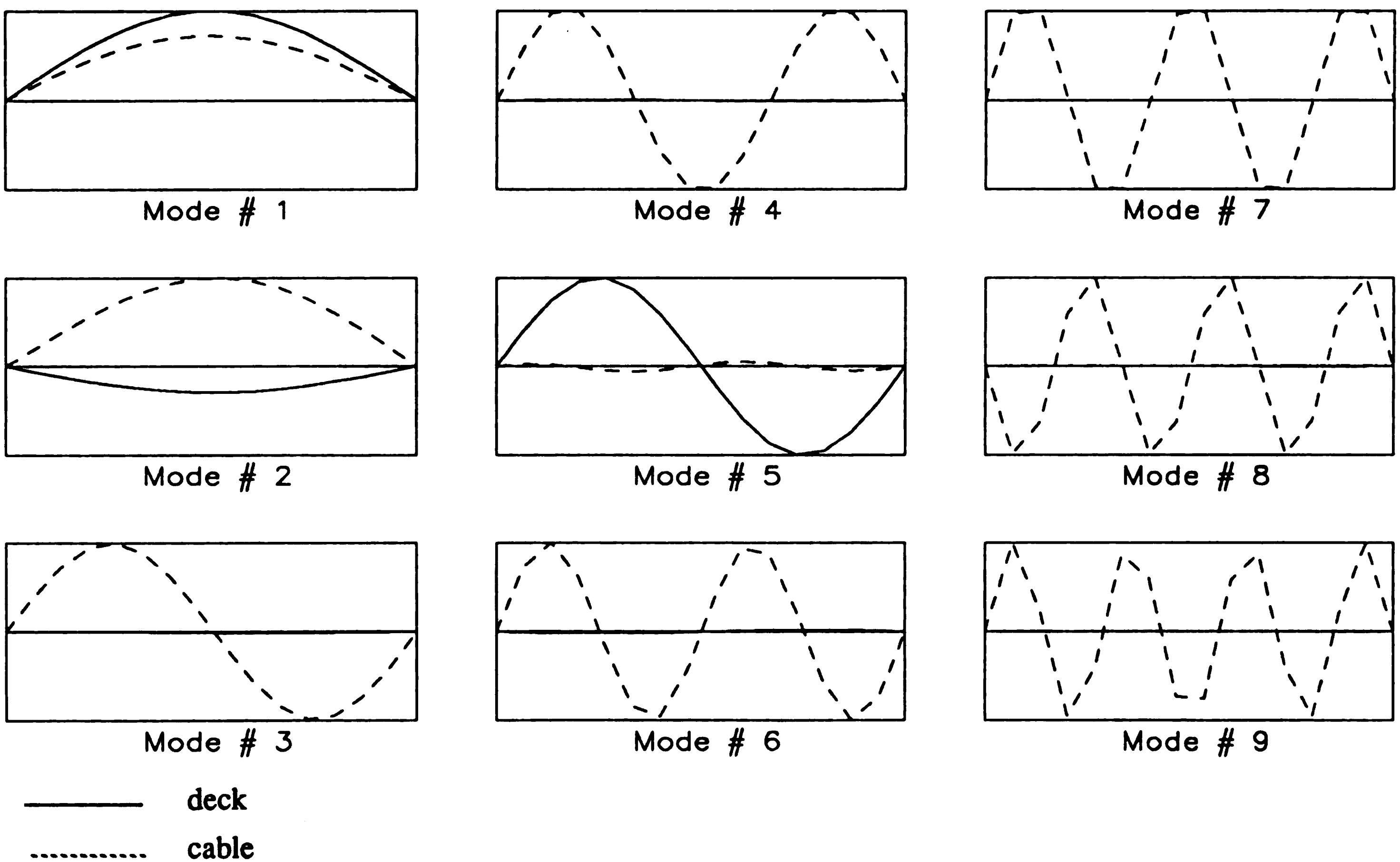

Figure 4.1 : First nine mode shapes of the bridge side span

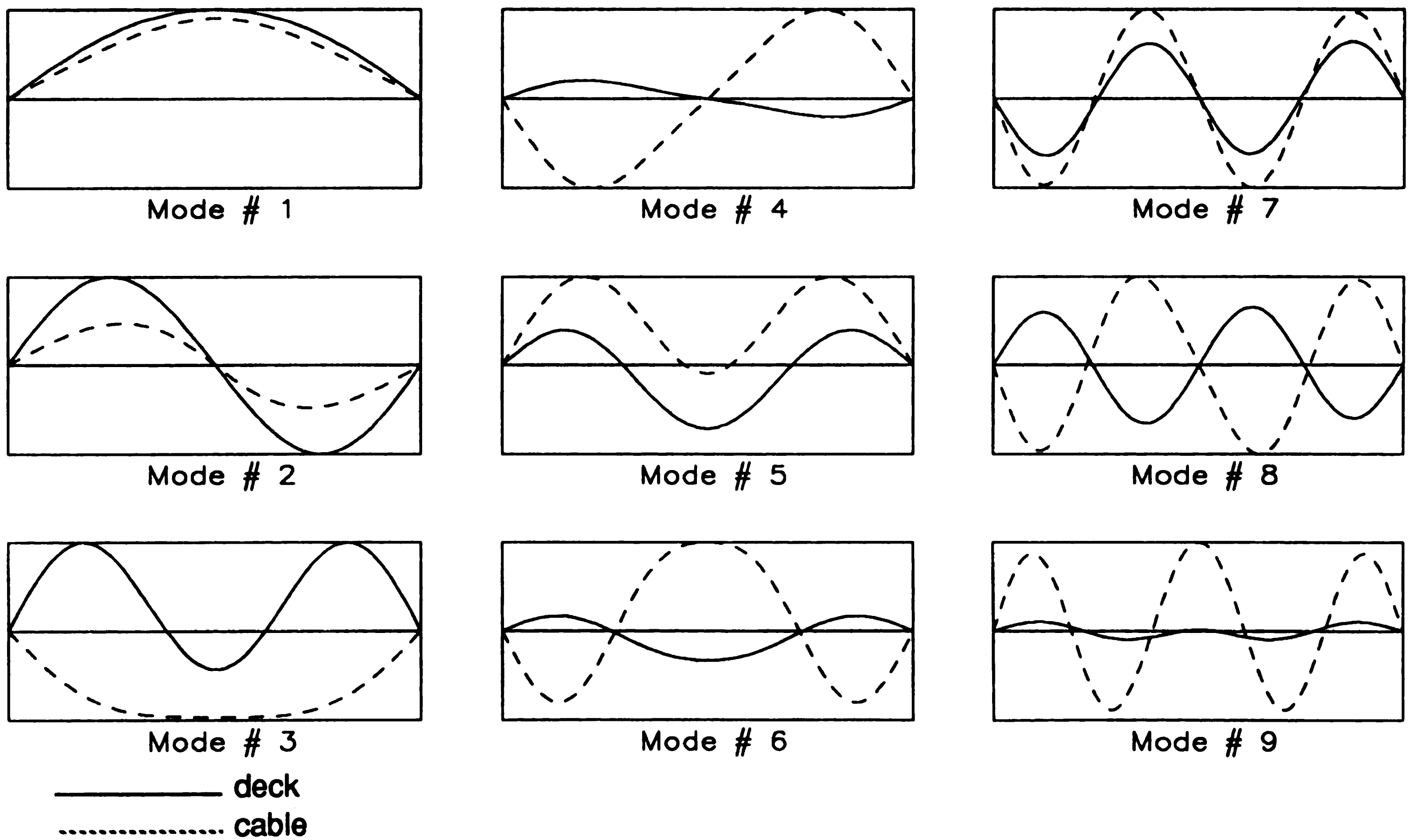

Figure 4.2 : First set of the center span mode shapes

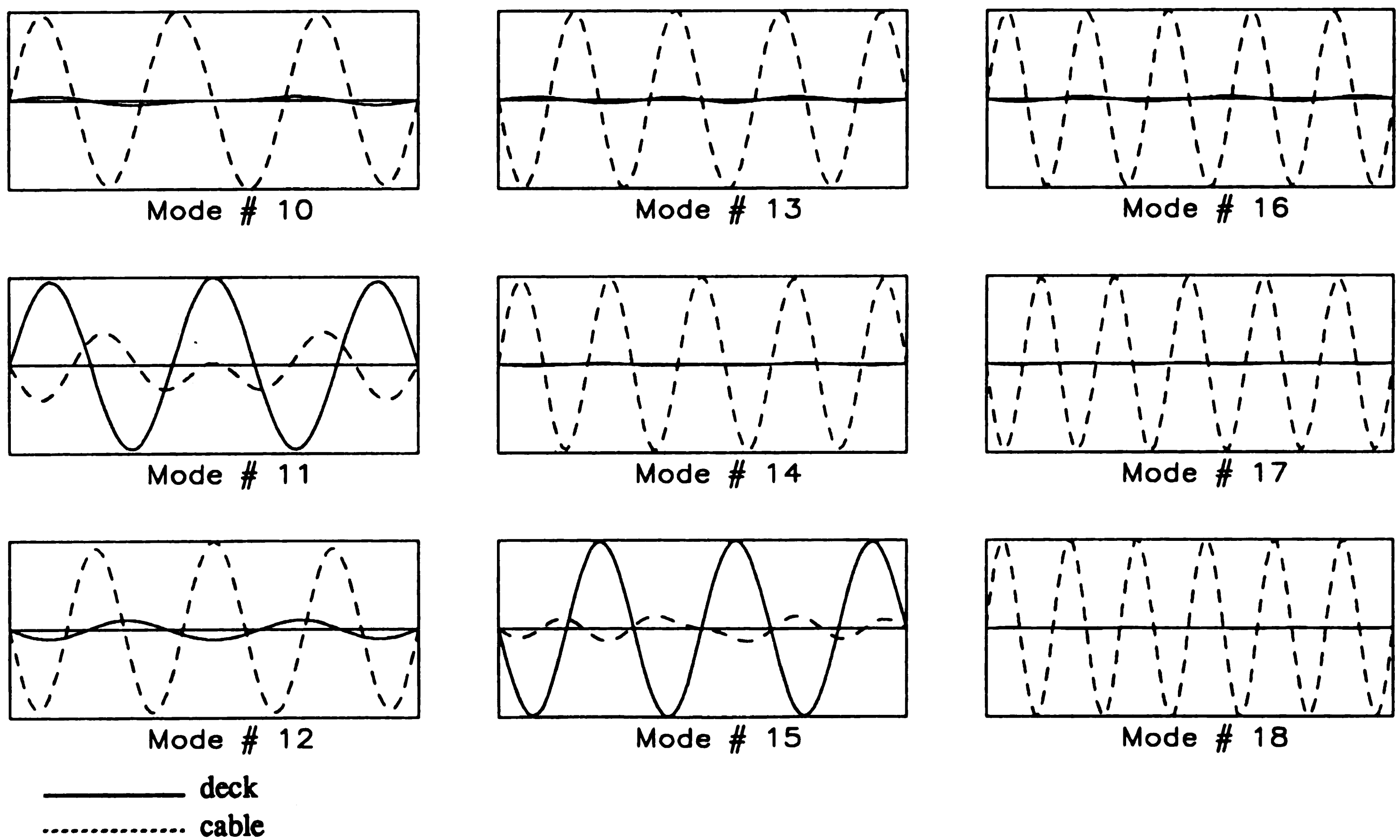

Figure 4.3 : Second set of the bridge center span mode shapes

3, 6, and 8 are examples of 180° out of phase between cables and deck. The first mode represents one fourth wave lateral motion of the cables and deck with a period of 20.85 seconds, while the second represents one half wave lateral motion of the cables and deck with a period of 9.27 seconds. A full-wave lateral motion is seen in the fifth mode. Relatively smooth mode shapes are achieved for high frequencies as a result of the fine discretization.

4.2 Ground Motion Models

The following three specialized ground motion models were considered in studying the response of the side and center spans of the Golden Gate bridge to seismic support excitation:

1. The most general form which includes both the wave propagation effect as well as correlation effects, as expressed in equation (3.58).
2. Fully correlated ground motion (which is commonly used in practice) for which $S_{\ddot{u}_A \ddot{u}_B}(\omega) = S_{\ddot{u}}(\omega)$ (i.e., $\rho(\nu, \omega) = 1$ and $V \to \infty$ in equation (3.58)).
3. Wave propagation without coherency loss for which $\rho(\nu, \omega) = 1$ and V is finite in equation (3.58).

4.3 Side Span

The response variances are normalized by dividing by the maximum total response along the span.

4.3.1 Side Span Response Components

As discussed earlier in Chapter 3, the variance of the total response comprises of three components: the variance of the dynamic response, the variance of the pseudo-static response, and the covariance between the pseudo-static and dynamic responses. It is instructive to deduce which component contributes most to the total response.

The first natural frequency of the side span is 0.31 Hz which is indicative of a flexible structure. The contribution of the three components to the total lateral displacement response along the cables and deck are presented in Figures 4.4 and 4.5, respectively for the general ground motion model. All response quantities are normalized by dividing by the maximum total response along the span. It is clear from these figures that the dynamic component dominates the total response. Examining the components of the total lateral displacement response at node 7 (which is 300 feet from the left support) reveals that the dynamic component contributes 100.04%, the static component contributes 4.1%, and the covariance contributes -4.2%. In a similar manner for node 15 (which is 600 feet from the left support), the dynamic component contributes 101.12%, the static component contributes 2.2%, and the covariance contributes -3.3%.

The moment and shear responses are dominated completely by the dynamic component and the effect of pseudo-static and covariance terms are negligible (see Figures 4.6 and 4.7).

4.3.2 Lateral Response of the Side Span

A comparison of the side span responses due to the three ground motion models are presented in Figures 4.8 to 4.11. The responses in each figure are normalized by dividing by the maximum response along the span due to the general ground motion model. Figures 4.8 and 4.9 represent the total lateral displacement response of the side span cables and deck, respectively, and show that the response due to fully correlated ground motion is the highest, while that due to the general ground motion model is the lowest. The responses of node 8 (on the cable) due to fully correlated and propagating excitations are essentially the same, and are 6.5% larger than the response due to general excitation. At node, 16 the response due to fully correlated and propagating excitations are 17.12% and 10.91% larger than that due to general excitation. The responses of node 7 (on the deck) due to fully correlated and propagating excitations are 13.67% and 10.41% larger than that due to general excitation. At node 15, the responses due to fully correlated and propagating excitaions are 16.87% and 11.21% larger than that due to general excitation.

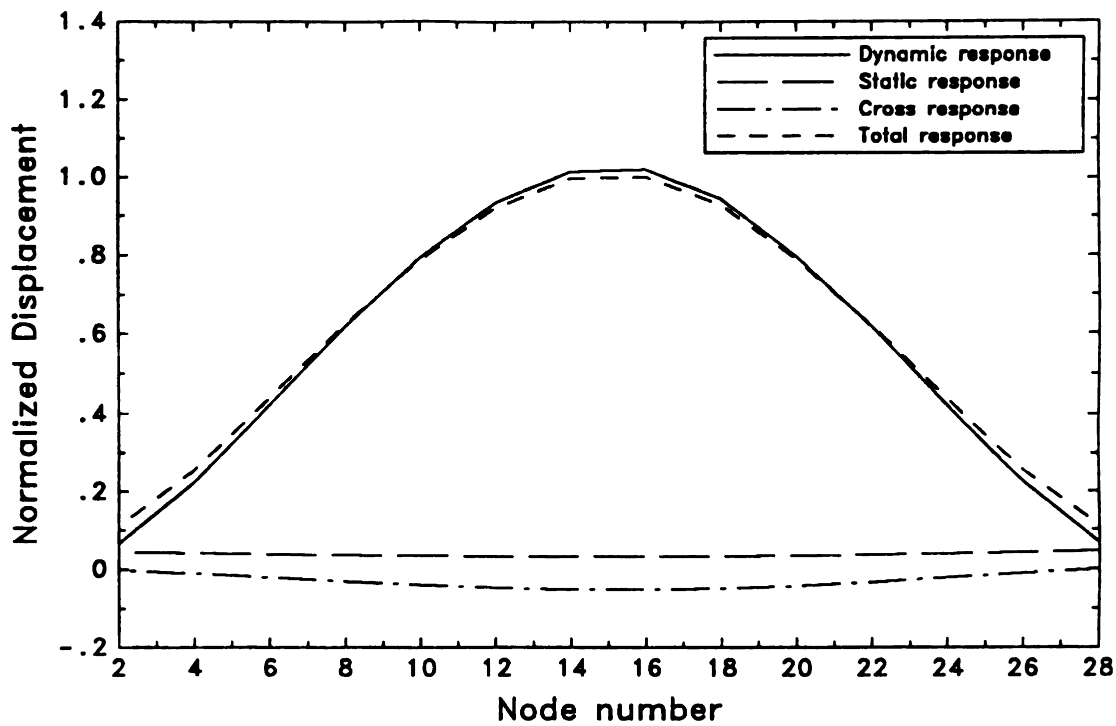

Figure 4.4 : Variation of normalized displacement variances of the side span cables

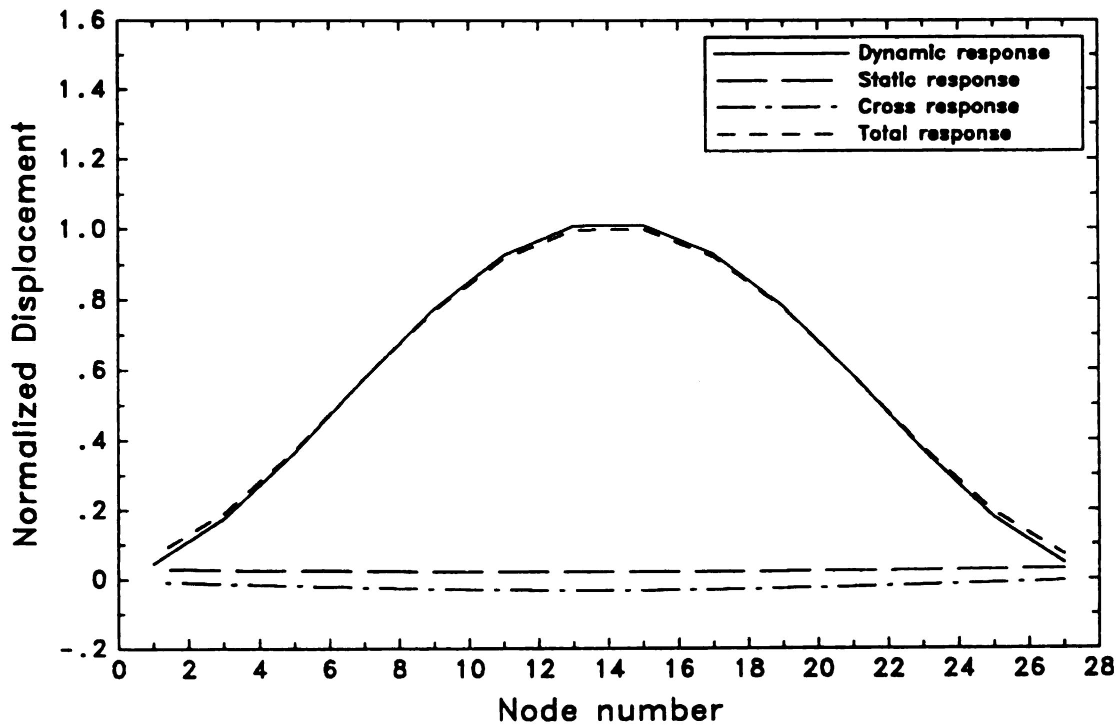

Figure 4.5 : Variation of normalized displacement variances of the side span deck

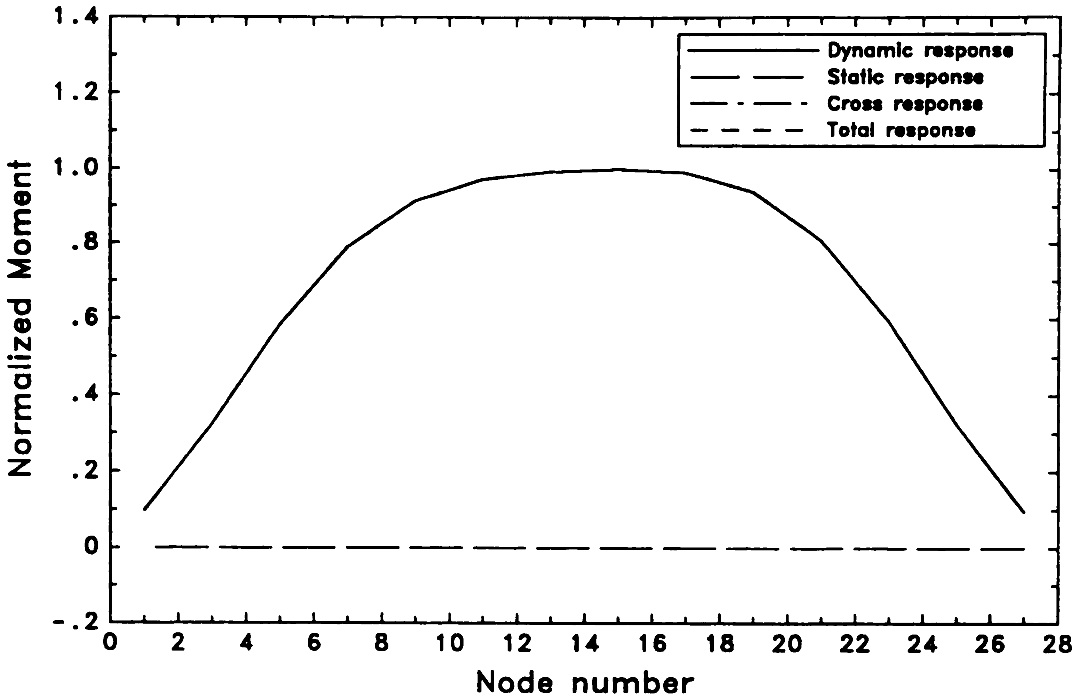

Figure 4.6 : Variation of normalized moment variances of the side span deck

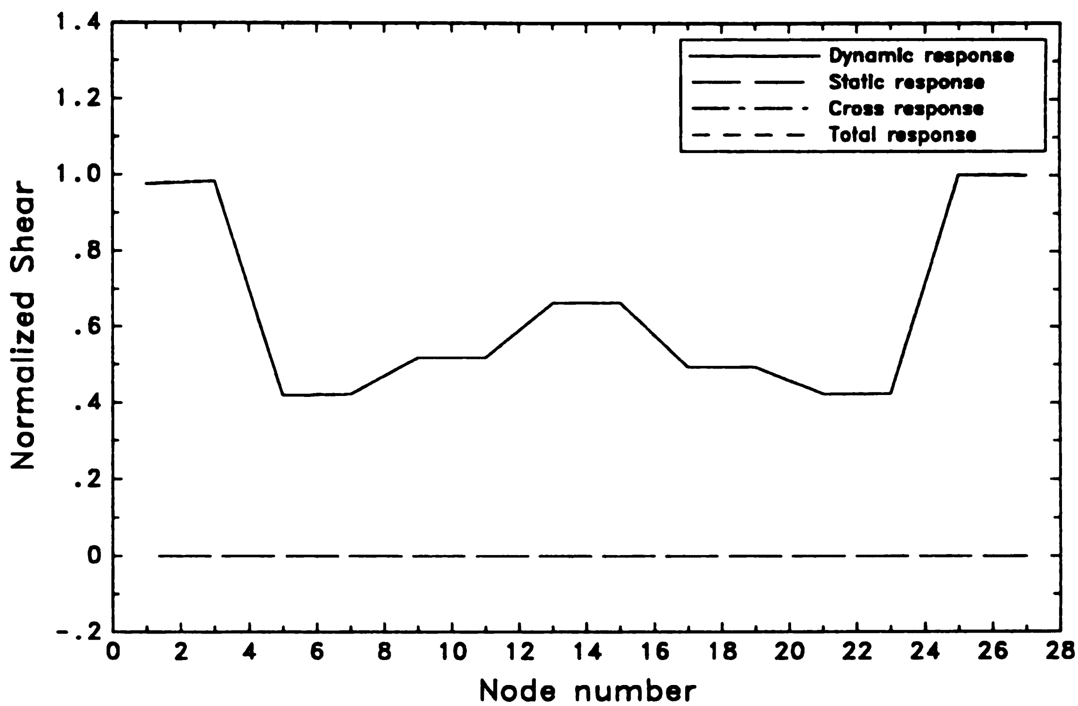

Figure 4.7 : Variation of normalized shear variances of the side span deck

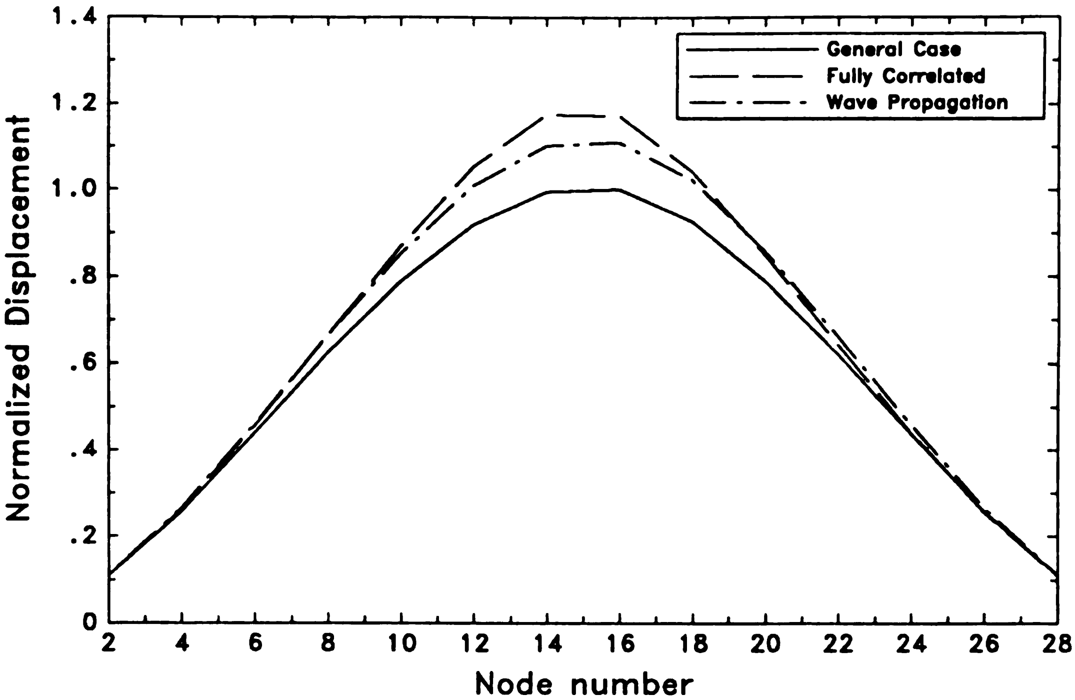

Figure 4.8 : Normalized displacement variances of the side span cables due to three ground motion models

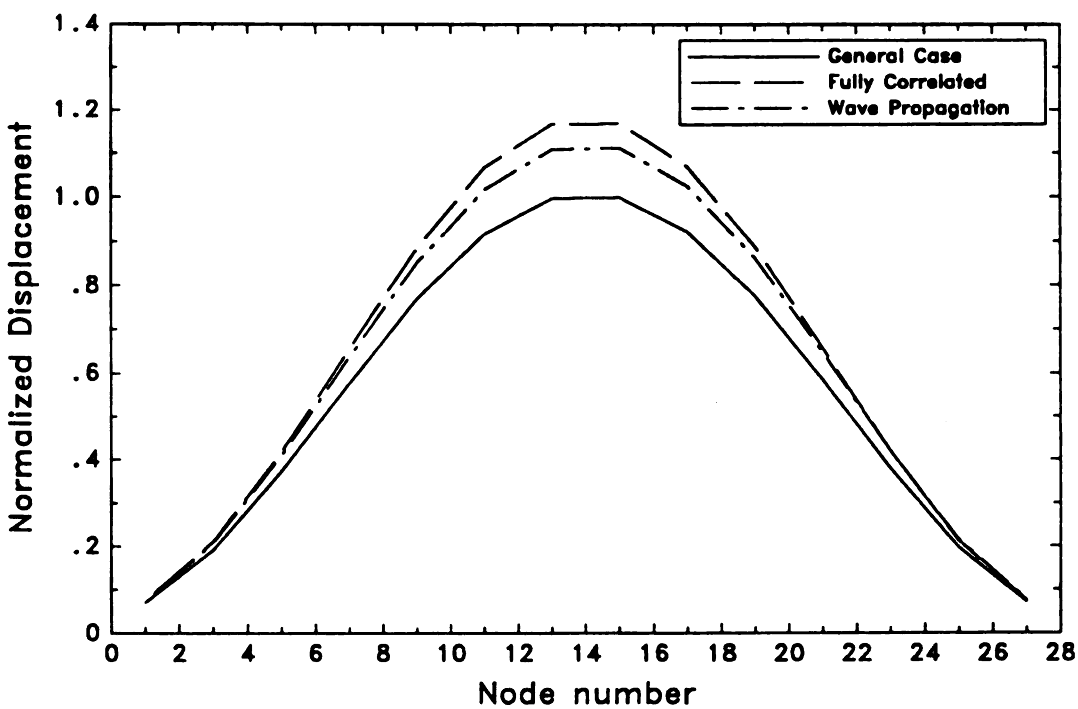

Figure 4.9 : Normalized displacement variances of the side span deck due to three ground motion models

The deck bending moment response due to the three ground motion models are presented in Figure 4.10. The maximum moment response for all three ground motion models occurs at the midspan. While the moments due to fully correlated excitation are greater than those due to general excitation near the midspan, the trend is reversed near the quarter spans. The moment response at node 7 due to fully correlated excitation is 17.4% lower than that due to general excitation.

The lateral shear responses of the side span deck due to the three ground motion models are presented in Figure 4.11. The figure indicates that the shear response due to fully correlated excitation underestimate the response due to general excitation by about 20% at the supports; overestimates the response by about 40% at the quarter span locations; and gives zero shear at the midspan. The rather unexpected behavior at midspan where the shear response drops to zero for fully correlated excitation can be explained by examining the modal contributions. Figure 4.12 shows the relative contributions of the dynamic modal covariances $F_{ij}F_{ik}I_{jk}$ to the total dynamic variance (see equations 3.33 and 3.52) for the first 23 modes, due to general excitation. Since the modal covariances are symmetric, i.e., $F_{ij}F_{ik}I_{jk} = F_{ik}F_{ij}I_{kj}$, the off diagonal elements that are shown, are twice the value of the corresponding covariance (i.e., the ij^{th} value shown is the relative contribution of $2F_{ij}F_{ik}I_{jk}$ to the overall dynamic variance). Figure 4.12 indicates that mode 5 contributes about 95% of the total dynamic shear response, while mode 17 contributes 4% to give a total contribution of 99%. The fully correlated excitation does not excite either mode 5 or mode 17 since they are anti-symmetric modes (see Table 4.1).

4.3.3 Effect of Apparent Wave Velocity

By choosing different apparent wave velocities in equation (3.58), a study was conducted to examine its effect on the side span response due to the general excitation. Figures 4.13 and 4.14 represent the effect of the apparent wave velocity on the displacement response of the cables and deck. It is found that increasing the lateral wave velocity from

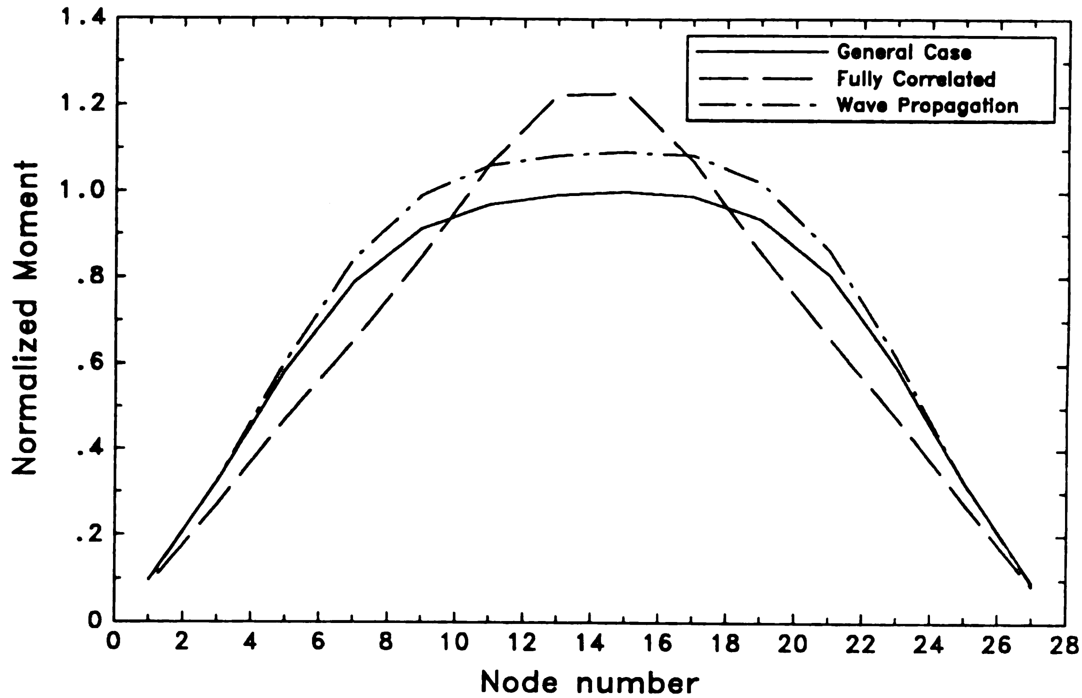

Figure 4.10 : Normalized moment variances of the side span deck due to three ground motion models

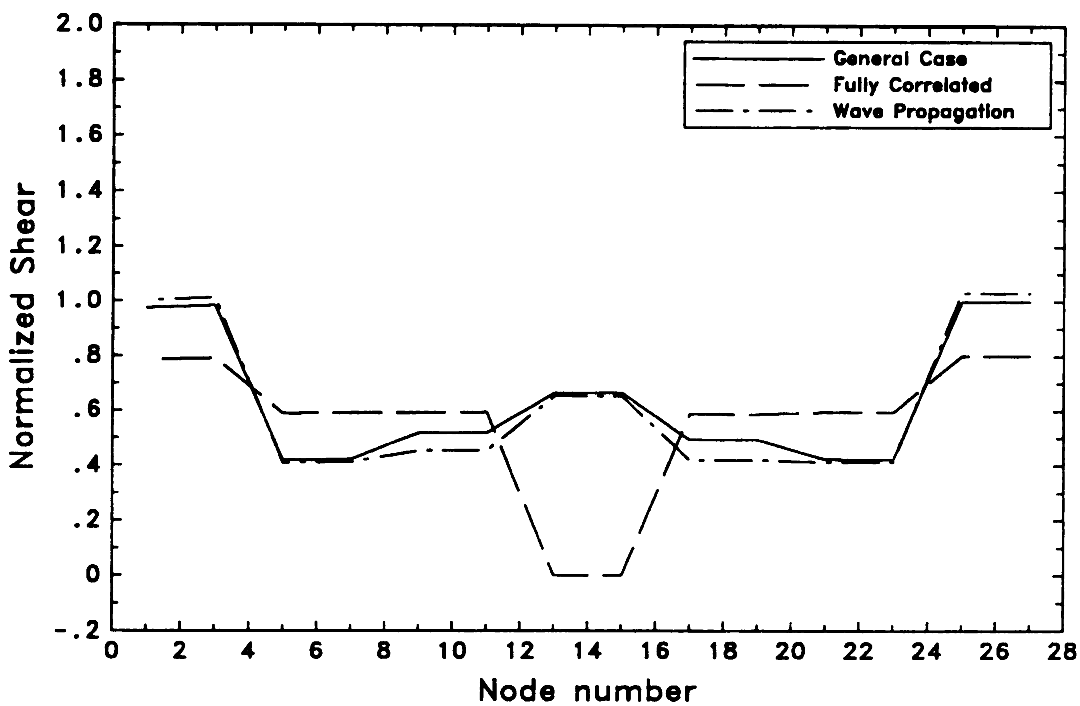

Figure 4.11 : Normalized shear variances of the side span deck due to three ground motion models

1	.000																						
2	.000	.000																					
3	.000	.000	.000																				
4	.000	.000	.000	0.000																			
5	.000	.000	.000	**-.001**	**0.949**																		
6	.000	.000	.000	0.000	**-.005**	.000																	
7	.000	.000	.000	0.000	0.000	.000	.000																
8	.000	.000	.000	0.000	0.000	.000	.000	.000															
9	.000	.000	.000	0.000	0.000	.000	.000	.000	.000														
10	.000	.000	.000	0.000	0.000	.000	.000	.000	.000	.00													
11	.000	.000	.000	0.000	0.000	.000	.000	.000	.000	.00	.000												
12	.000	.000	.000	0.000	0.000	.000	.000	.000	.000	.00	.000	.00											
13	.000	.000	.000	0.000	0.000	.000	.000	.000	.000	.00	.000	.00	.000										
14	.000	.000	.000	0.000	0.000	.000	.000	.000	.000	.00	.000	.00	.000	.000									
15	.000	.000	.000	0.000	0.000	.000	.000	.000	.000	.00	.000	.00	.000	.000	.00								
16	.000	.000	.000	0.000	0.000	.000	.000	.000	.000	.00	.000	.00	.000	.000	.00	.000							
17	.000	.000	.000	0.000	**0.019**	.000	.000	.000	.000	.00	.000	.00	.000	.000	.00	.000	**0.042**						
18	.000	.000	.000	0.000	0.000	.000	.000	.000	.000	.00	.000	.00	.000	.000	.00	.000	0.000	.000					
19	.000	.000	.000	0.000	0.000	.000	.000	.000	.000	.00	.000	.00	.000	.000	.00	.000	0.000	.000	.000				
20	.000	.000	.000	0.000	**-.007**	.000	.000	.000	.000	.00	.000	.00	.000	.000	.00	.000	**-.006**	.000	.000	**0.005**			
21	.000	.000	.000	0.000	0.000	.000	.000	.000	.000	.00	.000	.00	.000	.000	.00	.000	0.000	.000	.000	0.000	.000		
22	.000	.000	.000	0.000	**0.004**	.000	.000	.000	.000	.00	.000	.00	.000	.000	.00	.000	**0.003**	.000	.000	**-.001**	.000	**.001**	
23	.000	.000	.000	0.000	0.000	.000	.000	.000	.000	.00	.000	.00	.000	.000	.00	.000	0.000	.000	.000	0.000	.000	.000	.000
	1	**2**	**3**	**4**	**5**	**6**	**7**	**8**	**9**	**10**	**11**	**12**	**13**	**14**	**15**	**16**	**17**	**18**	**19**	**20**	**21**	**22**	**23**

Figure 4.12 : Relative modal contributions to the dynamic deck shear response - Node 15

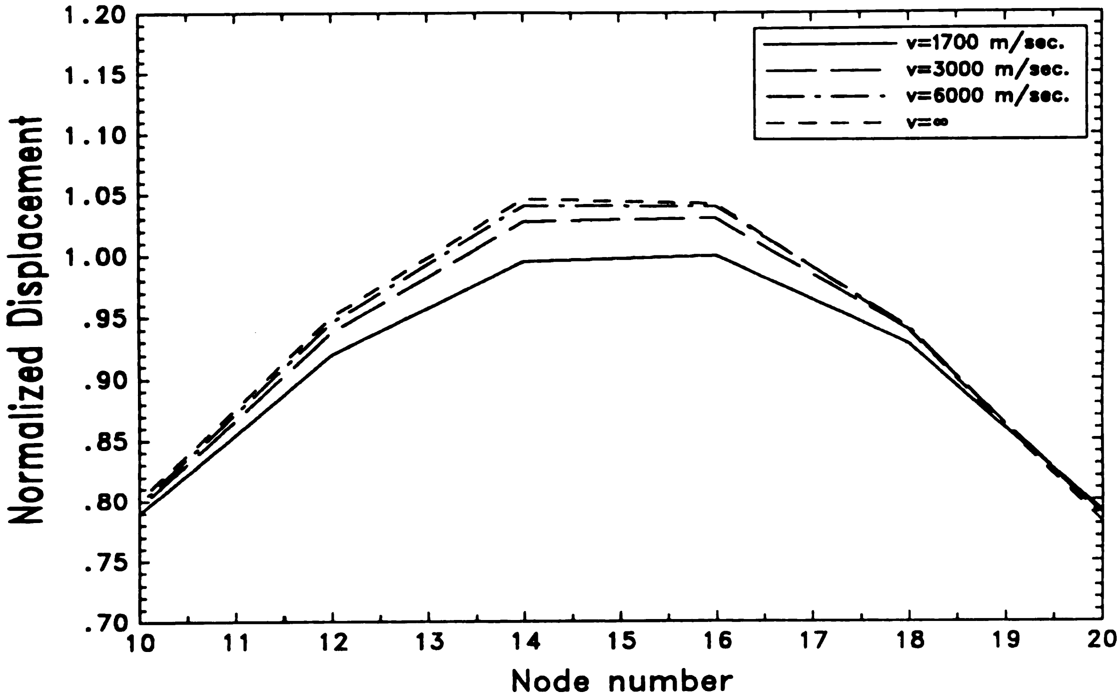

Figure 4.13 : Effect of apparent wave velocity on the side span cable displacement

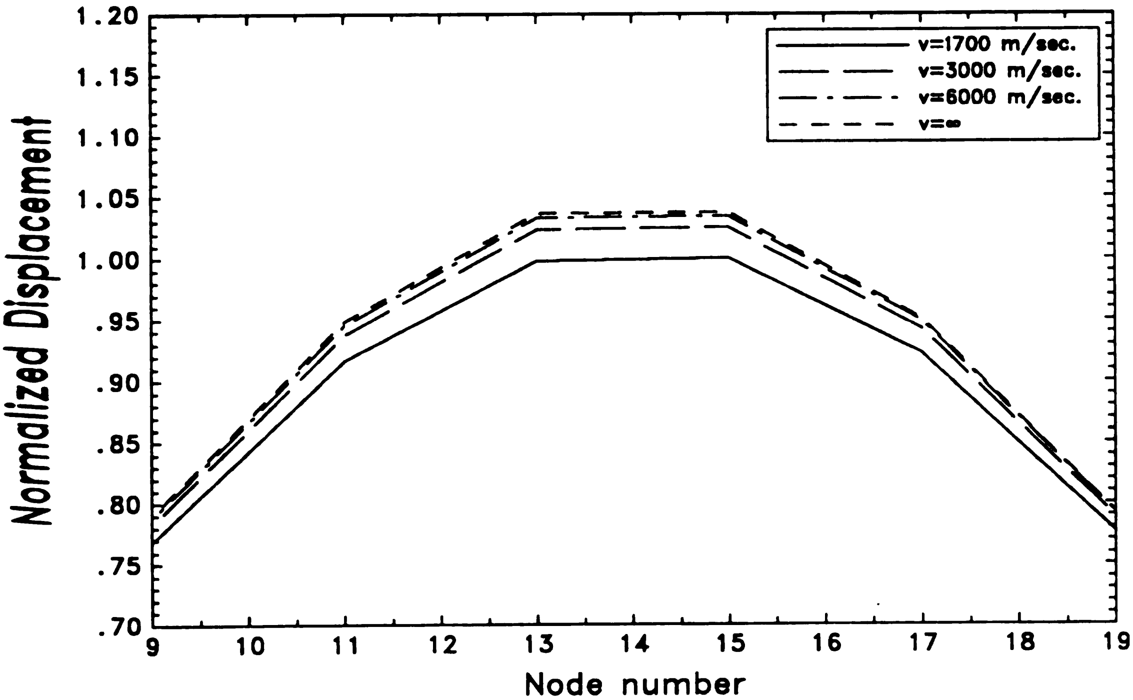

Figure 4.14 : Effect of apparent wave velocity on the side span deck displacement

1,700 m/sec to ∞ increases the cable displacement response by about 5.0% at midspan and the deck displacement response by about 4.0% at midspan.

The effect of the apparent wave velocity on the moment response of the deck is presented in Figure 4.15. It can be seen that the moment response at midspan increases as the apparent wave velocity is increased, while in the moment response near the quarter span (node 9) decreases as the apparent wave velocity is increased.

The effect of apparent wave velocity on the shear response of the deck is presented in Figure 4.16. The shear response at midspan (node 15) and near supports (nodes 3 and 27) decreases as the apparent wave velocity increases, while the shear response near the quarter span (node 7) increases as the velocity increases.

4.3.4 Modal Contributions

The dynamic response variances are composed of individual modal response variances and covariances between pairs of modal responses as indicated in equations (3.31) and (3.33). The relative modal contributions at nodes 7 and 15 in the deck located at (300 feet and 600 feet from left support, respectively), are presented in Figures 4.17 to 4.20 for the displacement and moment responses. Figures 4.17 and 4.18 reveal that modes 1, 2, and 5 contribute most to the lateral displacement. Mode 1 contributes 99.1% and 101.4% to the dynamic response at nodes 7 and 15, respectively. Only a very few of the off diagonal modal covariances have a noticeable contribution at these nodes. Figures 4.19 and 4.20 show that modes 1, 2, 5, 10, and 19 contribute most to the total dynamic moment response at nodes 7 and 15 with their total contribution being 102.4% for node 7 and 101% for node 15. It is clear that the contribution of mode 1 to the moment response of node 7 is less than that of node 15. The modal covariances participate more to the moment response than for the displacement response. A comparison between the displacement response and the moment force response indicates that the number of modes required to compute the moment response is higher than that required for the displacement response.

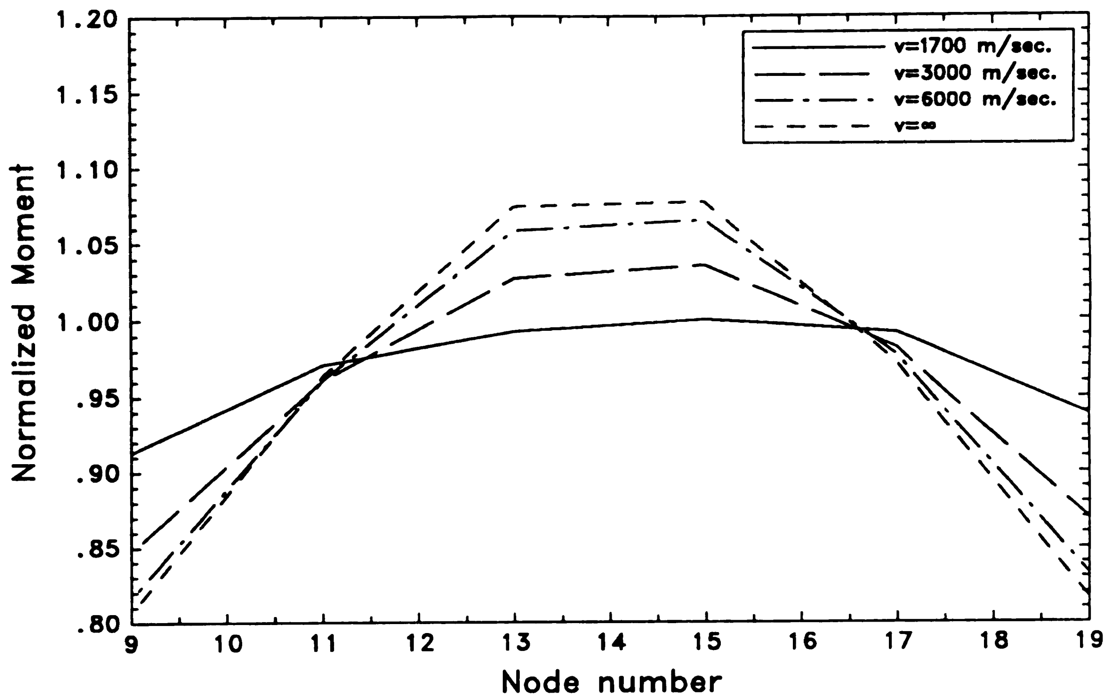

Figure 4.15 : Effect of apparent wave velocity on the side span deck moment

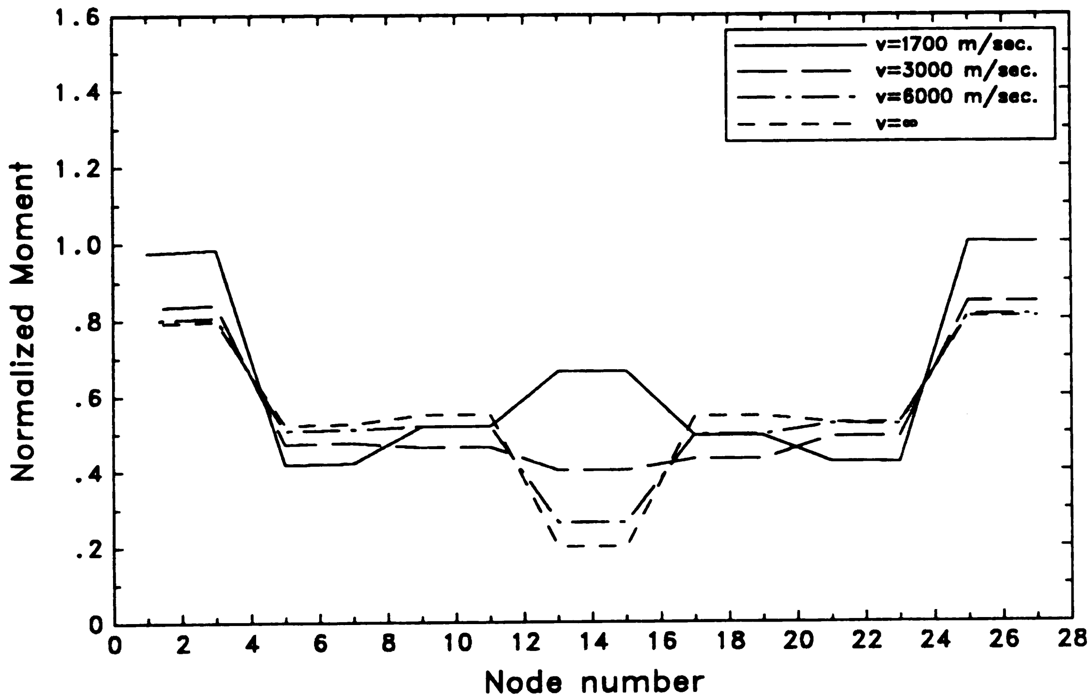

Figure 4.16 : Effect of apparent wave velocity on the side span deck shear

1	0.991																						
2	-.020	.004																					
3	0.000	.000	.000																				
4	0.000	.000	.000	.000																			
5	-.004	.000	.000	.000	.029																		
6	0.000	.000	.000	.000	.000	.000																	
7	0.000	.000	.000	.000	.000	.000	.000																
8	0.000	.000	.000	.000	.000	.000	.000	.000															
9	0.000	.000	.000	.000	.000	.000	.000	.000	.000														
10	-.001	.000	.000	.000	.000	.000	.000	.000	.000	.000													
11	0.000	.000	.000	.000	.000	.000	.000	.000	.000	.000	.000												
12	0.000	.000	.000	.000	.000	.000	.000	.000	.000	.000	.000	.000											
13	0.000	.000	.000	.000	.000	.000	.000	.000	.000	.000	.000	.000	.000										
14	0.000	.000	.000	.000	.000	.000	.000	.000	.000	.000	.000	.000	.000	.000									
15	0.000	.000	.000	.000	.000	.000	.000	.000	.000	.000	.000	.000	.000	.000	.000								
16	0.000	.000	.000	.000	.000	.000	.000	.000	.000	.000	.000	.000	.000	.000	.000	.000							
17	0.000	.000	.000	.000	.000	.000	.000	.000	.000	.000	.000	.000	.000	.000	.000	.000	.000						
18	0.000	.000	.000	.000	.000	.000	.000	.000	.000	.000	.000	.000	.000	.000	.000	.000	.000	.000					
19	0.000	.000	.000	.000	.000	.000	.000	.000	.000	.000	.000	.000	.000	.000	.000	.000	.000	.000	.000				
20	0.000	.000	.000	.000	.000	.000	.000	.000	.000	.000	.000	.000	.000	.000	.000	.000	.000	.000	.000	.000			
21	0.000	.000	.000	.000	.000	.000	.000	.000	.000	.000	.000	.000	.000	.000	.000	.000	.000	.000	.000	.000	.000		
22	0.000	.000	.000	.000	.000	.000	.000	.000	.000	.000	.000	.000	.000	.000	.000	.000	.000	.000	.000	.000	.000	.000	
23	0.000	.000	.000	.000	.000	.000	.000	.000	.000	.000	.000	.000	.000	.000	.000	.000	.000	.000	.000	.000	.000	.000	.000
	1	2	3	4	5	6	7	8	9	10	11	12	13	14	15	16	17	18	19	20	21	22	23

Figure 4.17 : Relative modal contributions to the dynamic deck displacement response - Node 7

	1	2	3	4	5	6	7	8	9	10	11	12	13	14	15	16	17	18	19	20	21	22	23
1	**1.014**																						
2	**-.021**	**.004**																					
3	0.000	.000	.000																				
4	0.000	.000	.000	.000																			
5	**0.001**	.000	.000	.000	**.001**																		
6	0.000	.000	.000	.000	.000	.000																	
7	0.000	.000	.000	.000	.000	.000	.000																
8	0.000	.000	.000	.000	.000	.000	.000	.000															
9	0.000	.000	.000	.000	.000	.000	.000	.000	.000														
10	**0.001**	.000	.000	.000	.000	.000	.000	.000	.000	.000													
11	0.000	.000	.000	.000	.000	.000	.000	.000	.000	.000	.000												
12	0.000	.000	.000	.000	.000	.000	.000	.000	.000	.000	.000	.000											
13	0.000	.000	.000	.000	.000	.000	.000	.000	.000	.000	.000	.000	.000										
14	0.000	.000	.000	.000	.000	.000	.000	.000	.000	.000	.000	.000	.000	.000									
15	0.000	.000	.000	.000	.000	.000	.000	.000	.000	.000	.000	.000	.000	.000	.000								
16	0.000	.000	.000	.000	.000	.000	.000	.000	.000	.000	.000	.000	.000	.000	.000	.000							
17	0.000	.000	.000	.000	.000	.000	.000	.000	.000	.000	.000	.000	.000	.000	.000	.000	.000						
18	0.000	.000	.000	.000	.000	.000	.000	.000	.000	.000	.000	.000	.000	.000	.000	.000	.000	.000					
19	0.000	.000	.000	.000	.000	.000	.000	.000	.000	.000	.000	.000	.000	.000	.000	.000	.000	.000	.000				
20	0.000	.000	.000	.000	.000	.000	.000	.000	.000	.000	.000	.000	.000	.000	.000	.000	.000	.000	.000	.000			
21	0.000	.000	.000	.000	.000	.000	.000	.000	.000	.000	.000	.000	.000	.000	.000	.000	.000	.000	.000	.000	.000		
22	0.000	.000	.000	.000	.000	.000	.000	.000	.000	.000	.000	.000	.000	.000	.000	.000	.000	.000	.000	.000	.000	.000	
23	0.000	.000	.000	.000	.000	.000	.000	.000	.000	.000	.000	.000	.000	.000	.000	.000	.000	.000	.000	.000	.000	.000	.000

Figure 4.18 : Relative modal contributions to the dynamic deck displacement response - Node 15

	1	2	3	4	5	6	7	8	9	10	11	12	13	14	15	16	17	18	19	20	21	22	23
1	**0.680**																						
2	**-.013**	**.002**																					
3	0.000	.000	.000																				
4	0.000	.000	.000	0.000																			
5	**-.010**	**.001**	.000	**-.001**	**0.330**																		
6	0.000	.000	.000	0.000	**-.001**	.000																	
7	0.000	.000	.000	0.000	0.000	.000	.000																
8	0.000	.000	.000	0.000	0.000	.000	.000	.000															
9	0.000	.000	.000	0.000	0.000	.000	.000	.000	.000														
10	**-.005**	.000	.000	0.000	**0.004**	.000	.000	.000	.000	**.011**													
11	0.000	.000	.000	0.000	0.000	.000	.000	.000	.000	.000	.000												
12	0.000	.000	.000	0.000	0.000	.000	.000	.000	.000	.000	.000	.000											
13	0.000	.000	.000	0.000	0.000	.000	.000	.000	.000	.000	.000	.000	.000										
14	0.000	.000	.000	0.000	0.000	.000	.000	.000	.000	.000	.000	.000	.000	.000									
15	0.000	.000	.000	0.000	0.000	.000	.000	.000	.000	.000	.000	.000	.000	.000	.000								
16	0.000	.000	.000	0.000	0.000	.000	.000	.000	.000	.000	.000	.000	.000	.000	.000	.000							
17	0.000	.000	.000	0.000	**0.001**	.000	.000	.000	.000	.000	.000	.000	.000	.000	.000	.000	.000						
18	0.000	.000	.000	0.000	0.000	.000	.000	.000	.000	.000	.000	.000	.000	.000	.000	.000	.000	.000					
19	**0.002**	.000	.000	0.000	**-.001**	.000	.000	.000	.000	.000	.000	.000	.000	.000	.000	.000	.000	.000	**.001**				
20	0.000	.000	.000	0.000	0.001	.000	.000	.000	.000	.000	.000	.000	.000	.000	.000	.000	.000	.000	.000	.000			
21	0.000	.000	.000	0.000	0.000	.000	.000	.000	.000	.000	.000	.000	.000	.000	.000	.000	.000	.000	.000	.000	.000		
22	0.000	.000	.000	0.000	0.000	.000	.000	.000	.000	.000	.000	.000	.000	.000	.000	.000	.000	.000	.000	.000	.000	.000	
23	0.000	.000	.000	0.000	0.000	.000	.000	.000	.000	.000	.000	.000	.000	.000	.000	.000	.000	.000	.000	.000	.000	.000	.000

Figure 4.19 : Relative modal contributions to the dynamic deck moment response - Node 7

1	0.972																						
2	-.020	0.004																					
3	0.000	0.000	.000																				
4	0.000	0.000	.000	.000																			
5	0.002	0.000	.000	.000	.011																		
6	0.000	0.000	.000	.000	.000	.000																	
7	0.000	0.000	.000	.000	.000	.000	.000																
8	0.000	0.000	.000	.000	.000	.000	.000	.000															
9	0.000	0.000	.000	.000	.000	.000	.000	.000	.000														
10	0.008	-.001	.000	.000	.001	.000	.000	.000	.000	.023													
11	0.000	0.000	.000	.000	.000	.000	.000	.000	.000	.000	.000												
12	0.000	0.000	.000	.000	.000	.000	.000	.000	.000	.000	.000	.000											
13	0.000	0.000	.000	.000	.000	.000	.000	.000	.000	.000	.000	.000	.000										
14	0.000	0.000	.000	.000	.000	.000	.000	.000	.000	.000	.000	.000	.000	.000									
15	0.000	0.000	.000	.000	.000	.000	.000	.000	.000	.000	.000	.000	.000	.000	.000								
16	0.000	0.000	.000	.000	.000	.000	.000	.000	.000	.000	.000	.000	.000	.000	.000	.000							
17	0.000	0.000	.000	.000	.000	.000	.000	.000	.000	.000	.000	.000	.000	.000	.000	.000	.000						
18	0.000	0.000	.000	.000	.000	.000	.000	.000	.000	.000	.000	.000	.000	.000	.000	.000	.000	.000					
19	-.002	0.000	.000	.000	.000	.000	.000	.000	.000	.000	.000	.000	.000	.000	.000	.000	.000	.000	.000				
20	0.000	0.000	.000	.000	.000	.000	.000	.000	.000	.000	.000	.000	.000	.000	.000	.000	.000	.000	.000	.000			
21	0.001	0.000	.000	.000	.000	.000	.000	.000	.000	.000	.000	.000	.000	.000	.000	.000	.000	.000	.000	.000	.000		
22	0.000	0.000	.000	.000	.000	.000	.000	.000	.000	.000	.000	.000	.000	.000	.000	.000	.000	.000	.000	.000	.000	.000	
23	0.000	0.000	.000	.000	.000	.000	.000	.000	.000	.000	.000	.000	.000	.000	.000	.000	.000	.000	.000	.000	.000	.000	.000
	1	2	3	4	5	6	7	8	9	10	11	12	13	14	15	16	17	18	19	20	21	22	23

Figure 4.20 : Relative modal contributions to the dynamic deck moment response - Node 15

Figure 4.21 shows the modal variances and covariances for the deck shear response at node 7. The modal variances and covariances for the cable displacement at nodes 8 and 16 are presented in Figures 4.22 and 4.23. Figure 4.21 indicates that a relatively large number of modes contribute to the dynamic shear response (modes 1, 2, 5, 10, 17, 19, 20, 21, 22, and 23). The higher frequency modes contribute about 10.0% at node 7. A greater number of modal covariances contribute to the shear responses than to the displacement and moment responses. Figure 4.12, presented earlier shows the contribution of the modal covariances to the shear response at node 15, and indicates that the first mode has zero contribution and 95% of the contribution is from mode 5.

Figures 4.22 and 4.23 indicates that mode 1 contributes about 54.5% and 53% to the lateral dynamic displacement at nodes 8 and 16, respectively. The relative contributions in the figures are shown only to the third decimal figure and smaller contributions are simply shown as 0.000. This is a little misleading since the sum of all the non-zero values is 70.8% in Figure 4.22 and 66.1% in Figure 4.22, and a very large number of small contribution from variances and covariances shown as 0.000 in the figures must additively contribute the remaining 29.2% and 33.9% at nodes 8 and 16, respectively. This indicates the need to consider a very large number of modes in the overall analysis.

4.3.5 Transient Response

It is of interest to determine whether the side span will reach its stationary response during typical durations of strong shaking (10 to 20 seconds). The variances of the cable displacement, deck displacement, deck moment, and deck shear are evaluated at times of 5, 15, 30, and 40 seconds and compared with the stationary responses for the general ground motion model in Figures 4.24 to 4.27. All variances have been normalized by dividing by the maximum stationary variance for the corresponding response.

Figure 4.24 shows the lateral displacement response of the side span cables. At node 8, 47.4%, 79.2%, 91.7%, and 96.9% of the general stationary response is achieved at times

1	0.791																						
2	-.017	0.004																					
3	0.000	0.000	.000																				
4	0.000	0.000	.000	.000																			
5	-.002	0.000	.000	.000	0.018																		
6	0.000	0.000	.000	.000	0.000	.000																	
7	0.000	0.000	.000	.000	0.000	.000	.00																
8	0.000	0.000	.000	.000	0.000	.000	.00	.00															
9	0.000	0.000	.000	.000	0.000	.000	.00	.00	.000														
10	0.016	-.001	.000	.000	-.003	.000	.00	.00	.000	0.105													
11	0.000	0.000	.000	.000	0.000	.000	.00	.00	.000	0.000	.00												
12	0.000	0.000	.000	.000	0.000	.000	.00	.00	.000	0.000	.00	.00											
13	0.000	0.000	.000	.000	0.000	.000	.00	.00	.000	0.000	.00	.00	.000										
14	0.000	0.000	.000	.000	0.000	.000	.00	.00	.000	0.000	.00	.00	.000	.000									
15	0.000	0.000	.000	.000	0.000	.000	.00	.00	.000	0.000	.00	.00	.000	.000	.00								
16	0.000	0.000	.000	.000	0.000	.000	.00	.00	.000	0.000	.00	.00	.000	.000	.00	.00							
17	0.001	0.000	.000	.000	0.003	.000	.00	.00	.000	0.005	.00	.00	.000	.000	.00	.00	0.063						
18	0.000	0.000	.000	.000	0.000	.000	.00	.00	.000	0.000	.00	.00	.000	.000	.00	.00	0.000	.000					
19	0.008	-.001	.000	.000	-.001	.000	.00	.00	.000	0.002	.00	.00	.000	.000	.00	.00	0.000	.000	0.013				
20	0.000	0.000	.000	.000	0.000	.000	.00	.00	.000	0.000	.00	.00	.000	.000	.00	.00	0.003	.000	0.000	0.001			
21	-.002	0.000	.000	.000	0.000	.000	.00	.00	.000	-.001	.00	.00	.000	.000	.00	.00	0.000	.000	-.001	0.000	.001		
22	0.000	0.000	.000	.000	-.001	.000	.00	.00	.000	-.001	.00	.00	.000	.000	.00	.00	-.004	.000	0.000	-.001	.000	.001	
23	-.003	0.000	.000	.000	0.000	.000	.00	.00	.000	-.001	.00	.00	.000	.000	.00	.00	0.000	.000	-.001	0.000	.000	.000	.001
	1	2	3	4	5	6	7	8	9	10	11	12	13	14	15	16	17	18	19	20	21	22	23

Figure 4.21 : Relative modal contributions to the dynamic deck shear response - Node 7

1	0.545																						
2	0.048	0.043																					
3	-.012	-.004	0.074																				
4	-.005	-.001	0.005	.012																			
5	0.000	0.000	0.000	.000	.000																		
6	0.000	0.000	0.000	.000	.000	.000																	
7	0.002	0.000	-.001	.000	.000	.000	.001																
8	0.000	0.000	0.000	.000	.000	.000	.000	.002															
9	0.000	0.000	0.000	.000	.000	.000	.000	.000	.000														
10	0.000	0.000	0.000	.000	.000	.000	.000	.000	.000	.000													
11	0.000	0.000	0.000	.000	.000	.000	.000	.000	.000	.000	.000												
12	0.000	0.000	0.000	.000	.000	.000	.000	.000	.000	.000	.000	.000											
13	0.000	0.000	0.000	.000	.000	.000	.000	.000	.000	.000	.000	.000	.000										
14	0.000	0.000	0.000	.000	.000	.000	.000	.000	.000	.000	.000	.000	.000	.000									
15	0.000	0.000	0.000	.000	.000	.000	.000	.000	.000	.000	.000	.000	.000	.000	.000								
16	0.000	0.000	0.000	.000	.000	.000	.000	.000	.000	.000	.000	.000	.000	.000	.000	.000							
17	0.000	0.000	0.000	.000	.000	.000	.000	.000	.000	.000	.000	.000	.000	.000	.000	.000	.00						
18	0.000	0.000	0.000	.000	.000	.000	.000	.000	.000	.000	.000	.000	.000	.000	.000	.000	.00	.00					
19	0.000	0.000	0.000	.000	.000	.000	.000	.000	.000	.000	.000	.000	.000	.000	.000	.000	.00	.00	.00				
20	0.000	0.000	0.000	.000	.000	.000	.000	.000	.000	.000	.000	.000	.000	.000	.000	.000	.00	.00	.00	.00			
21	0.000	0.000	0.000	.000	.000	.000	.000	.000	.000	.000	.000	.000	.000	.000	.000	.000	.00	.00	.00	.00	.000		
22	0.000	0.000	0.000	.000	.000	.000	.000	.000	.000	.000	.000	.000	.000	.000	.000	.000	.00	.00	.00	.00	.000	.000	
23	0.000	0.000	0.000	.000	.000	.000	.000	.000	.000	.000	.000	.000	.000	.000	.000	.000	.00	.00	.00	.00	.000	.000	.000
	1	2	3	4	5	6	7	8	9	10	11	12	13	14	15	16	17	18	19	20	21	22	23

Figure 4.22 : Relative modal contributions to the dynamic cable displacement response - Node 8

1	0.528																						
2	0.051	.048																					
3	0.002	.001	.001																				
4	0.006	.002	.001	.016																			
5	0.000	.000	.000	.000	.000																		
6	0.000	.000	.000	.000	.000	.001																	
7	-.001	.000	.000	.000	.000	.000	.001																
8	0.000	.000	.000	.000	.000	.000	.000	.000															
9	0.000	.000	.000	.000	.000	.000	.000	.000	.000														
10	0.000	.000	.000	.000	.000	.000	.000	.000	.000	.000													
11	0.000	.000	.000	.000	.000	.000	.000	.000	.000	.000	.000												
12	0.000	.000	.000	.000	.000	.000	.000	.000	.000	.000	.000	.000											
13	0.000	.000	.000	.000	.000	.000	.000	.000	.000	.000	.000	.000	.000										
14	0.000	.000	.000	.000	.000	.000	.000	.000	.000	.000	.000	.000	.000	.000									
15	0.000	.000	.000	.000	.000	.000	.000	.000	.000	.000	.000	.000	.000	.000	.000								
16	0.000	.000	.000	.000	.000	.000	.000	.000	.000	.000	.000	.000	.000	.000	.000	.000							
17	0.000	.000	.000	.000	.000	.000	.000	.000	.000	.000	.000	.000	.000	.000	.000	.000	.000						
18	0.000	.000	.000	.000	.000	.000	.000	.000	.000	.000	.000	.000	.000	.000	.000	.000	.000	.000					
19	0.000	.000	.000	.000	.000	.000	.000	.000	.000	.000	.000	.000	.000	.000	.000	.000	.000	.000	.000				
20	0.000	.000	.000	.000	.000	.000	.000	.000	.000	.000	.000	.000	.000	.000	.000	.000	.000	.000	.000	.000			
21	0.000	.000	.000	.000	.000	.000	.000	.000	.000	.000	.000	.000	.000	.000	.000	.000	.000	.000	.000	.000	.000		
22	0.000	.000	.000	.000	.000	.000	.000	.000	.000	.000	.000	.000	.000	.000	.000	.000	.000	.000	.000	.000	.000	.000	
23	0.000	.000	.000	.000	.000	.000	.000	.000	.000	.000	.000	.000	.000	.000	.000	.000	.000	.000	.000	.000	.000	.000	.000
	1	2	3	4	5	6	7	8	9	10	11	12	13	14	15	16	17	18	19	20	21	22	23

Figure 4.23 : Relative modal contributions to the dynamic cable displacement response - Node 16

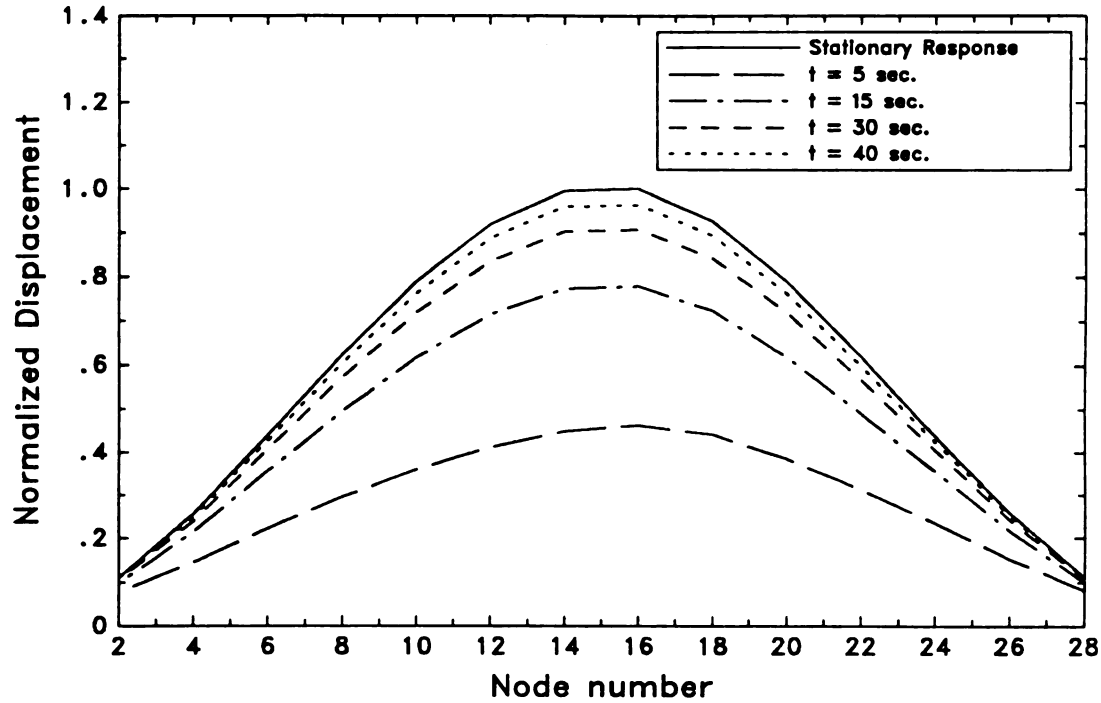

Figure 4.24 : Variation of normalized transient displacement variances of the side span cables

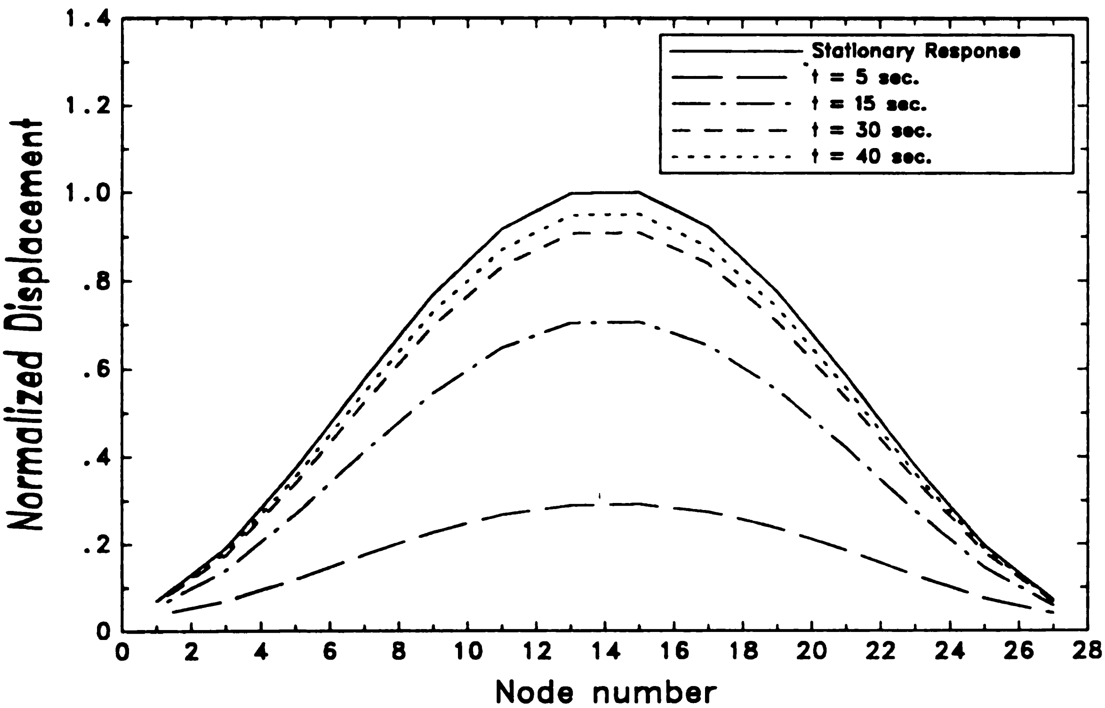

Figure 4.25 : Variation of normalized transient displacement variances of side span deck

of 5, 15, 30, and 40 seconds, respectively, while for node 16 the corresponding numbers are 46.2%, 77.9%, 90.8%, and 96.5%.

Figure 4.25 illustrates the lateral displacement of the deck. At node 7, 30.4%, 71.3%, 90.9%, and 95% of the general stationary response is achieved at times of 5, 15, 30, and 40 seconds, respectively, while for node 15 the corresponding numbers are 29.1%, 70.6%, 90.9%, and 95%. A comparison of the results between cable and deck responses reveal that the rate at which the responses grow is sensitive to the percentage contribution of the lower modes to the overall responses. While the contribution of mode 1 to the cable response at nodes 8 and 16 is 54.5% and 52.8%, it is 99.1% and 101.4%, respectively for deck nodes 7 and 15. The lower modes with longer periods take longer to attain stationarity, and therefore, total responses dominated by the lower modes take longer to attain stationarity.

Figure 4.26 shows the moment response of the side span deck. Results for node 7 show that 45.3%, 79.9%, 93.4%, and 96.2% of the stationary response is achieved at times of 5, 15, 30, and 40 seconds, respectively, while for node 15 the corresponding numbers are 32.3%, 71.7%, 90.8%, and 94.8%.

Finally Figure 4.27 illustrates the shear response of the side span deck. Mode 1 contributes 79.1% and 0.0% of the overall dynamic response at nodes 7 and 15 respectively (see Figures 4.12 and 4.21). The earlier statement reading the effect of the percentage contribution of the lower modes on the rate at which the responses grow is exemplified by the shear responses. At node 7, 45.1%, 78.4%, 94.2%, and 97.4% of the stationary response is achieved at times of 5, 15, 30, and 40 seconds, respectively, while for node 15 the corresponding numbers are 79.3%, 98.7%, 99.6%, and 99.6%. The results presented here indicate that for common ground motion durations, the assumption of stationarity may grossly over estimate the side span responses, and the transient nature of the responses should be taken into account.

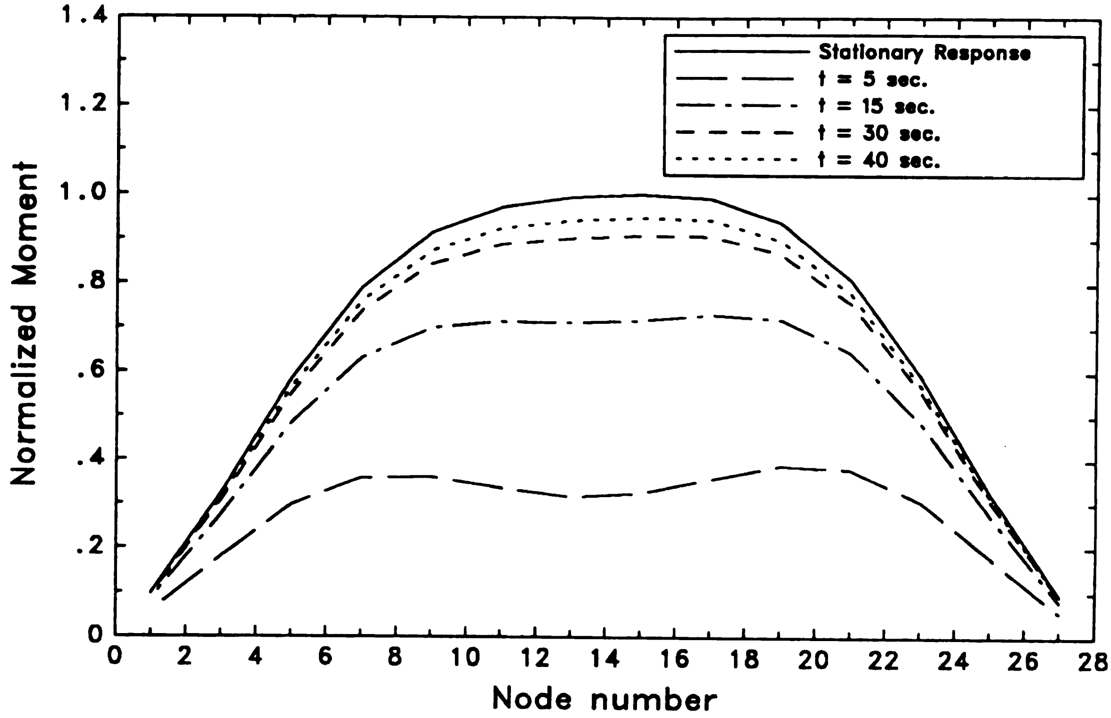

Figure 4.26 : Variation of normalized transient moment variances of the side span deck

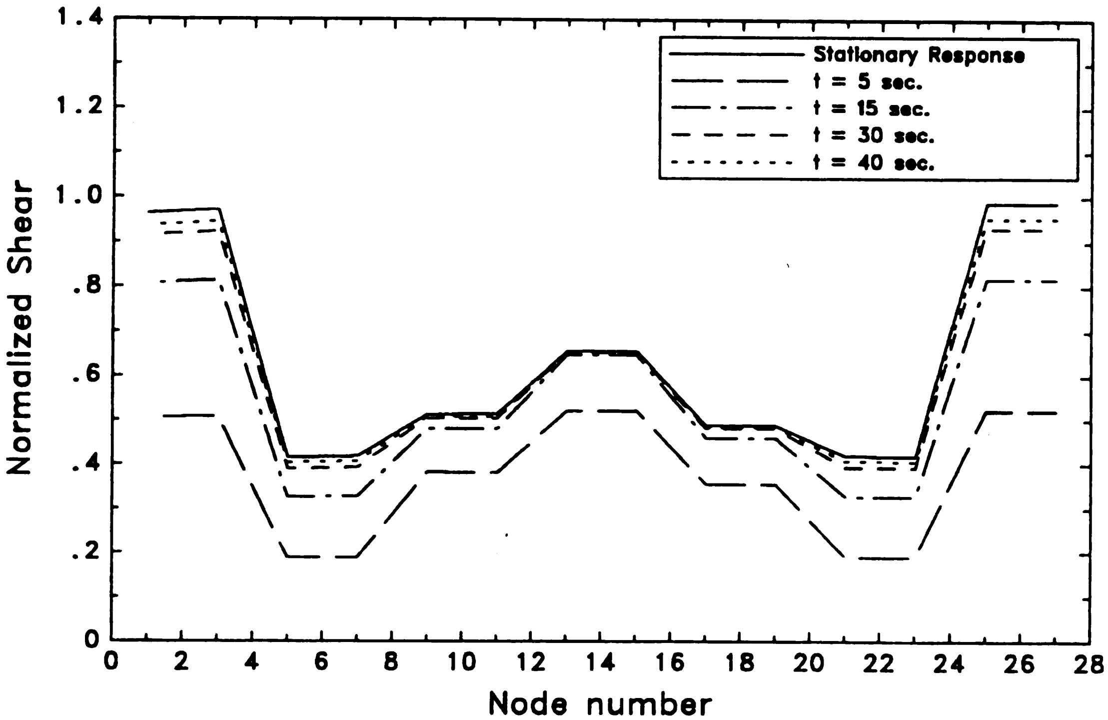

Figure 4.27 : Variation of normalized transient shear variances of the side span deck

The transient response of the side span was computed for the three ground motion models at time t=15 seconds. The responses of this study are normalized by dividing by the maximum response along the span due to the general ground motion model at time t=15 seconds. The results are presented in Figures 4.28 to 4.31 for displacement of the side span cable and for the displacement, moment, and shear of the side span deck, respectively. These figures are very similar to Figures 4.8 to 4.11, which are for stationary response. This indicates that the general conclusions drawn based on comparisons between the stationary response due to the three types of excitation are also valid for the transient response.

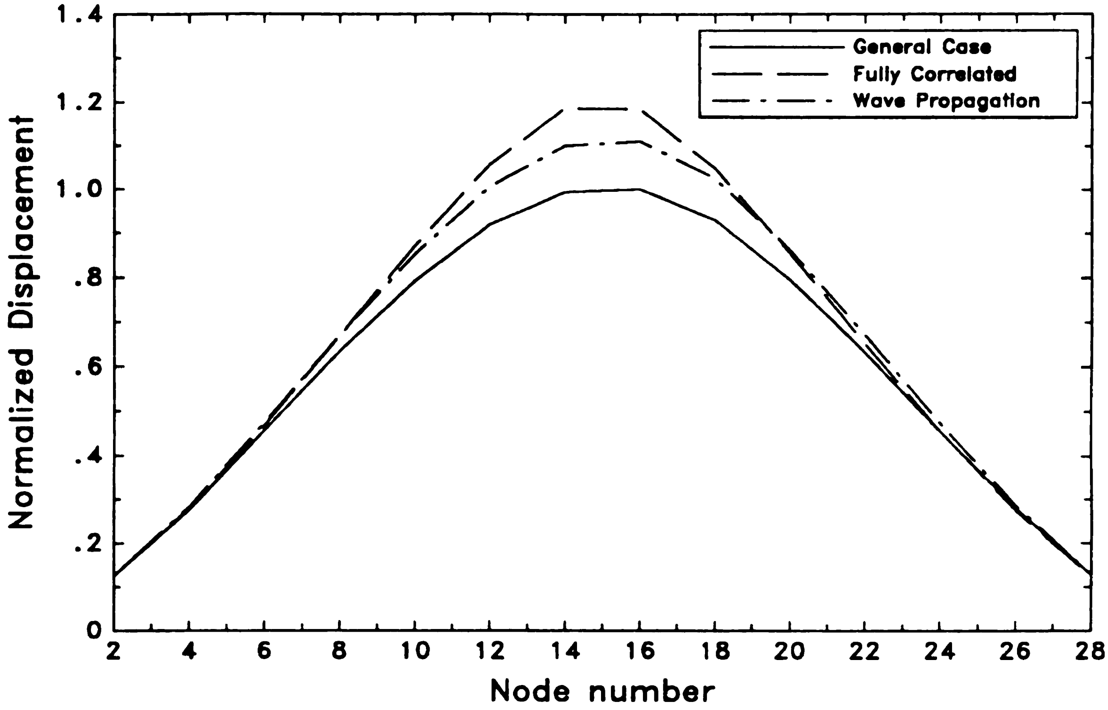

Figure 4.28 : Normalized transient displacement variances of the side span cables due to three ground motion models at t=15 seconds

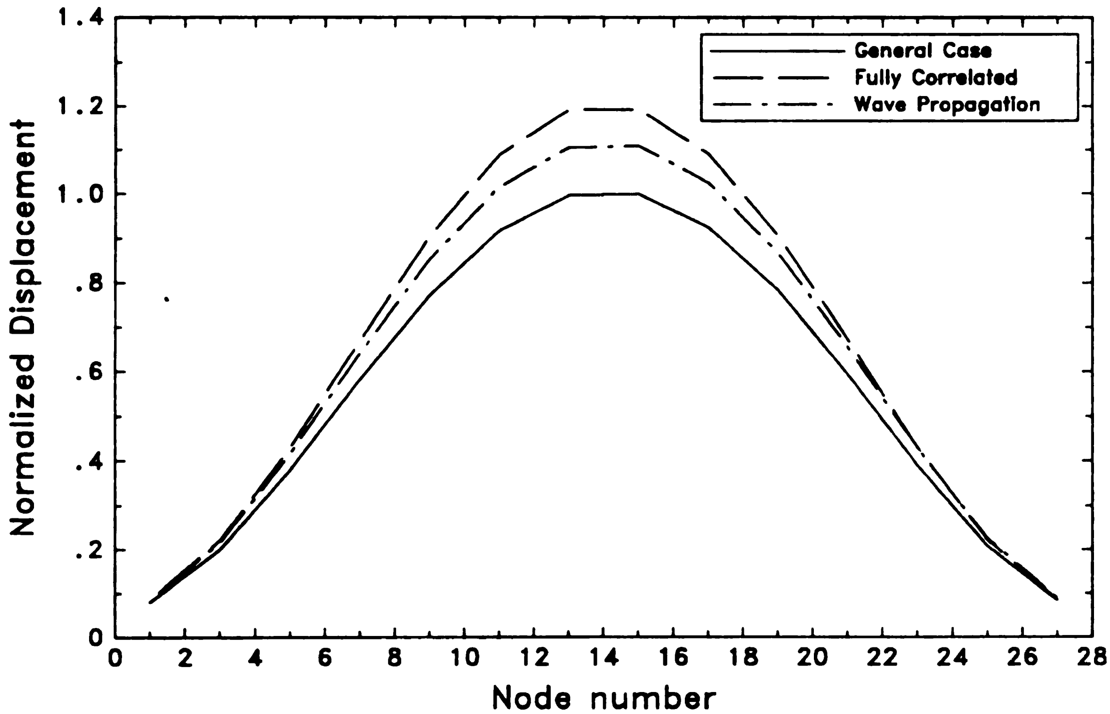

Figure 4.29 : Normalized transient displacement variances of the side span deck due to three ground motion models at t=15 seconds

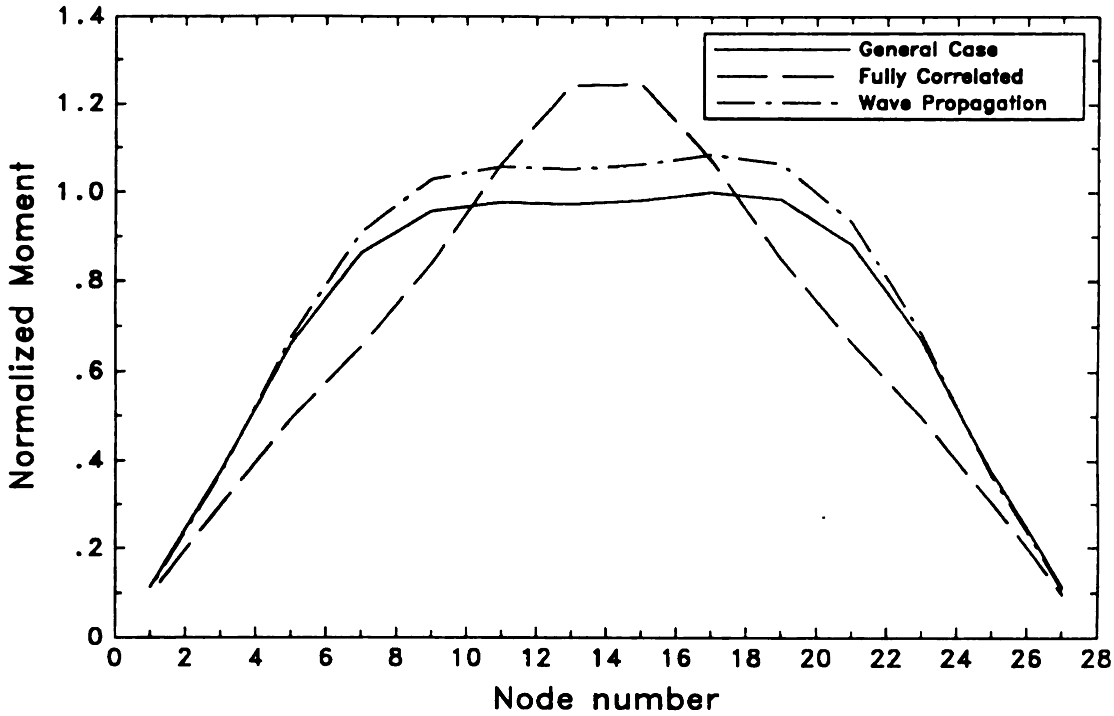

Figure 4.30 : Normalized transient moment variances of the side span deck due to three ground motion models at t=15 seconds

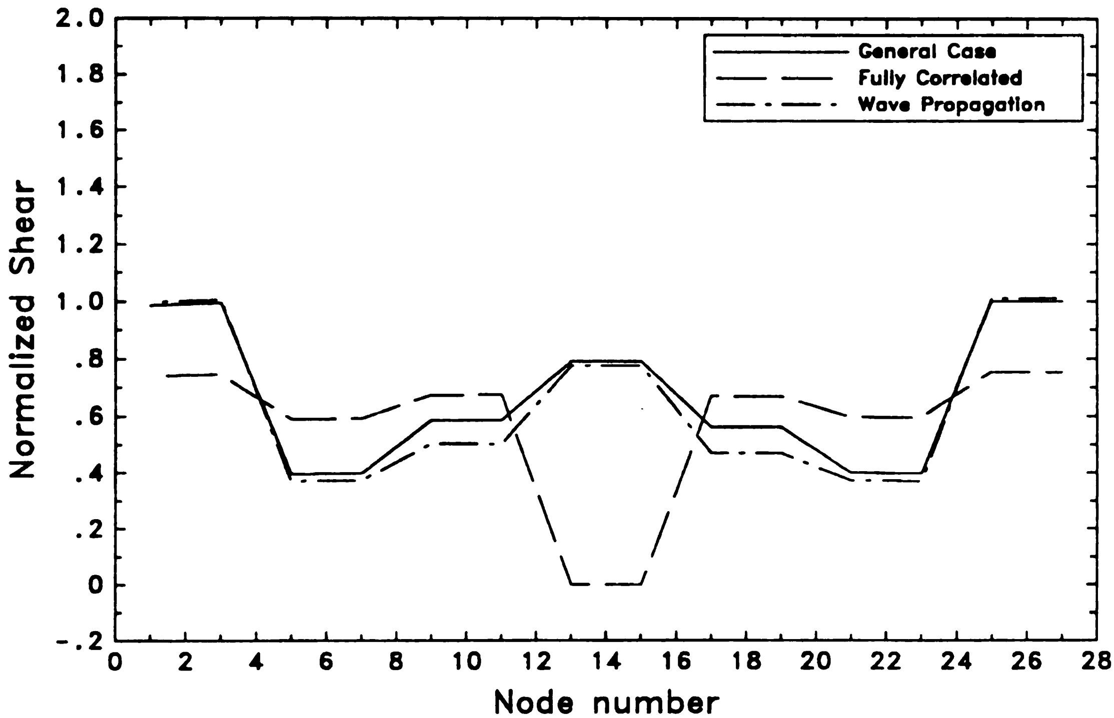

Figure 4.31 : Normalized transient shear variances of the side span deck due to three ground motion models at t=15 seconds

4.4 Center Span

It is very costly to consider all 251 modes in estimating the response of the Golden Gate bridge center span. For example, in equation (3.33) the required number of integrations is $(n^2 + n)\, r^2/2$. Table 4.3 presents the number of integrations that are required as a

Table 4.3 : Relation between the number of modes and the number of integrations.

No. of modes considered	Required No. of integrations
10	220
20	840
40	3,280
60	7,320
80	12,960
104	21,840
180	65,160
251	126,504

function of the number of modes used in the analysis. Therefore, it is important to determine the minimum number of modes required to acurately evaluate the response of the bridge center span. Several runs were performed with varying number of modes and it was found that using 104 modes gave at least 99% accuracy for all responses. Results for displacement and force responses using 20, 40, 60 and 104 modes are presented in Figures 4.28 to 4.31. Figure 4.32 indicates that if 40 modes are considered, the lateral displacement

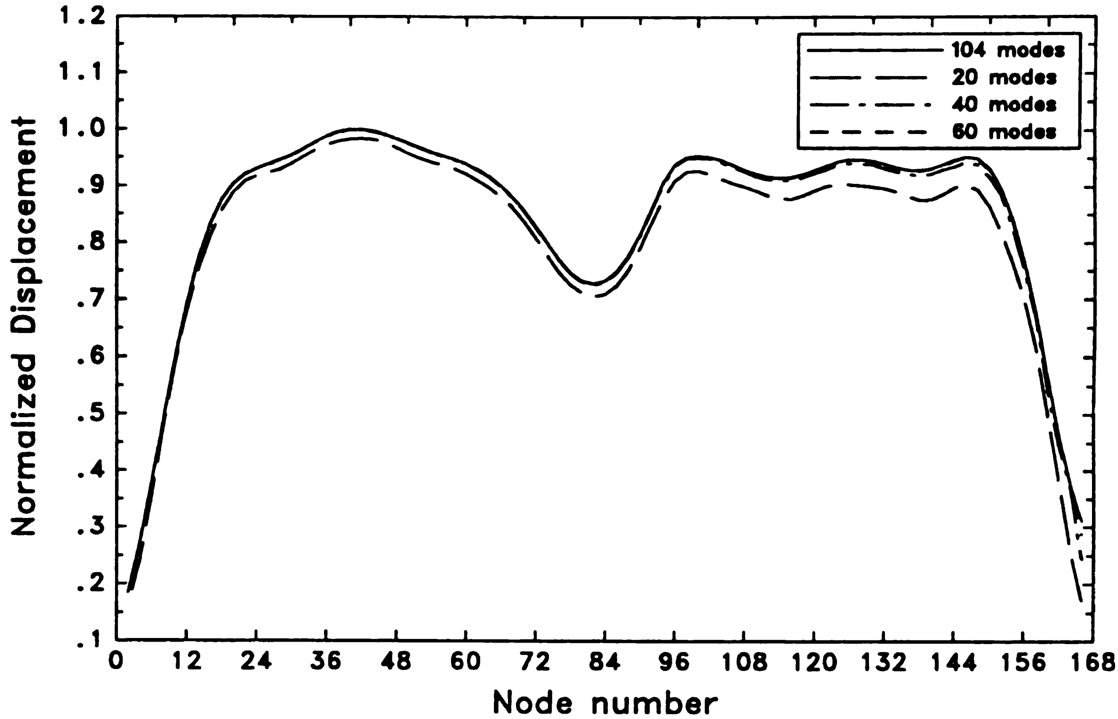

Figure 4.32 : Variation of normalized displacement variances of the center span cables

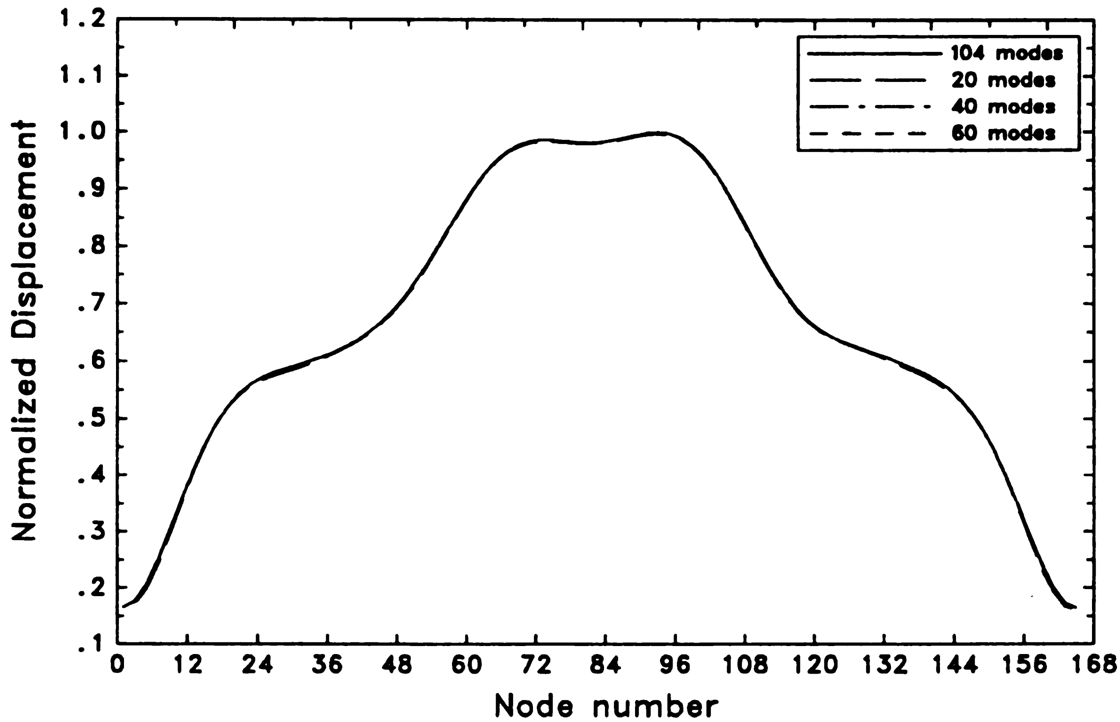

Figure 4.33 : Variation of normalized displacement variances of the center span deck

response of the cables will be represented with high accuracy, while the consideration of 60 modes will give almost an identical response to that of 104 modes. Figure 4.33 shows that the response of the center span deck lateral displacement estimated using 20 modes will give identical results to that of 104 modes.

Figure 4.34 and 4.31 show that using 60 modes represent the force responses accurately. It is clear that accurate computation of the force responses requires larger number of modes. Based on these results, 60 modes were considered in this study.

4.4.1 Center Span Response Components

The components of the total response variances are presented in Figures 4.32 to 4.37. The first three figures show the center span cable response for the three ground motion models, while the remaining figures show the displacement response of the center span deck for the three ground motion models. In Figures 4.32 to 4.37 the dynamic displacement response dominates the total response, but on the other hand the pseudo-static and covariance components contribute significantly more than for the side span.

Table 4.4 and 4.5 present the relative contribution of response components to the cable and deck displacement response at quarter span (node 42) and midspan (node 84). The results show the domination of the dynamic response and the significant relative contribution of the covariance components. The dynamic response contributes about 110% or more to the total response for all excitation models, and the covariance response contributes about 20% or more.

The results indicate that the correlation effect is not significant on the response, and that wave propagation alone yields good accuracy. In terms of the response components, neglecting the static variance and the covariance would over-estimate the lateral cable response by about 10% and the deck response by about 24%.

The force response components of the deck (i.e., moment and shear) are dominated totally by the dynamic component and the effect of the static component and cross covari-

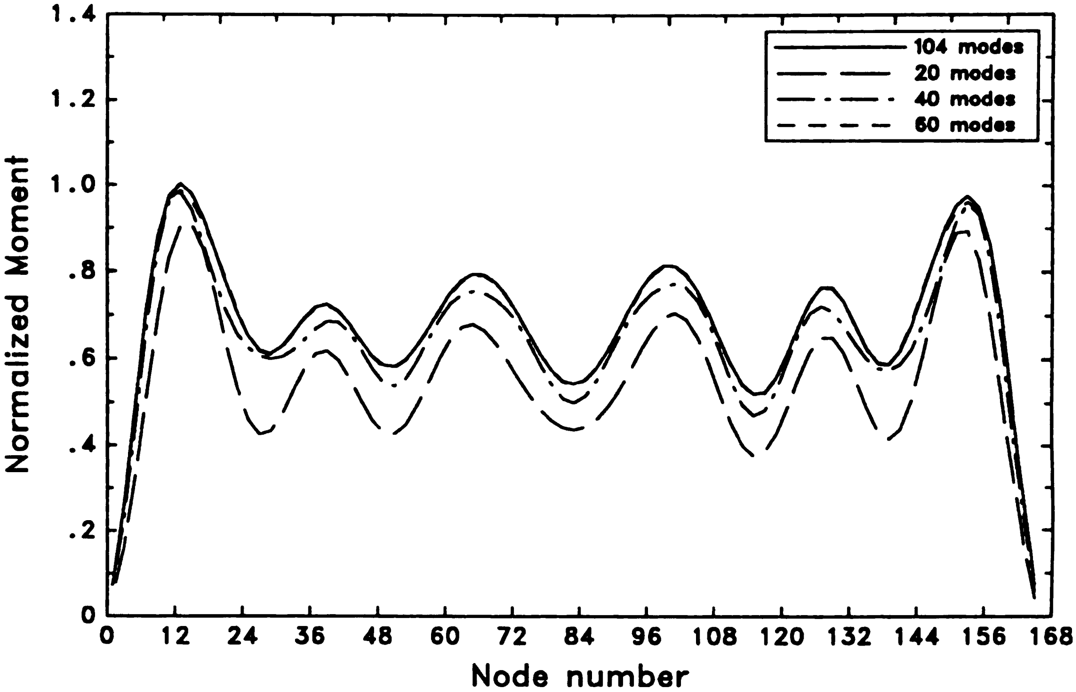

Figure 4.34 : Variation of normalized moment variances of the center span deck

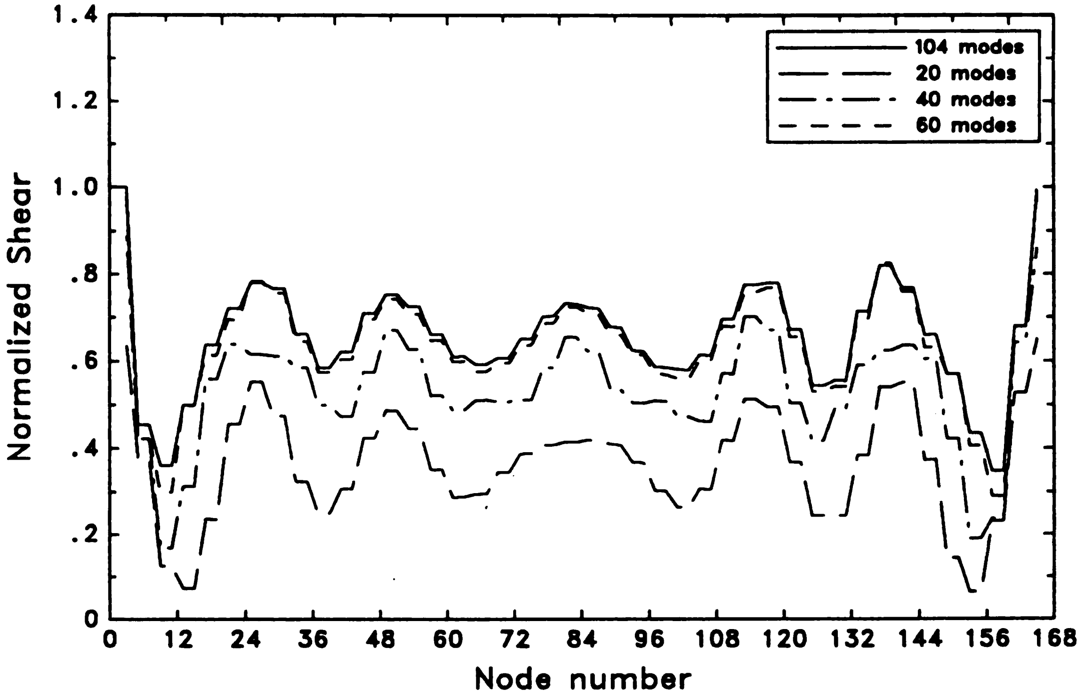

Figure 4.35 : Variation of normalized shear variances of the center span deck

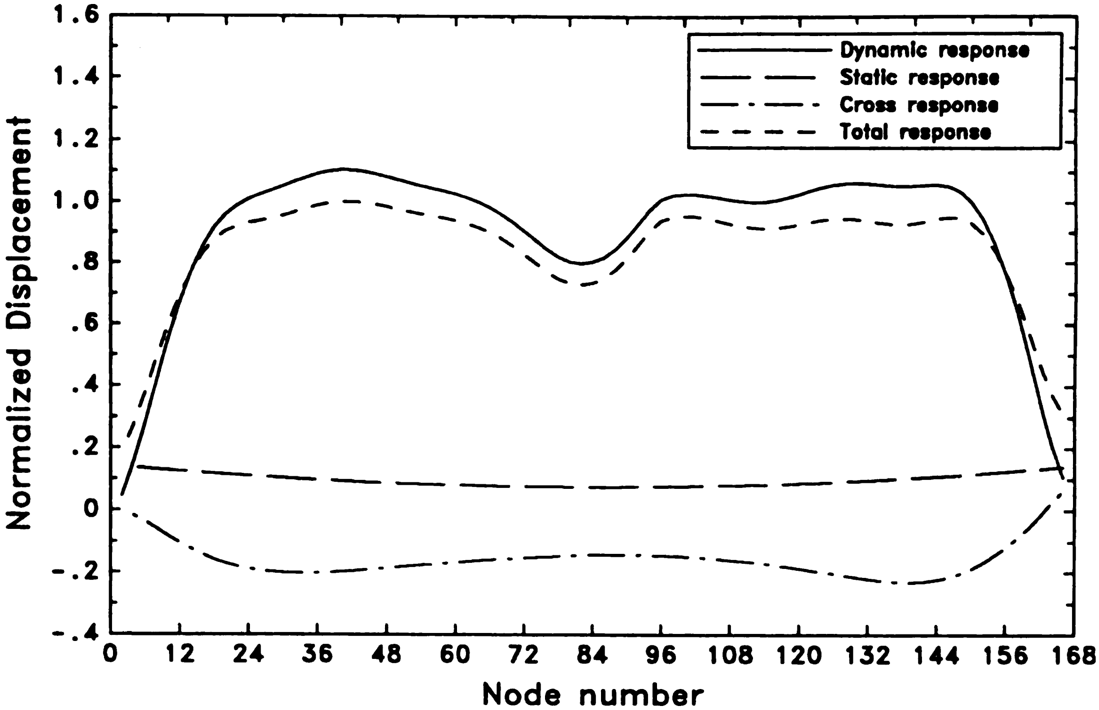

Figure 4.36 : Variation of normalized displacement variances of the center span cables (General ground motion model)

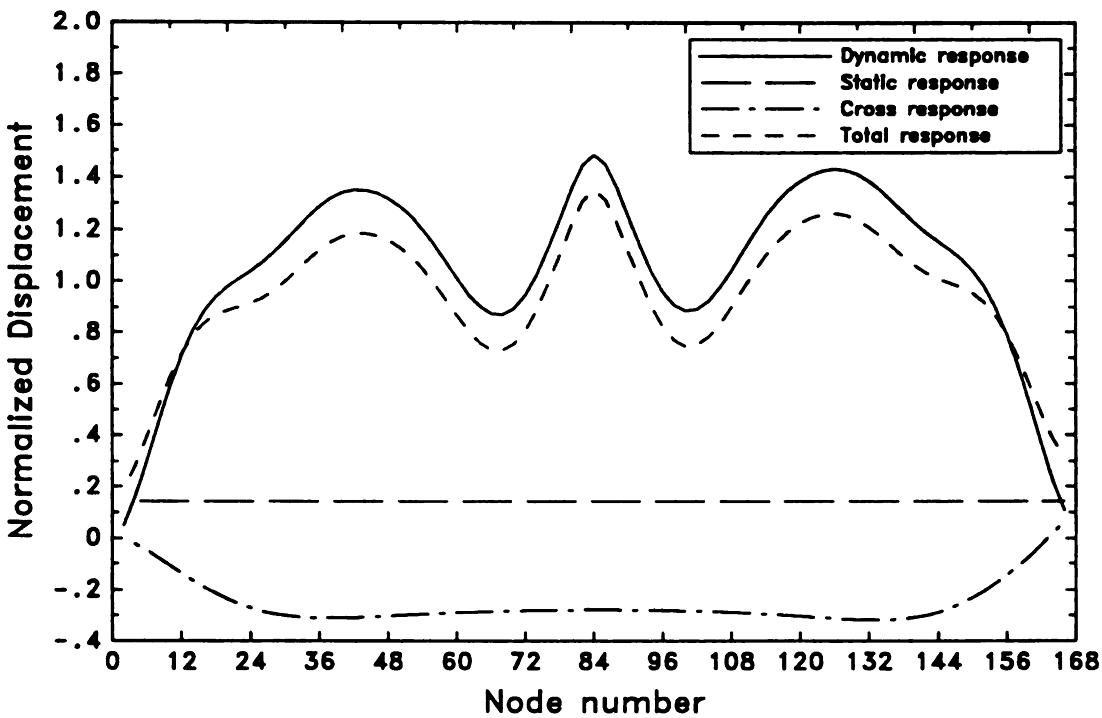

Figure 4.37 : Variation of normalized displacement variances of the center span cables (Fully correlated ground motion model)

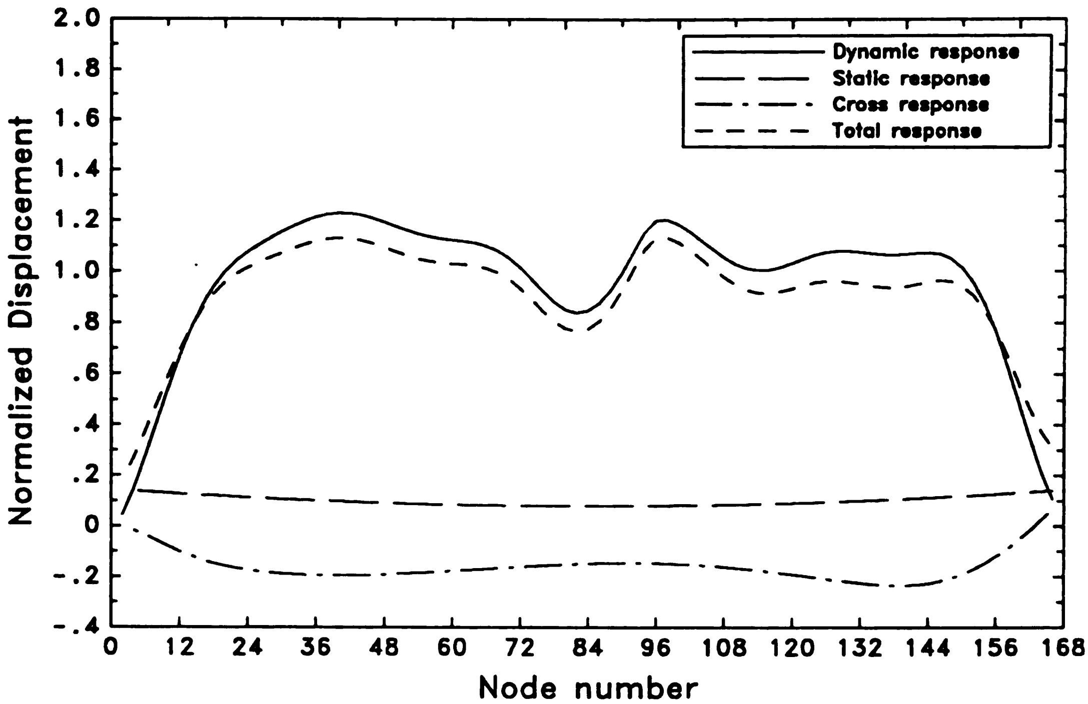

Figure 4.38 : Variation of normalized displacement variances of the center span cables (Wave propagation ground motion model)

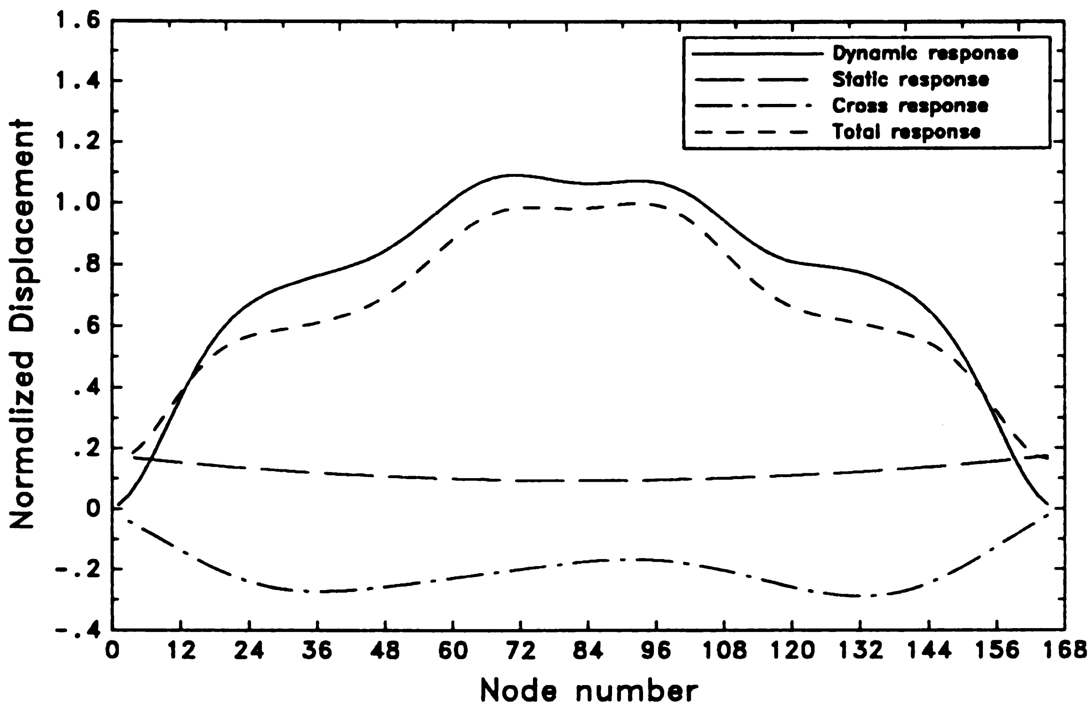

Figure 4.39 : Variation of normalized displacement variances of the center span deck (General ground motion model)

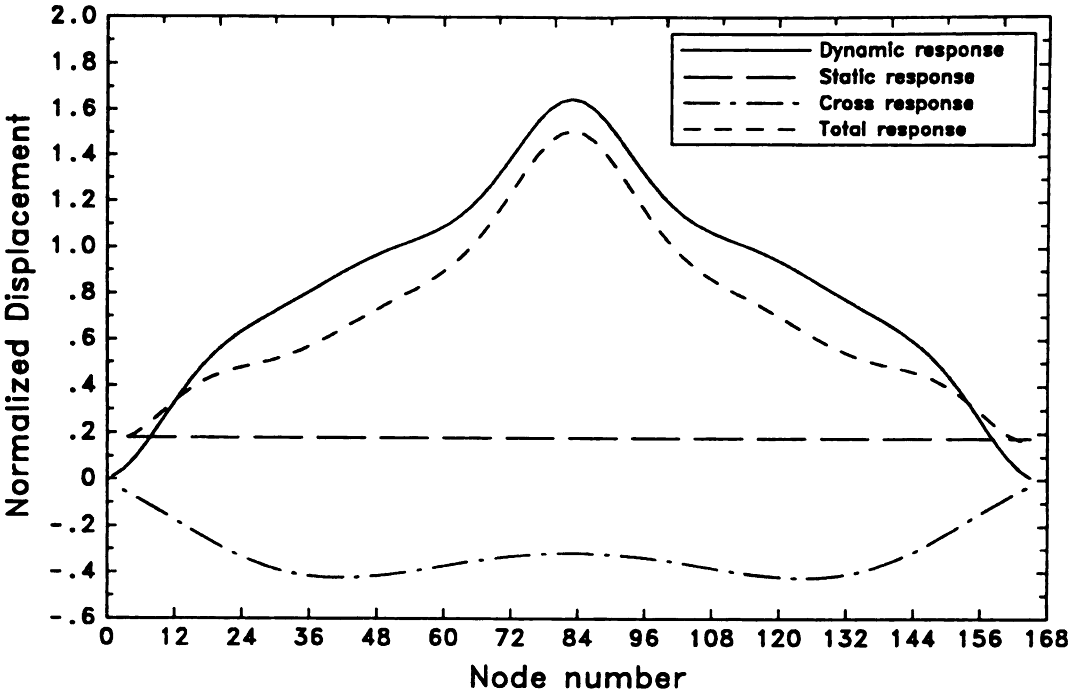

Figure 4.40 : Variation of normalized displacement variances of the center span deck (Fully correlated ground motion model)

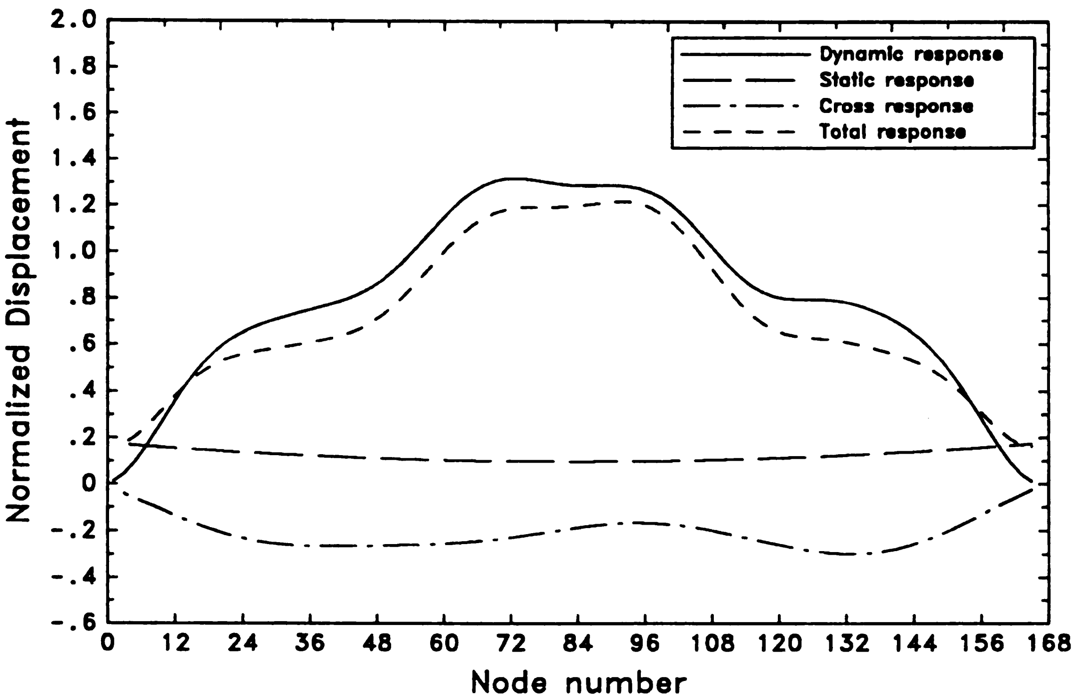

Figure 4.41 : Variation of normalized displacement variances of the center span deck (Wave propagation ground motion model)

Table 4.4 : Relative contribution of response components to cable displacement response at quarter and mid span.

Excitation model	Quarter-span (Node 42)			Mid-span (Node 84)		
	Dynamic	Static	Covariance	Dynamic	Static	Covariance
General excitation	110.3%	9.2%	-19.5%	109.4%	10.3%	-19.7%
Fully correlated excitation	113.9%	12.1%	-26.0%	110.0%	10.6%	-20.6%
Wave propagation	108.9%	8.4%	-19.2%	109.1%	10.1%	-19.2%

Table 4.5 : Relative contribution of response components to deck displacement response at quarter and mid span

Excitation model	Quarter-span (Node 41)			Mid-span (Node 83)		
	Dynamic	Static	Covariance	Dynamic	Static	Covariance
General excitation	124.3%	18.0%	-42.3%	108.3%	9.5%	-17.8%
Fully correlated excitation	139.1%	28.2%	-21.1%	109.8%	12.4%	-21.0%
Wave propagation	108.9%	18.6%	-42.1%	107.7%	8.13%	-15.8%

ance between pseudo-static and dynamic components is neglegible. The pseudo-static and cross covariance terms are essentially zero and the total response will essentially be the dynamic component similar to those in Figures 4.6 and 4.7.

4.4.2 Lateral Response of the Center Span

A comparison of the center span responses due to the three ground motion models are presented in Figures 4.42 to 4.45. The responses in each figure are normalized by dividing by the maximum response along the span due to the general ground motion model. Figures 4.42 and 4.43 represent the total lateral displacement response of the center span cables and deck, respectively.

Examining the total cable displacement response in Figure 4.42 at quarter span (node 42) reveals that the use of identical excitations overestimates the response by 18.5%, while the use of delayed excitation overestimates the response by 13% when compared to the response due to the general ground motion model. Similarly at mid-span (node 84), the use of identical excitation overestimates the response significantly (84.1%), while the use of delayed excitation overestimates the response slightly by 5.8% when compared to the response due to the general ground motion model. It is clear that the overestimation at mid-span when identical support excitation is used is very high. The response due to the delayed excitation also overestimates the general response near the midspan by as much as 20.6% (e.g. at node 96).

The lateral deck displacement shown in Figure 4.43 is overestimated by 53.6% and 21.9% at mid-span (node 83) for the fully correlated and wave propagation ground motion models, respectively, when compared to the general ground motion model.

The moment response of the center span deck presented in Figure 4.44 indicates that the use of fully correlated and wave propagation ground motion models overestimate or under estimate the response due to general excitation depending on the location. The moment response at node 83 is overestimated by 124.44% and underestimated by 11.52% for the

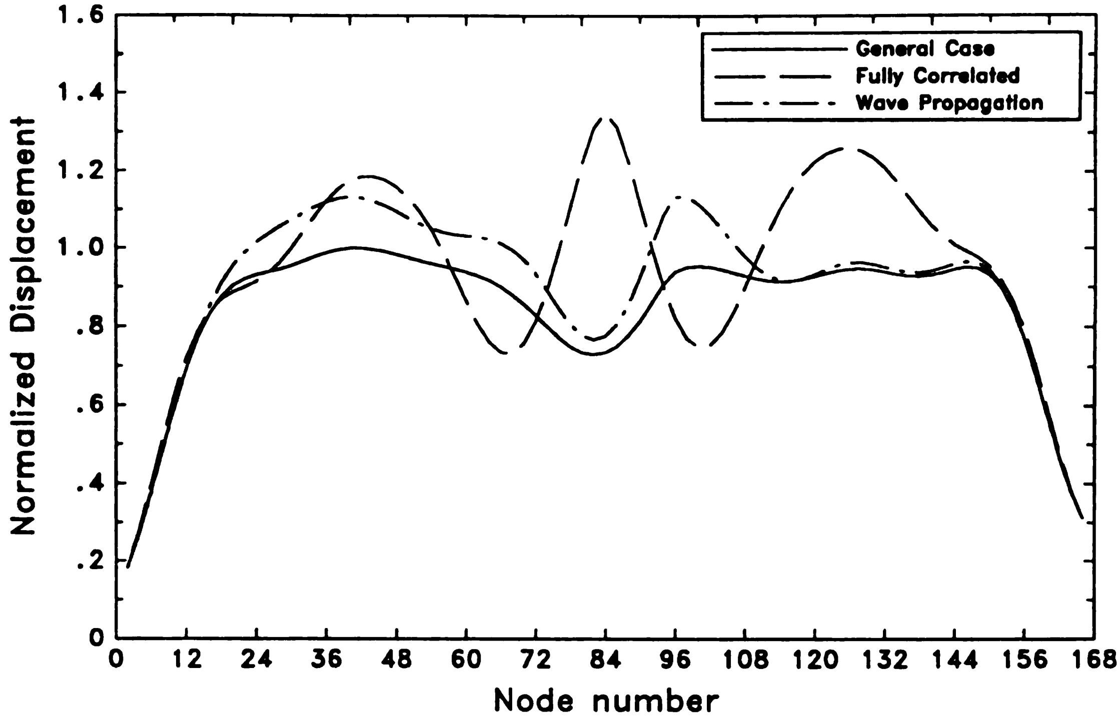

Figure 4.42 : Normalized displacement variances of the center span cables due to three ground motion models

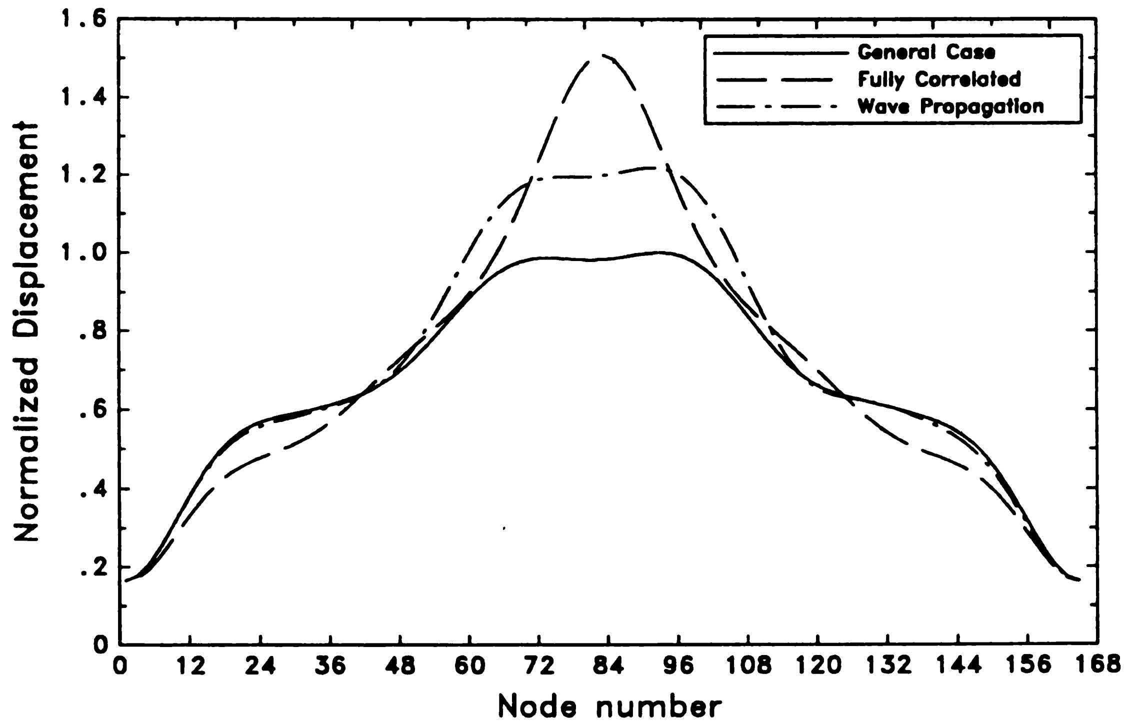

Figure 4.43 : Normalized displacement variances of the center span deck due to three ground motion models

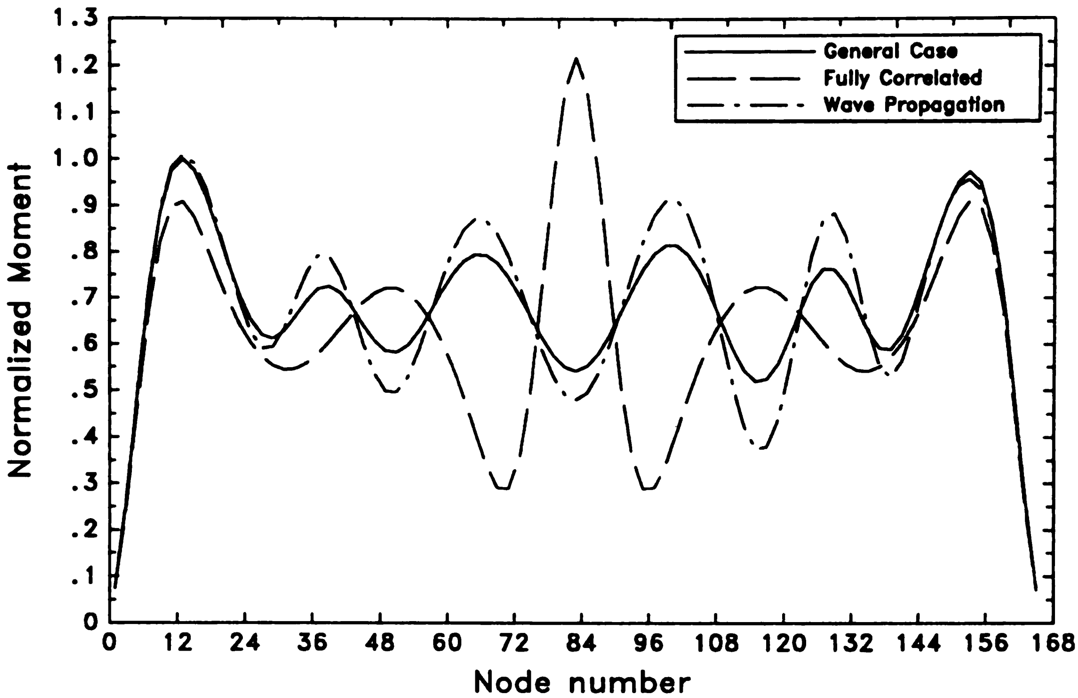

Figure 4.44 : Normalized moment variances of the center span deck due to three ground motion models

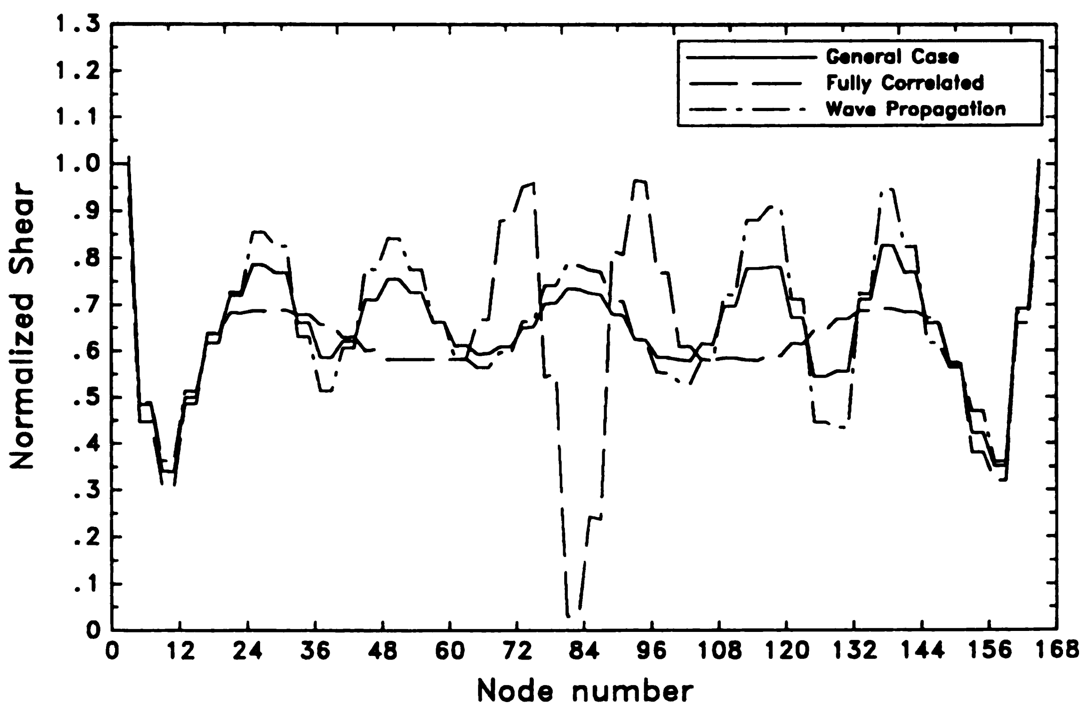

Figure 4.45 : Normalized shear variances of the center span deck due to three ground motion models

fully correlated and wave propagation ground motion models, respectively, when compared to that of the general ground motion model response. The identical support excitation may result in a serious underestimation of the moment response, for example at node 71 the moment is underestimated by 61.2% when compared to that of the general ground motion model. The large underestimation in the response is due to the fact that some of the anti-symmetric modes which are excited by the general response are not excited by the fully correlated ground motion model.

The shear response of the deck is presented in Figure 4.45. At node 83, the response due to fully correlated excitation underestimates the general response by 95.71% and the wave propagation case overestimates it by 7.1%. The reason for the 95.71% underestimation is again due to the fact that the fully correlated excitation does not excite many of the anti-symmetric modes. The results indicate that contribution of general correlated excitation is important for estimating the force response to avoid serious underestimation or overestimation of the force response at some locations along the bridge.

4.4.3 Effect of Apparent Wave Velocity

By choosing different apparent wave velocities in equation (3.58), a study similar to that done for the side span was conducted to examine its effect on the center span response due to the general and wave propagation excitation models.

Figures 4.46 and 4.47 show the effect of the apparent wave velocity on the displacement due to the general and wave propagation ground motion models, respectively. The increase in the velocity causes progressively higher displacements near nodes 83 and 130, and progressively lower displacements near node 100. The wave propagation ground motion shows a similar behavior to that of the general ground motion model but with higher increases and decreases in the response. As is expected, the response due to wave propagation excitation approaches that due to fully correlated excitation as $V \rightarrow \infty$.

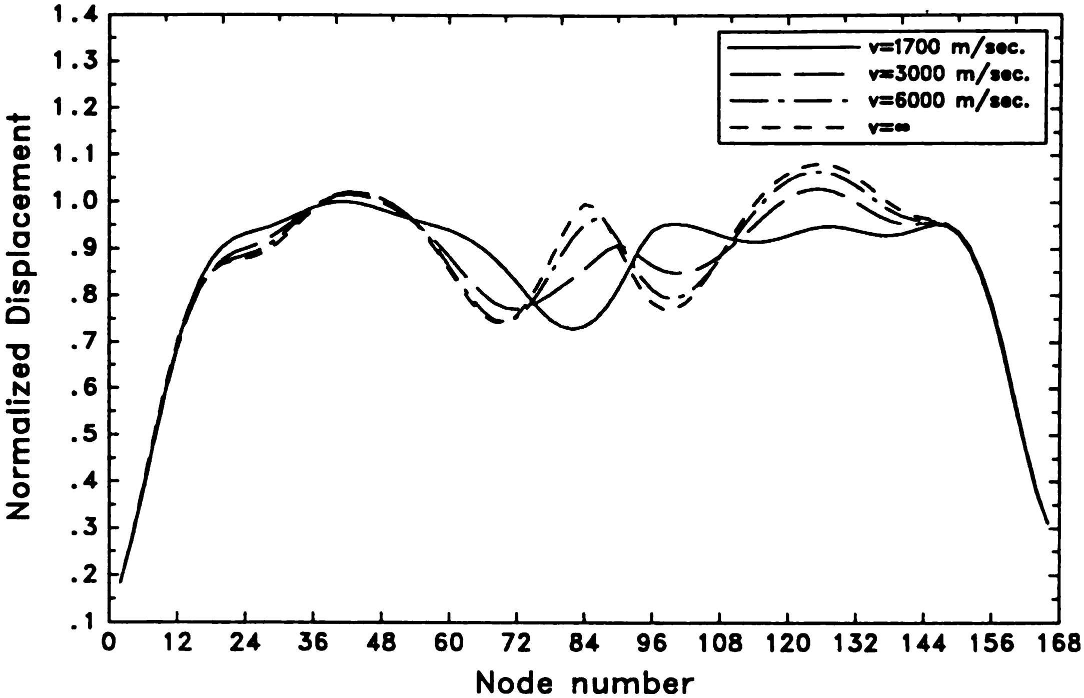

Figure 4.46 : Effect of apparent wave velocity on the center span cable displacement (General ground motion model)

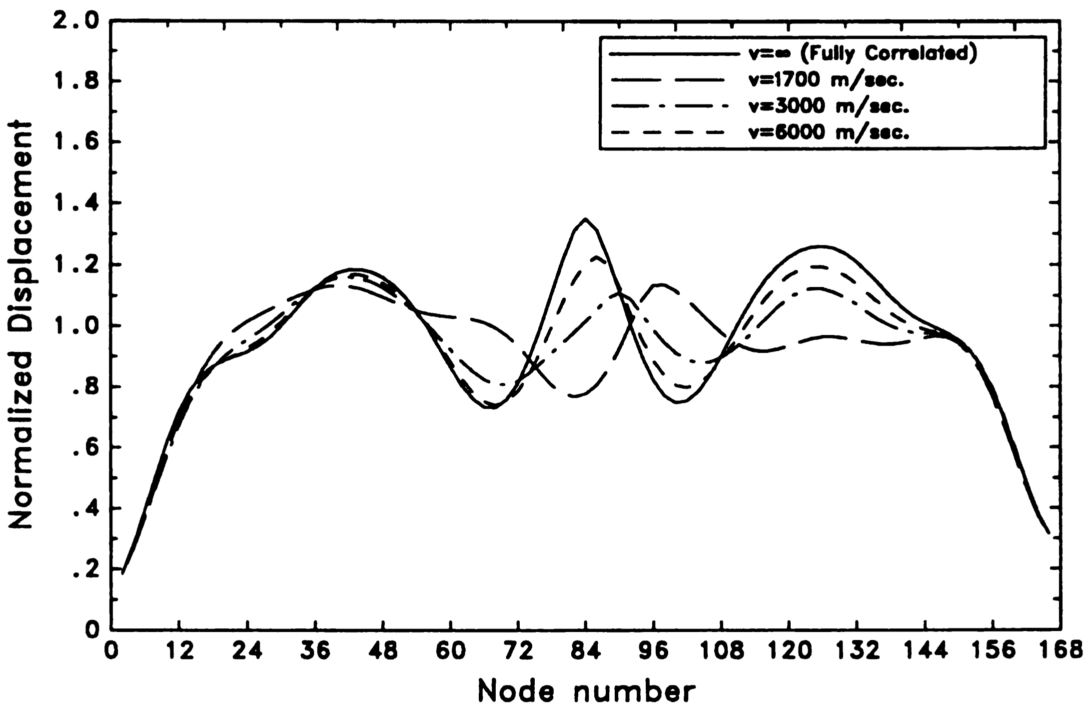

Figure 4.47 : Effect of apparent wave velocity on the center span cable displacement (wave propagation ground motion model)

Figure 4.48 and 4.49 show the effect of the apparent wave velocity on the lateral displacement of the center span deck due to the general and wave propagation ground motion models, respectively. The behavior of the response is similar to that of the cable, and for the wave propagation ground motion model the response approaches that of the fully correlated response as the velocity goes to ∞.

Figures 4.50 and 4.51 show the effect of the apparent wave velocity on the moment response of the center span deck due to general and wave propagation ground motion models. For the general ground motion model the maximum moment response occurs at nodes 13 and 155. For the general ground motion model the maximum moment response occurs at node 13. For the wave propagation ground motion model the maximum moment response occurs at node 83. Figures 4.52 and 4.53 represent the effect of apparent wave velocity on the shear response for the general and wave propagation ground motion models.

4.4.4 Modal Contributions

The relative contributions of the dynamic modal covariances to the total dynamic variances were computed for 23 modes at nodes 41 and 83 for the deck and nodes 42 and 84 for the cables due to the general ground motion model. The modal covariance matrix is symmetric as explained in section 4.3.2, and the off diagonal elements that are shown are twice the value of the corresponding covariances.

Figures 4.54 and 4.55 show the relative modal contributions to the total dynamic displacement response at quarter and mid-spans (nodes 41 and 83, respectively). The main conclusions are highlighted in Table 4.6. Significant contributions are obtained from three anti-symmetric modes at quarter-span, and there modes are not excited by identical ground excitations. The diagonal terms contribute most of the total dynamic response. Significant contributions are obtained from the off-diagonal terms at quarter-span, and neglecting them will result in an error of about 5%

Figures 4.56 and 4.57. show the relative modal contributions to the total dynamic mo-

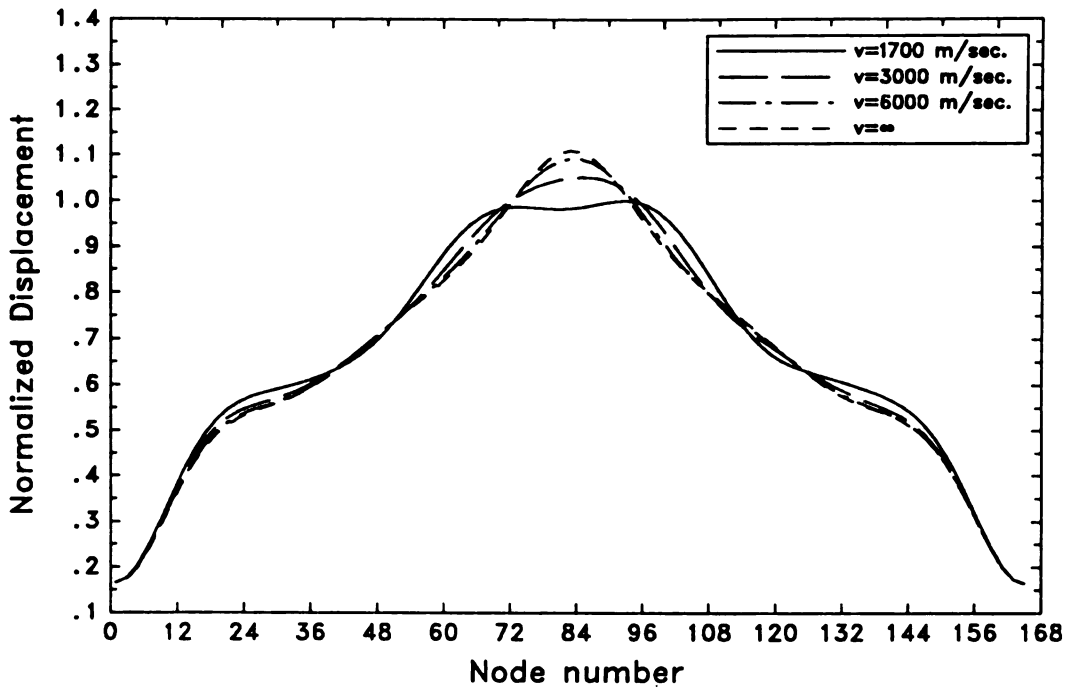

Figure 4.48 : Effect of apparent wave velocity on the center span deck displacement (General ground motion model)

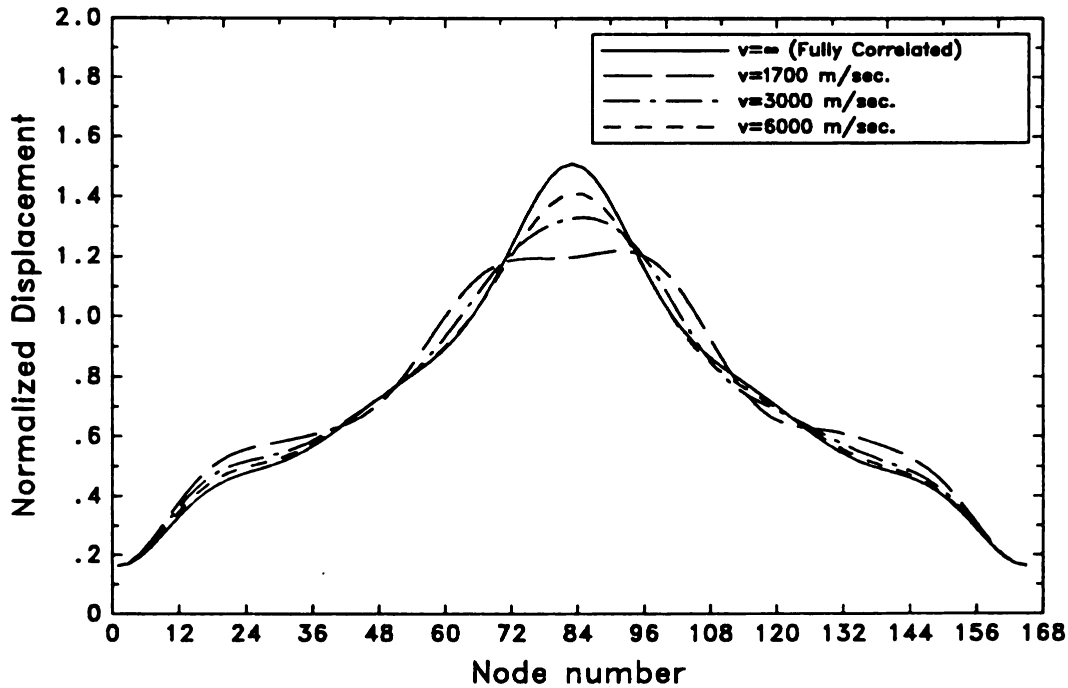

Figure 4.49 : Effect of apparent wave velocity on the center span deck displacement (Wave propagation ground motion model)

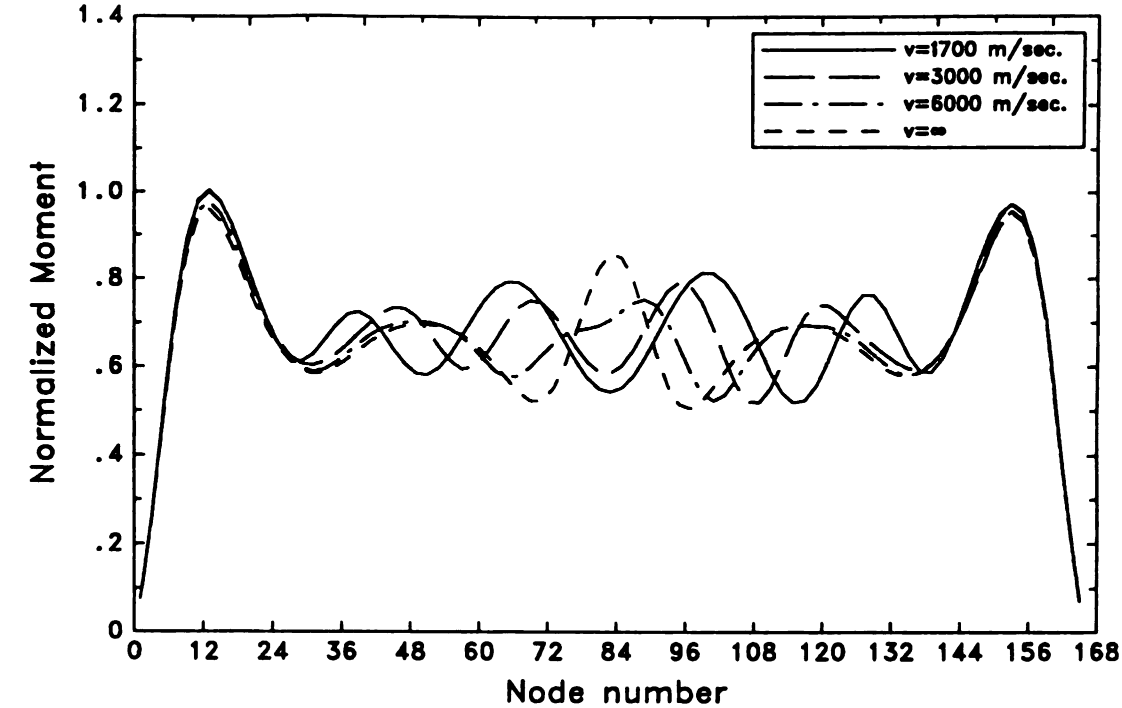

Figure 4.50 : Effect of apparent wave velocity on the center span deck moment (General ground motion model)

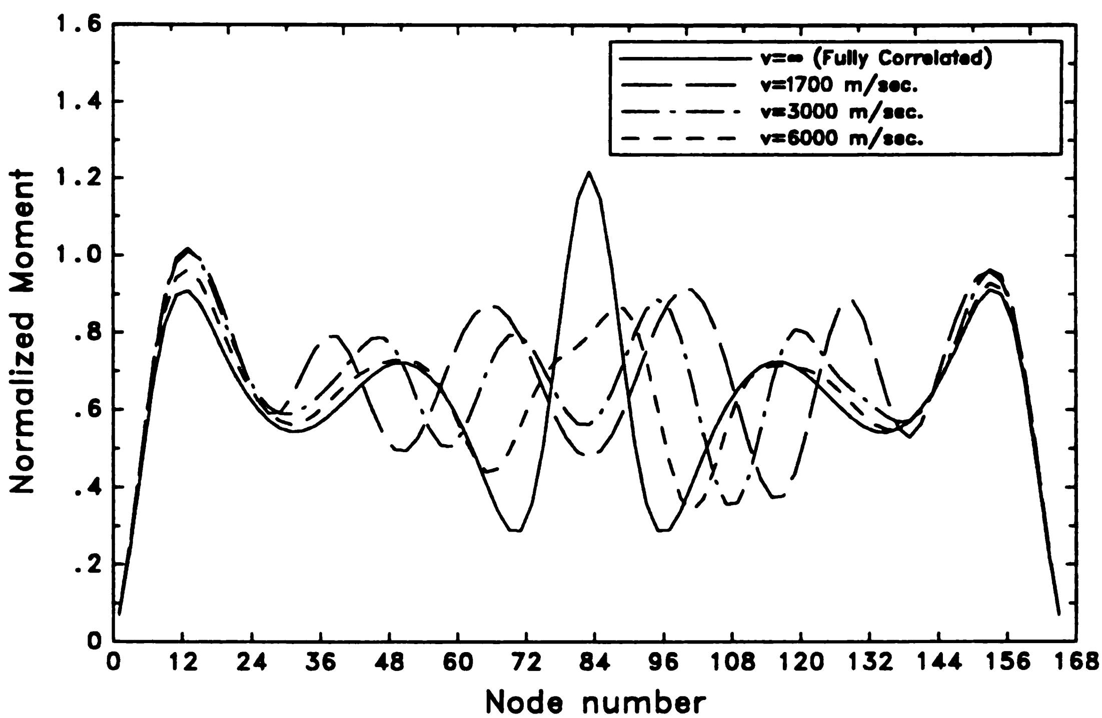

Figure 4.51 : Effect of apparent wave velocity on the center span deck moment (wave propagation ground motion model)

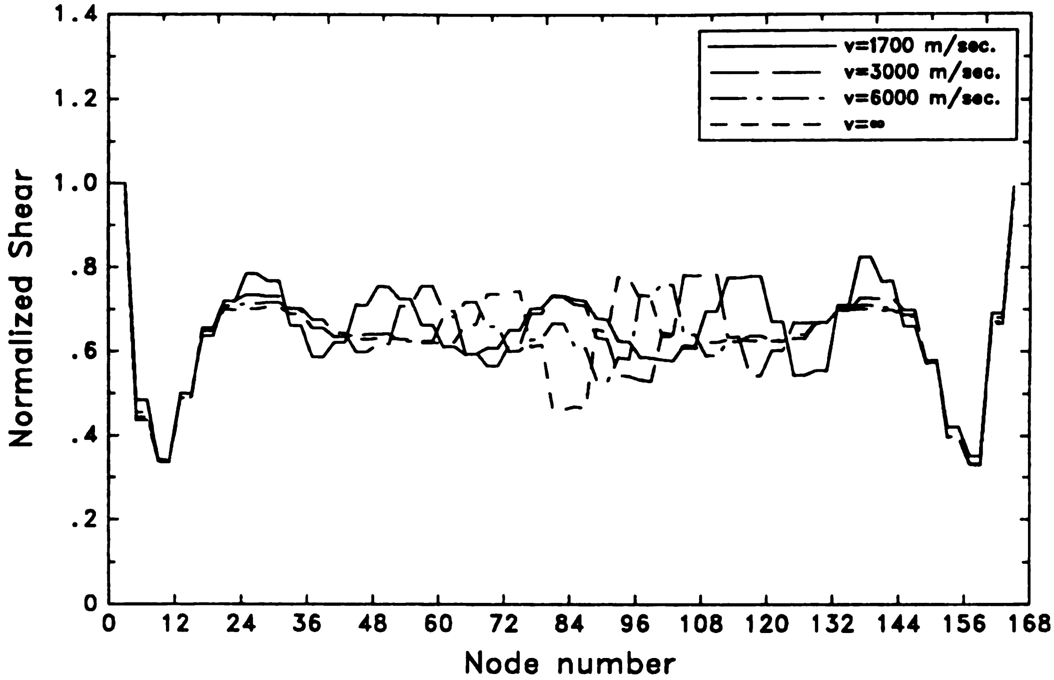

Figure 4.52 : Effect of apparent wave velocity on the center span deck shear (General ground motion model)

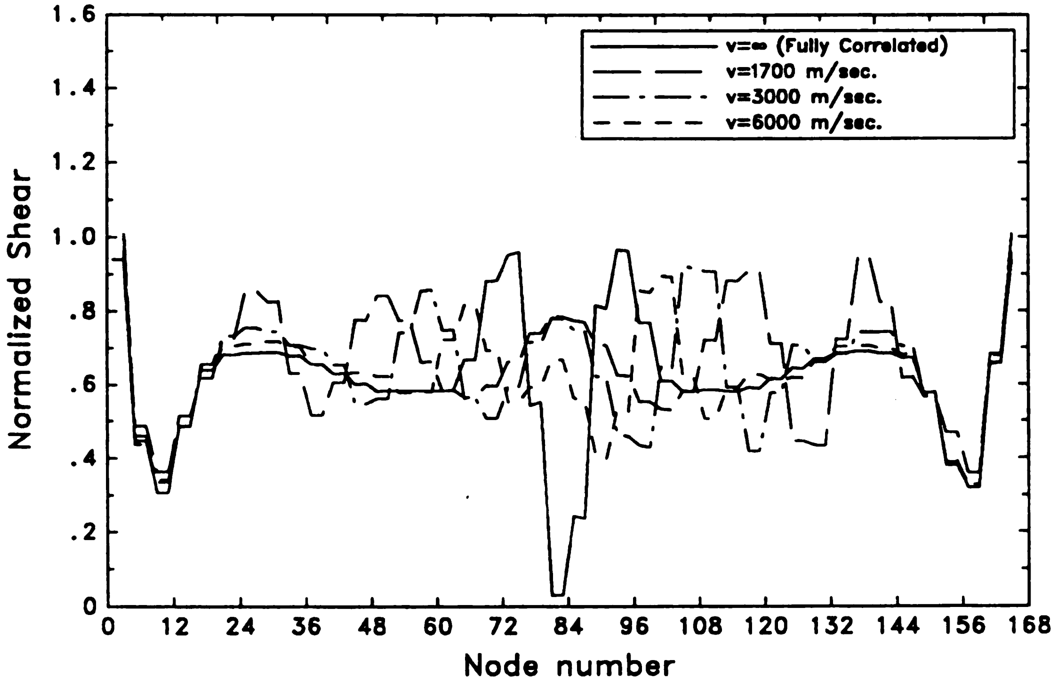

Figure 4.53 : Effect of apparent wave velocity on the center span deck shear (wave propagation ground motion model)

1	0.530																						
2	-.013	0.266																					
3	0.022	0.006	0.035																				
4	0.004	-.010	0.004	0.006																			
5	0.017	0.006	0.007	-.003	0.027																		
6	0.000	0.000	0.000	0.000	0.000	.000																	
7	-.001	0.001	0.000	0.000	0.000	.000	.000																
8	0.001	-.001	0.000	0.000	0.000	.000	.000	.000															
9	0.000	-.001	0.000	0.000	0.000	.000	.000	.000	.000														
10	0.000	0.000	0.000	0.000	0.000	.000	.000	.000	.000	.000													
11	0.006	-.003	0.002	0.001	0.001	.000	.000	.000	.000	.001	.022												
12	0.001	0.000	0.000	0.000	0.000	.000	.000	.000	.000	.000	.002	.001											
13	0.000	0.000	0.000	0.000	0.000	.000	.000	.000	.000	.000	.000	.000	.000										
14	0.000	0.000	0.000	0.000	0.000	.000	.000	.000	.000	.000	.000	.000	.000	.000									
15	-.004	0.012	-.001	-.002	-.001	.000	.000	.000	.000	.000	.000	.000	.000	.000	0.052								
16	0.000	0.000	0.000	0.000	0.000	.000	.000	.000	.000	.000	.000	.000	.000	.000	-.001	.000							
17	0.000	0.000	0.000	0.000	0.000	.000	.000	.000	.000	.000	.000	.000	.000	.000	0.000	.000	.000						
18	0.000	0.000	0.000	0.000	0.000	.000	.000	.000	.000	.000	.000	.000	.000	.000	0.000	.000	.000	.000					
19	0.002	0.001	0.000	0.000	0.000	.000	.000	.000	.000	.000	.000	.000	.000	.000	-.002	.000	.000	.000	.007				
20	0.000	0.000	0.000	0.000	0.000	.000	.000	.000	.000	.000	.000	.000	.000	.000	0.000	.000	.000	.000	.000	.00			
21	0.000	0.000	0.000	0.000	0.000	.000	.000	.000	.000	.000	.000	.000	.000	.000	0.000	.000	.000	.000	.000	.00	.00		
22	0.000	0.000	0.000	0.000	0.000	.000	.000	.000	.000	.000	.000	.000	.000	.000	0.000	.000	.003	.000	.000	.00	.00	.00	
23	0.000	0.000	0.000	0.000	0.000	.000	.000	.000	.000	.000	.000	.000	.000	.000	0.000	.000	.000	.000	.000	.00	.00	.00	.00
	1	2	3	4	5	6	7	8	9	10	11	12	13	14	15	16	17	18	19	20	21	22	23

Figure 4.54 : Relative modal contributions to the dynamic deck displacement response - Node 41

1	0.736																						
2	0.000	.000																					
3	-.011	.000	.006																				
4	0.000	.000	.000	.000																			
5	-.062	.000	.012	.000	0.269																		
6	0.004	.000	.000	.000	-.001	0.004																	
7	0.000	.000	.000	.000	0.000	0.000	.000																
8	0.000	.000	.000	.000	0.000	0.000	.000	.000															
9	0.000	.000	.000	.000	0.000	0.000	.000	.000	.000														
10	0.000	.000	.001	.000	0.000	0.000	.000	.000	.000	.000													
11	-.007	.000	.000	.000	0.005	-.001	.000	.000	.000	.000	.033												
12	-.001	.000	.000	.000	0.001	0.000	.000	.000	.000	.000	.002	.001											
13	0.000	.000	.000	.000	0.000	0.000	.000	.000	.000	.000	.000	.000	.000										
14	0.000	.000	.000	.000	0.000	0.000	.000	.000	.000	.000	.000	.000	.000	.000									
15	0.000	.000	.000	.000	0.000	0.000	.000	.000	.000	.000	.000	.000	.000	.000	.000								
16	0.000	.000	.000	.000	0.000	0.000	.000	.000	.000	.000	.000	.000	.000	.000	.000	.000							
17	0.000	.000	.000	.000	0.000	0.000	.000	.000	.000	.000	.000	.000	.000	.000	.000	.000	.000						
18	0.000	.000	.000	.000	0.000	0.000	.000	.000	.000	.000	.000	.000	.000	.000	.000	.000	.000	.000					
19	0.003	.000	.000	.000	-.001	0.000	.000	.000	.000	.000	.000	.000	.000	.000	.000	.000	.000	.000	.011				
20	0.000	.000	.000	.000	0.000	0.000	.000	.000	.000	.000	.000	.000	.000	.000	.000	.000	.000	.000	.000	.000			
21	0.000	.000	.000	.000	0.000	0.000	.000	.000	.000	.000	.000	.000	.000	.000	.000	.000	.000	.000	.000	.000	.000		
22	0.000	.000	.000	.000	0.000	0.000	.000	.000	.000	.000	.000	.000	.000	.000	.000	.000	.000	.000	.000	.000	.000	.000	
23	0.000	.000	.000	.000	0.000	0.000	.000	.000	.000	.000	.000	.000	.000	.000	.000	.000	.000	.000	.000	.000	.000	.000	.000
	1	2	3	4	5	6	7	8	9	10	11	12	13	14	15	16	17	18	19	20	21	22	23

Figure 4.55 : Relative modal contributions to the dynamic deck displacement response - Node 83

Table 4.6 : Relative modal contributions to the dynamic deck displacement.

	Quarter-span (Node 41)	Mid-span (Node 83)
No. of significant diagonal terms.	9	7
Contribution from significant diagonal terms.	94.6%	106.0%
No. of significant diagonal terms due to anti-symmetric modes.	3	0
Contribution of significant diagonal terms due to anti-symmetric modes.	32.4%	0.0%
No. of significant off-diagonal terms.	32	13
Contribution from significant off-diagonal terms.	5.3%	-5.9%
Total contribution from all terms with individual relative contributions less than 0.0005.	0.1%	0.1%

1	**0.005**																						
2	0.000	**0.032**																					
3	**0.001**	**0.001**	**0.011**																				
4	0.000	**-.001**	**0.001**	**0.001**																			
5	**0.002**	**0.003**	**0.005**	**-.001**	**0.045**																		
6	0.000	0.000	0.000	0.000	0.000	.00																	
7	0.000	0.000	0.000	0.000	0.000	.00	.000																
8	0.000	0.000	0.000	0.000	0.000	.00	.000	.00															
9	0.000	**-.001**	0.000	0.000	0.000	.00	.000	.00	**.002**														
10	0.000	0.000	0.000	0.000	0.000	.00	.000	.00	.000	**0.001**													
11	**0.001**	**-.002**	**0.001**	0.000	**0.003**	.00	.000	.00	.000	**0.002**	**0.100**												
12	0.000	0.000	0.000	0.000	0.000	.00	.000	.00	.000	0.000	**0.007**	**.003**											
13	0.000	0.000	0.000	0.000	0.000	.00	.000	.00	.000	0.000	0.000	.000	**0.001**										
14	0.000	0.000	0.000	0.000	0.000	.00	.000	.00	.000	0.000	0.000	.000	0.000	.000									
15	**-.001**	**0.013**	**-.001**	**-.002**	**-.002**	.00	**.001**	.00	.000	**-.001**	**0.002**	**.002**	**-.001**	**.001**	**0.496**								
16	0.000	0.000	0.000	0.000	0.000	.00	.000	.00	.000	0.000	0.000	.000	0.000	.000	**-.007**	.000							
17	0.000	0.000	0.000	0.000	0.000	.00	.000	.00	.000	0.000	0.000	.000	0.000	.000	0.000	.000	.00						
18	0.000	0.000	0.000	0.000	0.000	.00	.000	.00	.000	0.000	0.000	.000	0.000	.000	0.000	.000	.00	.00					
19	**0.001**	**0.001**	**0.001**	0.000	**0.002**	.00	.000	.00	.000	0.000	**-.001**	.000	0.000	.000	**-.018**	**.001**	.00	.00	**.125**				
20	0.000	0.000	0.000	0.000	0.000	.00	.000	.00	.000	0.000	0.000	.000	0.000	.000	0.000	.000	.00	.00	**.005**	.00			
21	0.000	0.000	0.000	0.000	0.000	.00	.000	.00	.000	0.000	0.000	.000	0.000	.000	0.000	.000	.00	.00	.000	.00	.00		
22	0.000	0.000	0.000	0.000	0.000	.00	.000	.00	.000	0.000	0.000	.000	0.000	.000	0.000	.000	.00	.00	.000	.00	.00	.00	
23	0.000	0.000	0.000	0.000	0.000	.00	.000	.00	.000	0.000	0.000	.000	0.000	.000	0.000	.000	.00	.00	.000	.00	.00	.00	.00
	1	**2**	**3**	**4**	**5**	**6**	**7**	**8**	**9**	**10**	**11**	**12**	**13**	**14**	**15**	**16**	**17**	**18**	**19**	**20**	**21**	**22**	**23**

Figure 4.56 : Relative modal contributions to the dynamic deck moment response - Node 41

1	0.007																						
2	0.000	.000																					
3	-.002	.000	0.023																				
4	0.000	.000	0.000	.000																			
5	-.004	.000	0.014	.000	0.141																		
6	0.000	.000	0.000	.000	0.000	0.001																	
7	0.000	.000	0.000	.000	0.000	0.000	.000																
8	0.000	.000	0.000	.000	0.000	0.000	.000	.000															
9	0.000	.000	0.000	.000	0.001	0.000	.000	.000	.008														
10	0.000	.000	0.000	.000	0.000	0.000	.000	.000	.000	.000													
11	-.002	.000	0.003	.000	0.009	-.001	.000	.000	.000	.000	.003												
12	0.000	.000	0.000	.000	0.001	0.000	.000	.000	.000	.000	.000	.00											
13	0.000	.000	0.000	.000	0.000	0.000	.000	.000	.000	.000	.000	.00	.00										
14	0.000	.000	0.000	.000	0.000	0.000	.000	.000	.000	.000	.000	.00	.00	.000									
15	0.000	.000	0.000	.000	0.000	0.000	.000	.000	.000	.000	.000	.00	.00	.000	.000								
16	0.000	.000	0.000	.000	0.000	0.000	.000	.000	.000	.000	.000	.00	.00	.000	.000	.000							
17	0.000	.000	0.000	.000	0.000	0.000	.000	.000	.000	.000	.000	.00	.00	.000	.000	.000	.000						
18	0.000	.000	-.002	.000	-.005	0.000	.000	.000	.001	.000	.000	.00	.00	.000	.000	.001	.000	.332					
19	0.002	.000	0.000	.000	0.000	0.000	.000	.000	.000	.000	.000	.00	.00	.000	.000	.000	.000	.009	.000				
20	0.000	.000	0.000	.000	0.000	0.000	.000	.000	.000	.000	.000	.00	.00	.000	.000	.000	.000	.000	.000	.000			
21	0.000	.000	0.000	.000	0.000	0.000	.000	.000	.000	.000	.000	.00	.00	.000	.000	.000	.000	.000	.000	.000	.000		
22	0.000	.000	0.000	.000	0.000	0.000	.000	.000	.000	.000	.000	.00	.00	.000	.000	.000	.000	.000	.000	.000	.000	.000	
23	0.000	.000	0.000	.000	0.000	0.000	.000	.000	.000	.000	.000	.00	.00	.000	.000	.000	.000	.000	.000	.000	.000	.000	.000
	1	2	3	4	5	6	7	8	9	10	11	12	13	14	15	16	17	18	19	20	21	22	23

Figure 4.57 : Relative modal contributions to the dynamic deck moment response - Node 83

ment response at quarter and mid-spans, the results are summarized in Table 4.7. A larger number of diagonal terms contribute to the moment response at quarter span. The anti-symmetric modes are large contributers to the moment response at quarter-span (about 53.1% of the total response). The total contribution from all terms with individual relative contributions less than 0.0005 add to 16% of the total dynamic response at quarter-span, while it is 46% at mid-span. These results show the importance of considering a large number of modes and the various cross-covariance terms associated with them.

Figures 4.58 and 4.59 show the relative modal contributions to the total dynamic cable displacement responses at quarter and mid-spans and Table 4.8 summarizes this information. A large number of diagonal and off-diagonal terms are needed to estimate the total dynamic response at quarter-span. The individual off-diagonal terms have small relative contributions, whith 76 of them contributing about 5.4% at quarter-span. The anti-symmetric modes are important in estimating the displacement response, with contributions of about 24.4%.

4.4.5 Transient Response

The results discussed in Section 4.3.5 for the side span revealed that the percentage contribution of the first mode of the side span influenced the rate at which the displacement responses grow to attain stationary. It is also of interest to determine the time required for the center span to attain its stationary response especially since its first few modes have frequencies far lower than that of the first mode of the side span. The transient variances of the cable displacement, deck displacement, deck moment, and deck shear were computed for various durations of stationary excitation; and compared with the stationary responses for the general ground motion model. All variances were normalized by dividing by the maximum stationary variance.

Figures 4.60 and 4.61 show the lateral displacement response of the center span cables and deck, respectively. The behavior is opposite to that observed for the side span and

Table 4.7 : Relative modal contributions to the dynamic deck moment.

	Quarter-span (Node 41)	Mid-span (Node 83)
No. of significant diagonal terms.	12	7
Contribution from significant diagonal terms.	82.2%	51.5%
No. of significant diagonal terms due to anti-symmetric modes.	5	0
Contribution of significant diagonal terms due to anti-symmetric modes.	53.1%	0.0%
No. of significant off-diagonal terms.	35	15
Contribution from significant off-diagonal terms.	1.8%	2.5%
Total contribution from all terms with individual relative contributions less than 0.0005.	16.%	46.%

1	0.204																				
2	-.003	0.034																			
3	-.011	-.002	0.022																		
4	-.009	0.015	0.012	0.081																	
5	0.037	0.007	-.022	0.043	0.353																
6	0.001	0.001	0.000	0.001	0.001	.002															
7	0.001	-.001	0.000	-.001	0.002	.001	.002														
8	-.001	0.001	0.000	0.001	-.001	.000	.000	0.001													
9	0.002	-.004	-.001	-.005	0.005	.000	.002	-.002	0.072												
10	0.005	0.001	-.001	0.002	0.005	.001	.000	0.000	-.015	0.112											
11	-.001	0.000	0.000	0.001	-.002	.000	.000	0.000	0.000	-.004	0.003										
12	0.003	-.001	-.001	-.001	0.003	.000	.000	0.000	0.000	0.003	-.003	0.014									
13	0.000	0.000	0.000	0.000	0.000	.000	.000	0.000	0.000	0.000	0.000	0.000	.00								
14	-.002	0.000	0.000	0.000	-.002	.000	.000	0.000	0.000	-.001	0.000	-.001	.00	.007							
15	0.000	0.000	0.000	-.001	0.000	.000	.000	0.000	0.000	0.000	0.000	0.000	.00	.000	.001						
16	0.002	-.003	0.000	-.003	0.002	.000	.000	0.000	0.000	0.003	0.000	-.001	.00	.001	.002	0.015					
17	-.001	0.000	0.000	0.000	-.001	.000	.000	0.000	0.000	0.000	0.000	0.000	.00	.000	.000	-.004	.005				
18	0.000	0.000	0.000	0.000	0.000	.000	.000	0.000	0.000	0.000	0.000	0.000	.00	.000	.000	0.000	.000	.00			
19	0.000	0.000	0.000	0.000	0.000	.000	.000	0.000	0.000	0.000	0.000	0.000	.00	.000	.000	0.000	.000	.00	0.000		
20	0.002	0.000	0.000	0.000	0.001	.000	.000	0.000	0.000	0.000	0.000	0.000	.00	.000	.000	0.001	.000	.00	-.001	0.005	
21	-.001	0.001	0.000	0.002	-.001	.000	.000	0.000	0.000	-.001	0.000	0.000	.00	.000	.000	0.000	.000	.00	0.000	-.001	0.005
22	0.001	0.000	0.000	0.000	0.001	.000	.000	0.000	0.000	0.000	0.000	0.000	.00	.000	.000	0.000	.000	.00	0.000	0.000	-.002
	1	2	3	4	5	6	7	8	9	10	11	12	13	14	15	16	17	18	19	20	21

Figure 4.58 : Relative modal contributions to the dynamic cable displacement response - Node 42

1	**0.637**																						
2	0.000	.000																					
3	**-.025**	.000	**0.037**																				
4	0.000	.000	0.000	.00																			
5	**-.008**	.000	**0.004**	.00	**0.005**																		
6	**-.010**	.000	**0.001**	.00	0.000	**0.038**																	
7	0.000	.000	0.000	.00	0.000	0.000	.00																
8	0.000	.000	0.000	.00	0.000	0.000	.00	.000															
9	**-.005**	.000	**0.002**	.00	**0.001**	**0.003**	.00	.000	**0.185**														
10	0.000	.000	0.000	.00	0.000	0.000	.00	.000	0.000	.00													
11	0.000	.000	**-.002**	.00	0.000	0.000	.00	.000	0.000	.00	0.000												
12	**0.010**	.000	0.000	.00	**-.001**	**-.002**	.00	.000	0.000	.00	**-.001**	**0.059**											
13	0.000	.000	**0.001**	.00	0.000	0.000	.00	.000	0.000	.00	0.000	0.000	.00										
14	**-.005**	.000	0.000	.00	0.000	**0.001**	.00	.000	**-.001**	.00	0.000	**-.002**	.00	**0.018**									
15	0.000	.000	0.000	.00	0.000	0.000	.00	.000	0.000	.00	0.000	0.000	.00	0.000	.000								
16	0.000	.000	**-.001**	.00	0.000	0.000	.00	.000	0.000	.00	0.000	0.000	.00	0.000	.000	.00							
17	**0.004**	.000	0.000	.00	**0.003**	**-.001**	.00	.000	**0.001**	.00	0.000	0.000	.00	**-.001**	.000	.00	**0.016**						
18	0.000	.000	0.000	.00	0.000	0.000	.00	.000	0.000	.00	0.000	0.000	.00	0.000	.000	.00	0.000	.00					
19	0.000	.000	**0.001**	.00	0.000	0.000	.00	.000	0.000	.00	0.000	0.000	.00	0.000	.000	.00	0.000	.00	.00				
20	**-.004**	.000	0.000	.00	0.000	**0.001**	.00	.000	**-.001**	.00	0.000	**0.001**	.00	0.000	.000	.00	**-.001**	.00	.00	**0.013**			
21	0.000	.000	**-.001**	.00	0.000	0.000	.00	.000	0.000	.00	0.000	0.000	.00	0.000	.000	.00	0.000	.00	.00	0.000	.000		
22	**0.004**	.000	0.000	.00	0.000	**-.001**	.00	.000	**0.001**	.00	0.000	**-.001**	.00	**0.001**	.000	.00	0.000	.00	.00	**-.001**	.000	**.009**	
23	0.000	.000	0.000	.00	0.000	0.00	.000	.000	0.000	.00	0.000	0.000	.00	0.000	.000	.00	0.000	.00	.00	0.000	.000	.000	.000
	1	**2**	**3**	**4**	**5**	**6**	**7**	**8**	**9**	**10**	**11**	**12**	**13**	**14**	**15**	**16**	**17**	**18**	**19**	**20**	**21**	**22**	**23**

Figure 4.59 : Relative modal contributions to the dynamic cable displacement response - Node 84

Table 4.8 : Relative modal contributions to the dynamic cable displacements.

	Quarter-span (Node 42)	Mid-span (Node 84)
No. of significant diagonal terms.	18	10
Contribution from significant diagonal terms.	93.7%	101.7%
No. of significant diagonal terms due to anti-symmetric modes.	7	0
Contribution of significant diagonal terms due to anti-symmetric modes.	24.4%	0.0%
No. of significant off-diagonal terms.	76	38
Contribution from significant off-diagonal terms.	5.4%	-3.7%
Total contribution from all terms with individual relative contributions less than 0.0005.	0.90%	-2.%

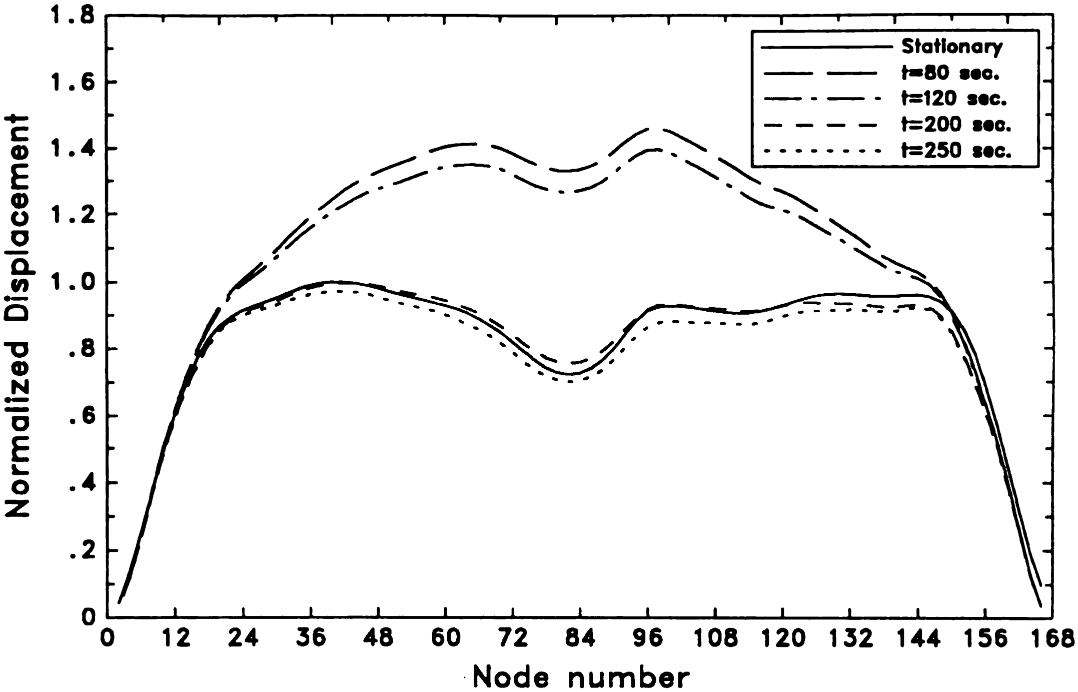

Figure 4.60 : Variation of normalized transient displacement variances of the center span cables

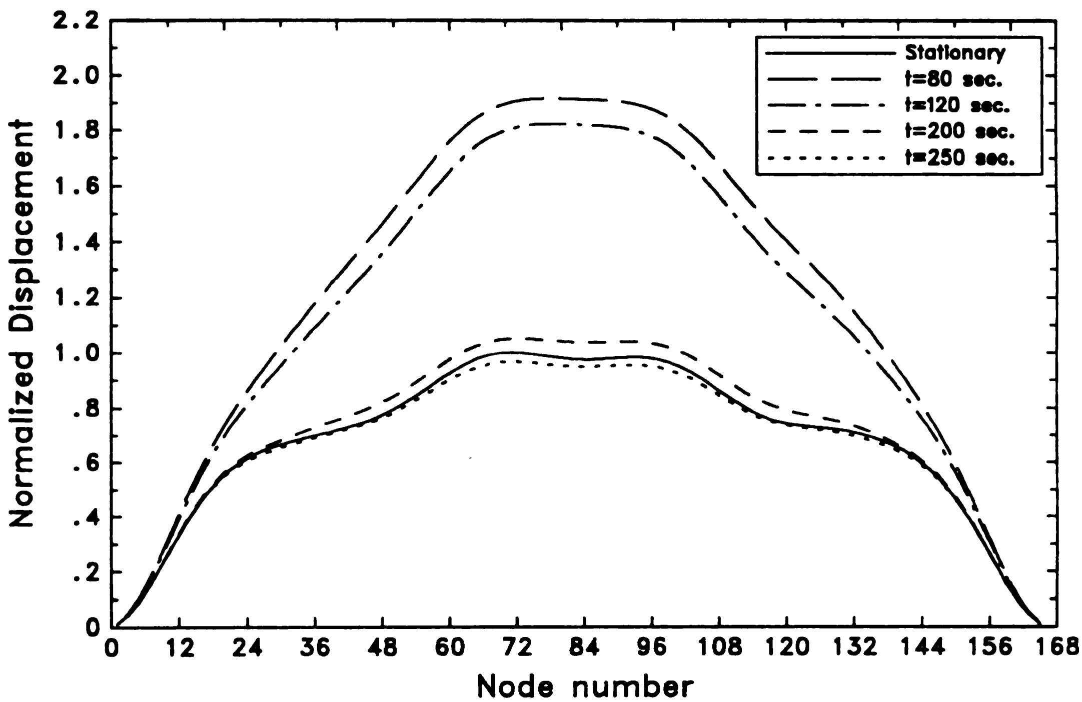

Figure 4.61 : Variation of normalized transient displacement variances of the center span deck

to what would intuitively be expected. Instead of the response gradually growing to the stationary response, there is a strong overshoot of the response for short durations, and then it gradually approaches the stationary variance from above. In order to explain this behavior a thorough study was conducted on the integrand in equation (3.31). This function can be written as

$$H_j(-\omega, t)\, H_k(\omega, t)\, S_{\ddot{u}_{Rl}\ddot{u}_{Rm}}(\omega) \tag{4.1}$$

where $H_j(\omega, t)$ is expressed by equation (3.57). For the diagonal element j, equation (4.1) can be written as

$$|H_j(\omega, t)|^2 S_{\ddot{u}_{Rl}\ddot{u}_{Rm}}(\omega) \tag{4.2}$$

Caughy and Stumpf (1961) studied the transient response of a single-degree-of-freedom system under ideal white noise excitation using equation (4.2). The response was evaluated for different natural frequencies and different damping factors of the single d.o.f. system. As expected the response variance approaches the stationary value as time increases, and the larger damping values result in lower stationary values and allow the response to become stationary in a shorter time. The transient variance did not overshoot the stationary variance. This, however, is not always the case with the transient response. Barnoski and Maurer (1969) studied the response of a single-degree-of-freedom system, with excitation having the input autocorrelation function

$$R_F(\tau) = R_0 e^{-\alpha|\tau|} \cos\omega\tau \tag{4.3}$$

where α = decay coefficient of noise correlation function

ω = frequency of noise correlation function

and found that the mean-square response does indeed overshoot the stationary value. Whether or not an overshoot is obtained depends on the shape of the excitation spectrum and on the frequency and damping of the oscillator. An overshoot is obtained only when the frequency of the oscillator is very low and the excitation spectrum varies sharply at low frequencies.

The integrand function of equation (4.2) is studied for two different modes (mode 1 of the center span and mode 1 of the side span) at two different times (5 and 10 seconds). A plot of the integrand function is presented in Figure 4.62 and 4.63. Figure 4.62 indicates that the area under the integrand function for t = 5 seconds is substantialy larger than that for t = 10 seconds, which would result in the first mode response at 5 seconds being much larger than that at 10 seconds. In Figure 4.63, however, the area under the integrand function at t = 5 seconds is smaller than that at t = 10 seconds, which results in the first mode response at 5 seconds being smaller than that at 10 seconds. These results indicate that the integration of equation (4.2) is dominated by the behavior of the cross spectral density function around the natural frequencies ω_j. The first natural frequency of the center span is very low compared to most structures and, because of this the nature of the fitted autospectra at low frequencies strongly affects the estimated displacement response of the low frequency modes.

Both the estimated autospectrum and the fit of the autospectrum shown in Figure 3.2 are not accurate at very low frequencies. In estimating the spectrum from the accelerogram, the band width of the smoothing window used to achieve stability was 0.5 Hz. This adversely affects the resolution in the estimated spectrum, and the estimates are expected to be biased, especially at very low frequencies. It is not possible to get good resolution unless the recorded accelerogram has a very long duration of strong motion, or several similar accelerograms are recorded. In view of the inaccuracy in the excitation spectrum at very low frequencies, and in view of the fact that the nature of the excitation autospectrum at very low frequencies strongly affects the transient response of the low frequency modes, the overshoot in the transient displacement response should be considered as qualitative information, and the magnitude of the overshoot should not be considered as accurate.

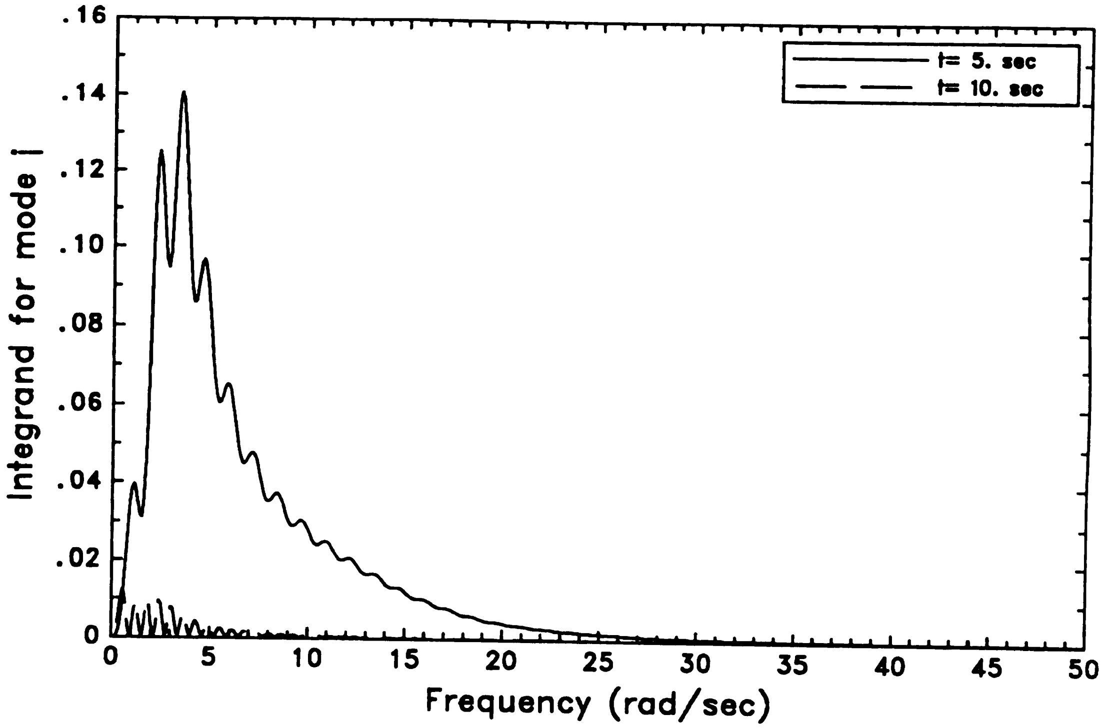

Figure 4.62 : Integrand function for mode 1 of the center span

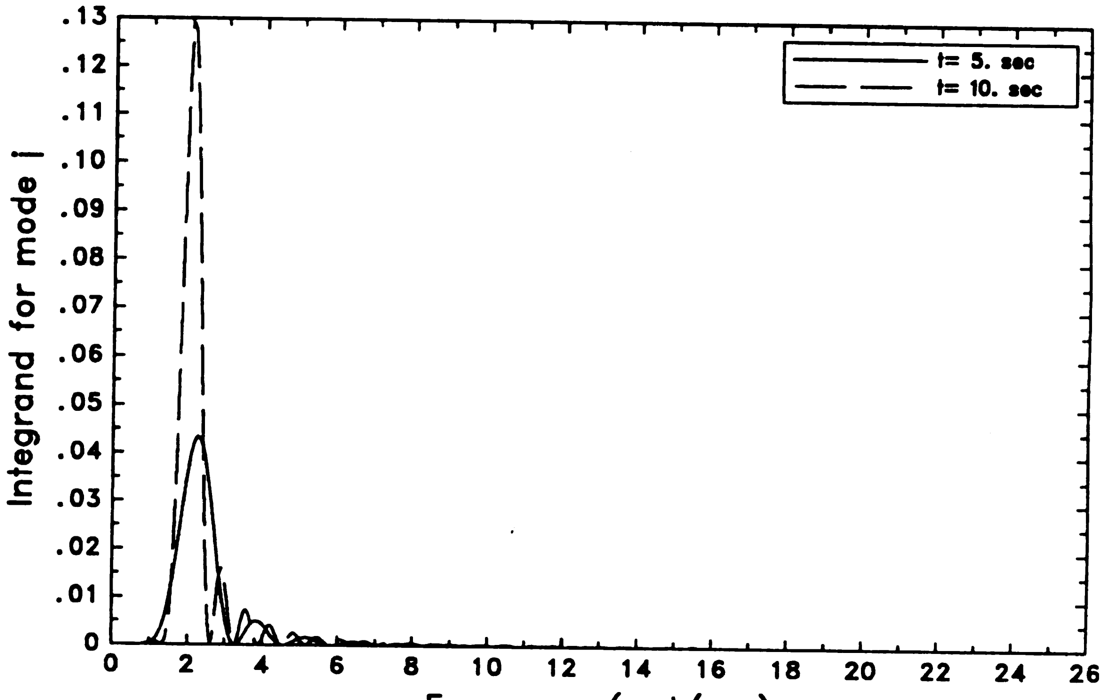

Figure 4.63 : Integrand function for mode 1 of the side span

The modal contributions to the center span *force* response presented in Section 4.4.4 reveal that the lower modes hardly contribute. Since only the first few modes display the overshoot behavior, and these do not contribute significantly to the force responses, the transient force responses do not overshoot their stationary values. This behavior is seen in Figures 4.64 and 4.65. Figure 4.64 show the transient moment response of the center span deck at various times. Results of node 41 indicates that 76.6%, 98.3%, and 99.1% of the stationary response is achieved at times of 5, 40, and 60 seconds, while for node 83 the corresponding numbers are 62.7%, 97.9%, and 99.2%.

The results presented here indicate that for usual ground motion durations, the assumption of stationarity may grossly overestimate the center span force responses, and significantly under-estimate the displacement response. Therefore transient response must be considered when analyzing the center span. However, to accurately estimate the transient displacement response, the excitation autospectrum should be specified carefully at very low frequencies based on more abundant data.

The transient responses of the center span using the three ground motion models were computed at t=20 seconds. The responses, normalized by dividing by the maximum response along the span due to the general ground motion model at t=20 seconds, are presented in Figures 4.66 to 4.69 for the cable and deck displacements , moment and shear of the center span. The normalized transient force responses (moment and shear) of the center span deck presented in Figures 4.68 and 4.69 reveal almost an identical behavior to the normalized stationary responses presented previously in Figures 4.44 and 4.45. This means that the conclusions based on comparing the force responses along the center span due to the three stationary ground motion models are also valid for the transient responses. However, the normalized transient displacement response of the center span cable and deck (Figures 4.66 and 4.67) are significantly different from the normalized stationary responses in Figures 4.42 and 4.43. This is due to the strong participation from the first few low fre-

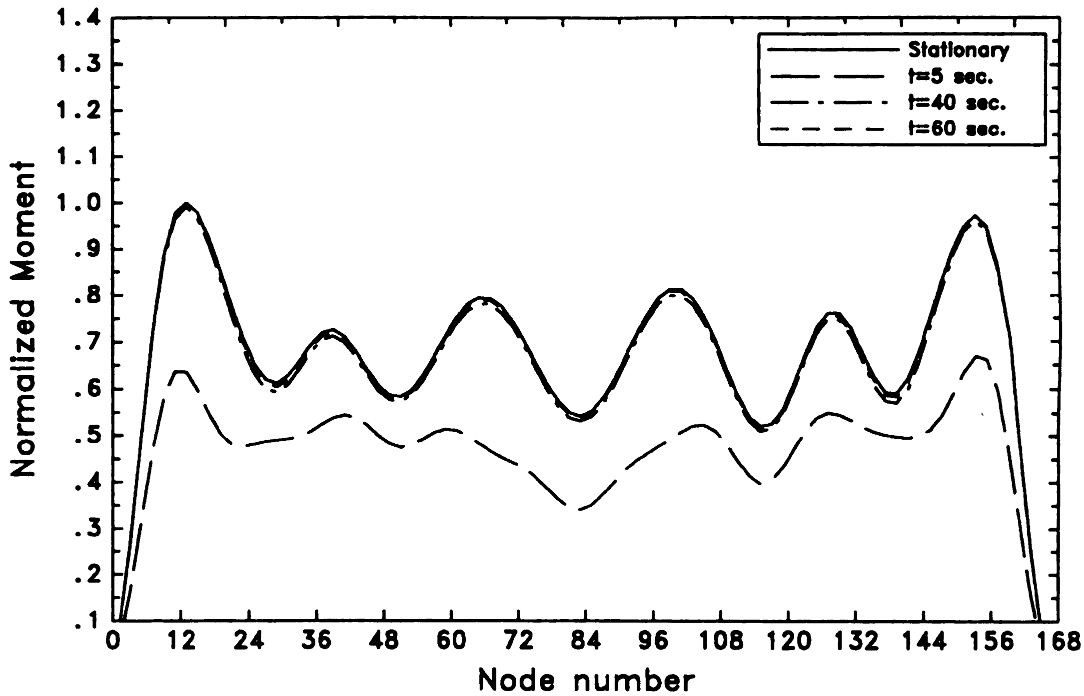

Figure 4.64 : Variation of normalized transient moment variances of the center span deck

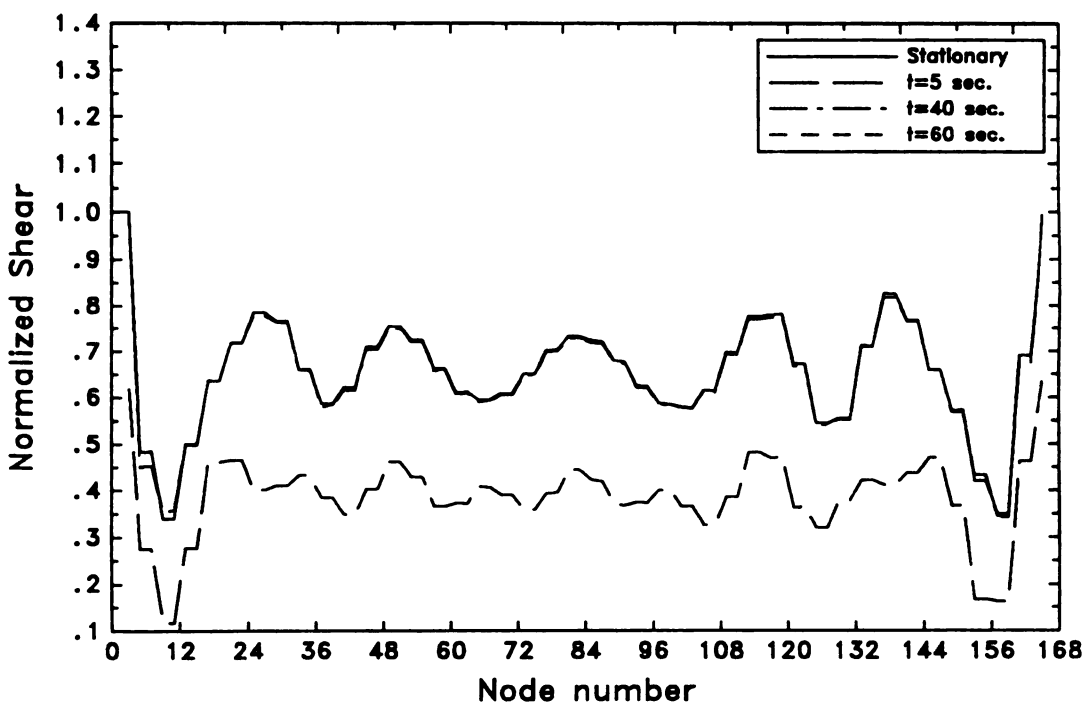

Figure 4.65 : Variation of normalized transient shear variances of the center span deck

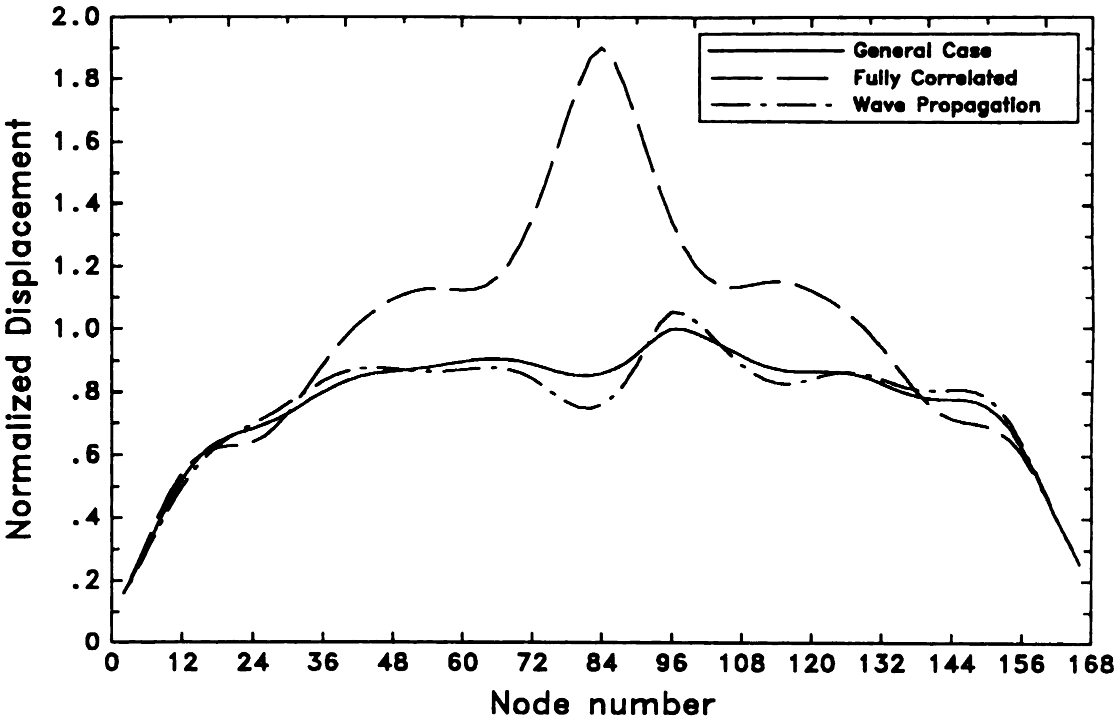

Figure 4.66 : Normalized transient displacement variances of the center span cables due to three ground motion models at t=20 seconds

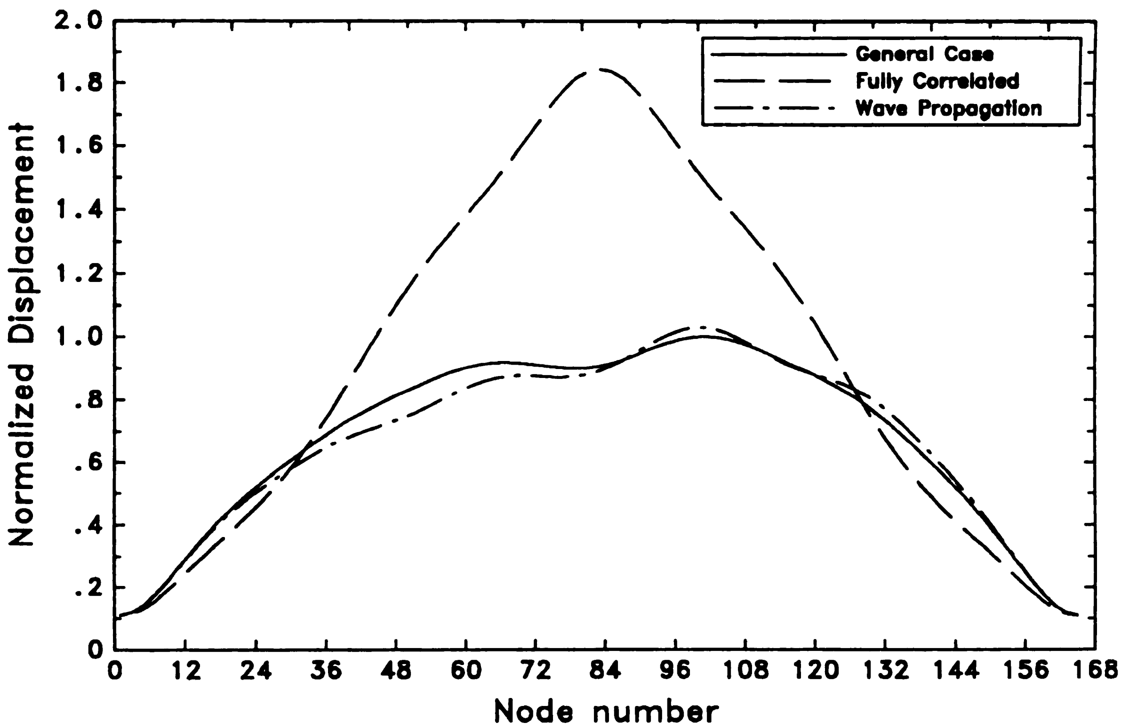

Figure 4.67 : Normalized transient displacement variances of the center span deck due to three ground motion models at t=20 seconds

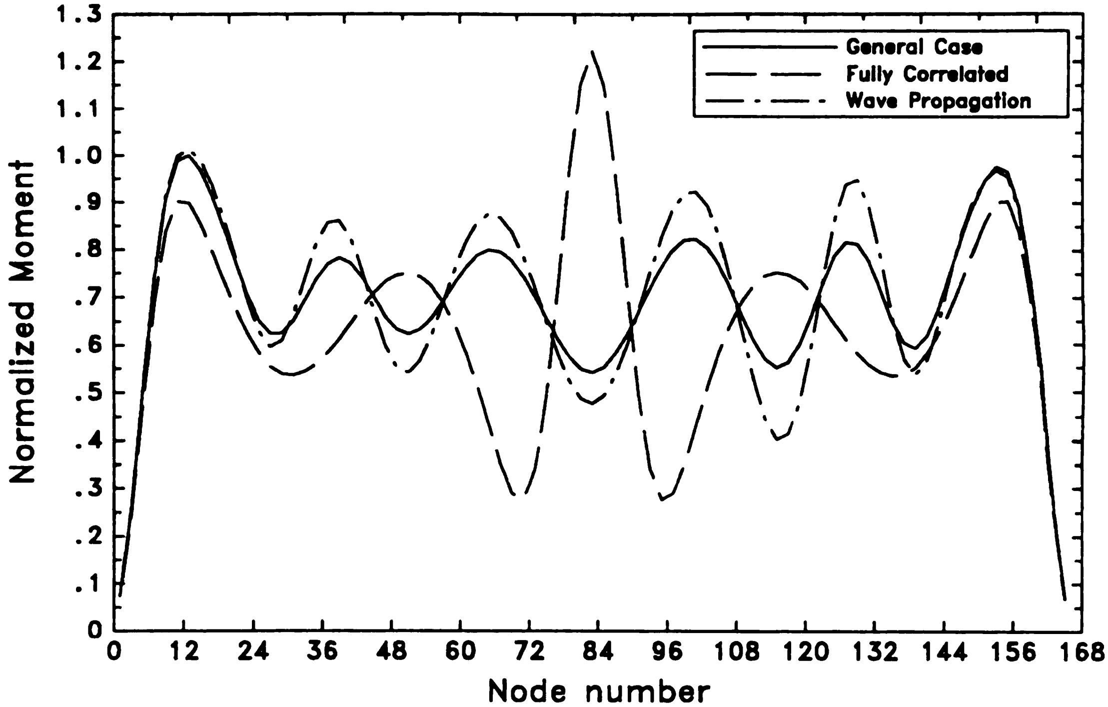

Figure 4.68 : Normalized transient moment variances of the center span deck due to three ground motion models at t=20 seconds

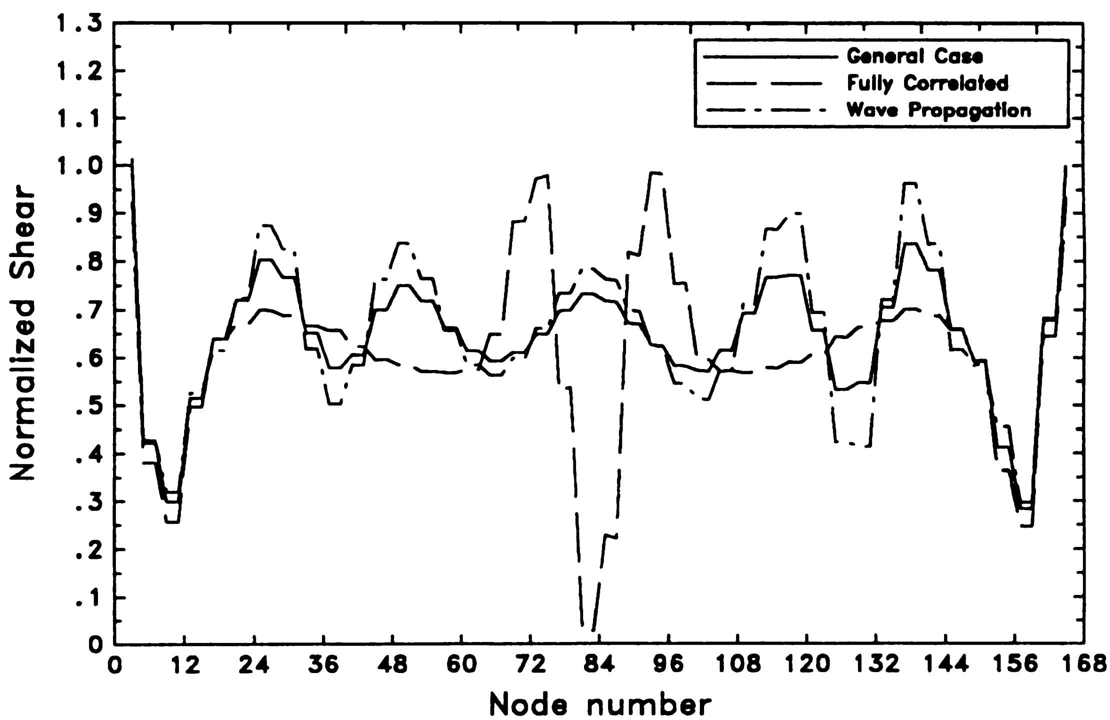

Figure 4.69 : Normalized transient shear variances of the center span deck due to three ground motion models at t=20 seconds

quency modes, whose relative contributions are quite different for transient and stationary responses.

4.5 Shear Deformation

It is of interest to study the effect of including shear deformation on the seismic response of the suspension bridge. Shear deformation was included in calculating the response of the side and center spans by substituting equations (2.23) and (2.28) in place of equations (2.22) and (2.27), respectively, with the remainder of the analysis being the same.

4.5.1 Side Span

The eigenvalue problem in equation (3.9) was assembled and solved for the side span natural frequencies and mode shapes. A softening behavior of the side span occured with a drop in the value of the first natural frequency to 0.27 Hz compared to 0.31 Hz when shear deformation was excluded. The spectrum of the undamped natural frequencies with and without the effect of shear deformation are presented in Figures 4.62 and 4.63. Figure 4.71

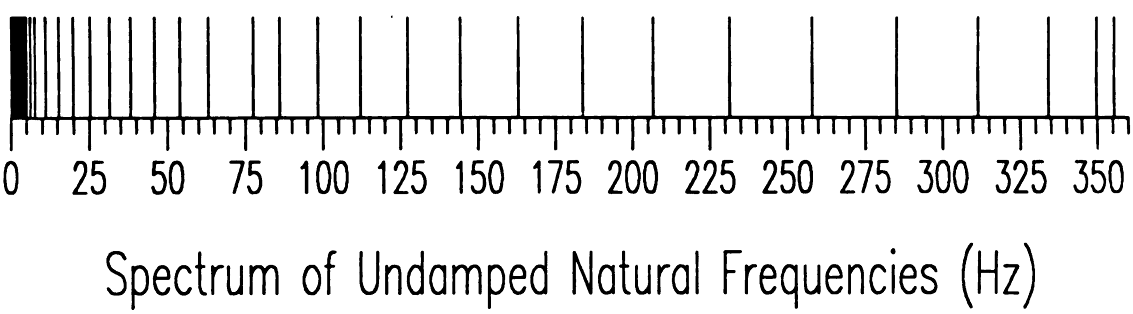

Figure 4.70 : Undamped natural frequencies of the side span excluding shear deformation

indicates that many of the modes are closely spaced and span a small range of frequencies when the shear deformation is included. Comparing Figure 4.71 with Figure 4.70, shows

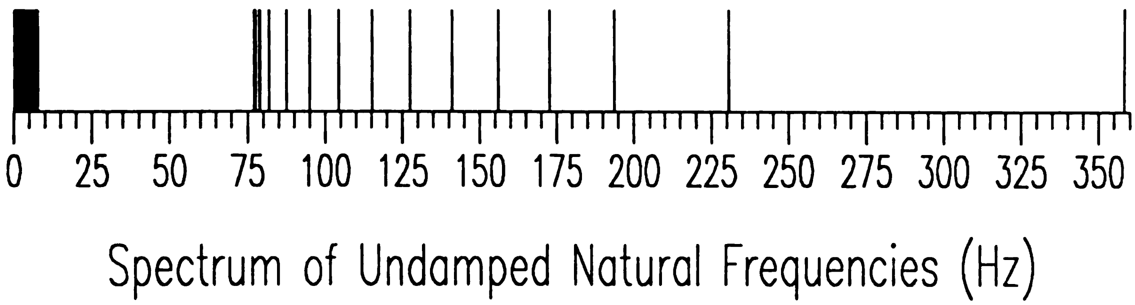

Figure 4.71 : Undamped natural frequencies of the side span including shear deformation

that modes with frequencies between 11.2 Hz and 63 Hz are shifted to between 4.6 Hz and 7.6 Hz.

The first nine mode shapes of the side span are presented in Figure 4.72. A comparison of the mode shapes for the two cases (including and excluding shear deformation) in Figures 4.1 and 4.64 reveal that the shapes of the first mode are similar, with the lateral displacement of the cables being smaller when shear deformation is included. The same behavior is seen for the second mode but the lateral displacement of the deck is now smaller when shear deformation is included. The mode order is also switched, with modes 4,5, 6, and 7 (for the analysis excluding shear deformation) becoming modes 5, 4, 7, and 8 (for the analysis including shear deformation).

The total lateral displacement response of the side span cables and deck are presented in Figures 4.73 and 4.74, respectively, for the two analyses including and excluding shear deformation using the general ground motion model. Figure 4.73 indicates that the cable displacement response when shear deformation included is consistently lower than that when shear deformation is excluded. Figure 4.74 shows a similar behavior for the deck displacement response.

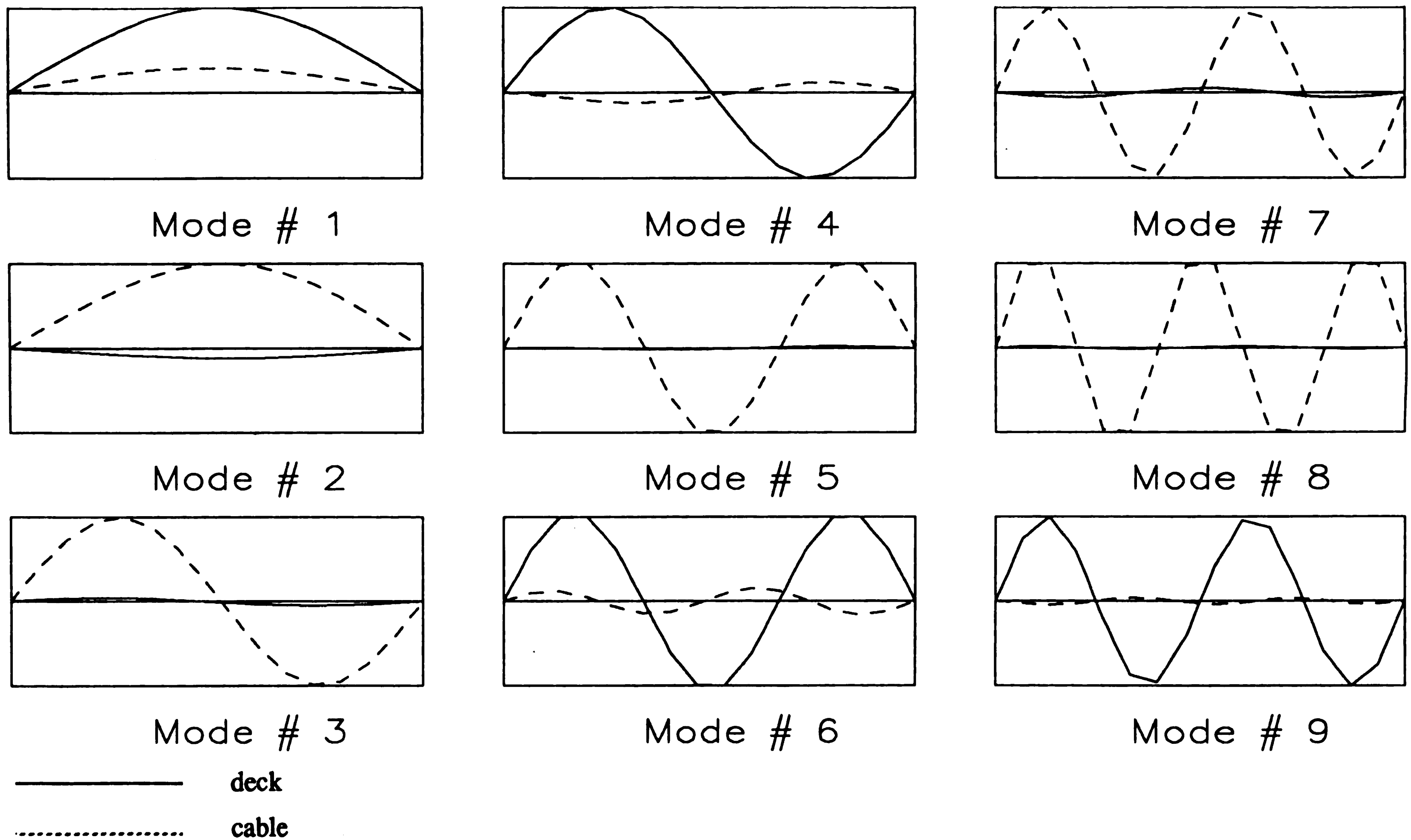

Figure 4.72 : First nine mode shapes of the side span including shear deformation

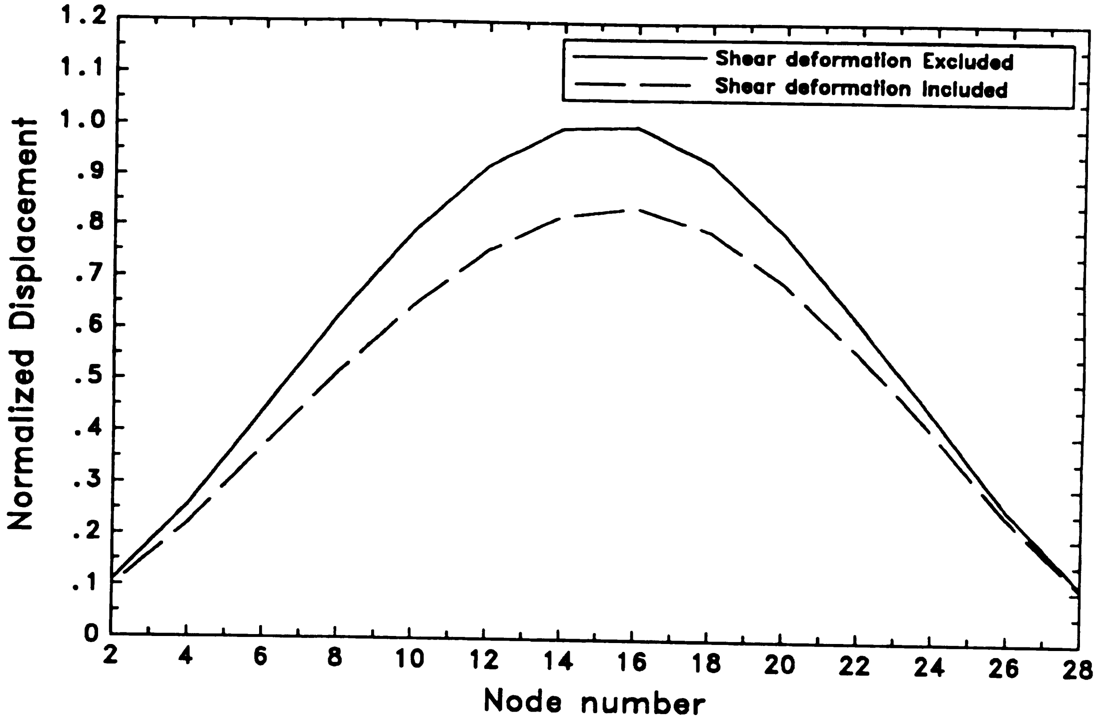

Figure 4.73 : Normalized displacement variances of the side span cables

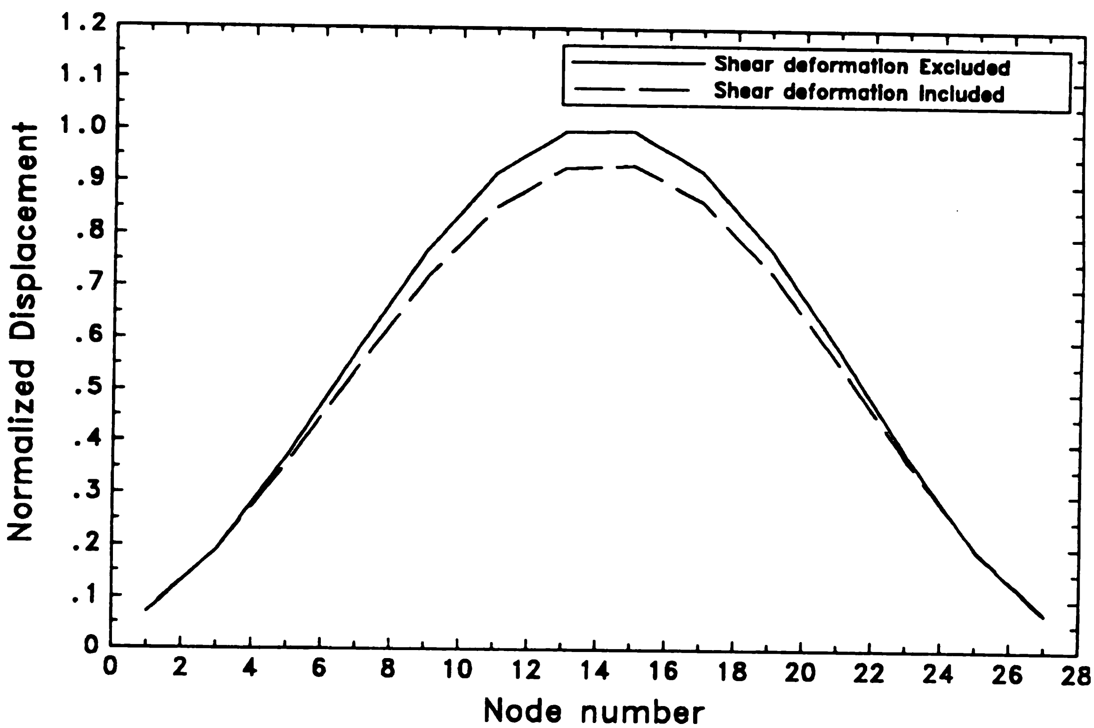

Figure 4.74 : Normalized displacement variances of the side span deck

Figures 4.75 and 4.76 show the side span deck moment and shear responses for the analyses excluding and including shear deformation using the general ground motion model. Figure 4.75 shows a severe drop in the deck moment response (53% at mid-span) when shear deformation is included. Figure 4.76 indicates a similar behavior for the shear response, with the maximum drop of 60% occuring at nodes close to the supports.

The reduction in the lateral displacement response of the side span deck when shear deformation is included is primarily due to the drop in the first natural frequency which contributes the most (see Figures 4.17 and 4.18). The excitation spectrum has lower power at the reduced first modal frequency, hence giving rise to a smaller response. This behavior is illustrated in Table 4.9 which shows the ratios of corresponding modal displacement responses for the analyses excluding and including shear deformation. The first mode response is reduced by about 9% when shear deformation is included.

The moment response of the side span deck has dominant contributions from modes 1, 2, and 5 for nodes 7 and 8 (see Figures 4.19 and 4.20). The ratios of corresponding modal moment responses shown in Table 4.9 reveal that the moment response of mode 1 when shear deformation is included is 44% and 33% of that when shear deformation is excluded at quarter and mid-span, respectively. Mode 5 is switched to mode 4 when shear deformation is included, and its response is 24% and 21% of that when shear deformation is excluded. The large reductions in the responses of modes 1 and 5 explain the severe drop in moment response when shear is included.

4.5.2 Center Span

As for the side span, the eigenvalue problem of equation (3.9) was assembled and solved for the center span natural frequencies and mode shapes. The first natural frequency remains the same as that when shear deformation is excluded. Results indicate that the first 120 modes span a frequency range between 0 Hz to 7.25 Hz compared to a range of 0 Hz to 30.95 Hz when shear deformation is not included. Furthermore, the first 166 modes span

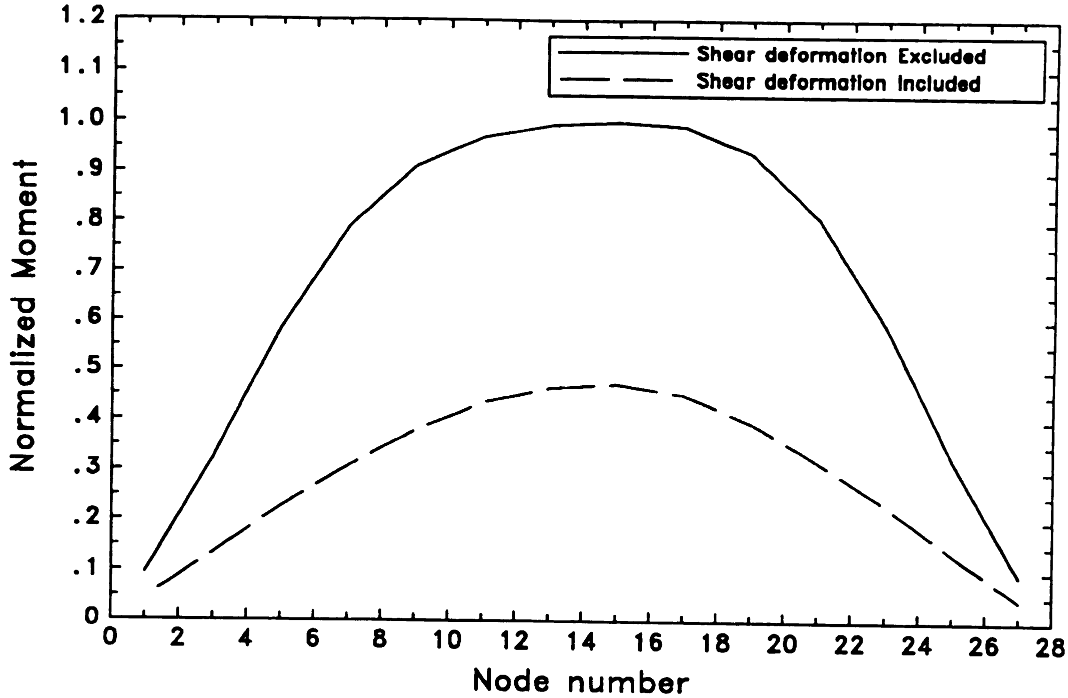

Figure 4.75 : Normalized moment variances of the side span deck

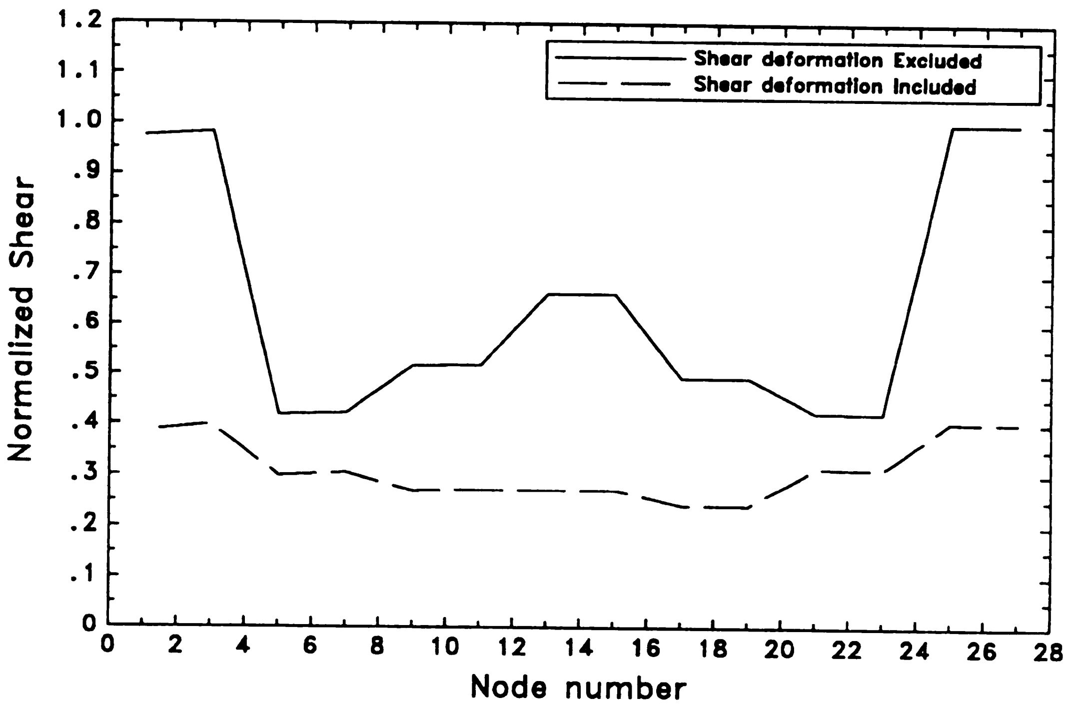

Figure 4.76 : Normalized shear variances of the side span deck

Table 4.9 : Ratio of corresponding modal responses of the side span from analyses including and excluding shear deformation

Mode Number				Quarter-span (Node 7)		Mid-span (Node 15)	
Shear deformation excluded Case # 1		Shear deformation included Case # 2		$\frac{\text{Modal variance for case \# 2}}{\text{Modal variance for case \# 1}}$		$\frac{\text{Modal variance for case \# 2}}{\text{Modal variance for case \# 1}}$	
No.	Frequency(Hz)	No.	Frequency(Hz)	Displacement	Moment	Displacement	Moment
1	0.3133	1	0.2678	0.9068	0.4400	0.9162	0.3297
2	0.3435	2	0.3407	1.1763	0.5829	1.6336	0.7074
3	0.6561	3	0.6555	0.0000	0.0000	0.0000	0.0000
4	0.9841	5	0.9834	0.0000	0.0000	0.0000	0.0000
5	1.2450	4	0.7609	1.8171	0.2402	1.0000	0.2144
6	1.3235	7	1.3228	0.0000	0.0000	0.0000	0.0000
7	1.6769	8	1.6762	0.0000	0.0000	0.0000	0.0000

a frequency range from 0 Hz to 11.82 Hz, and mode 167 jump to a frequency of 150.78 Hz. Therefore, modes in the frequency range between 12 Hz and 150 Hz are completely lost when shear deformation is included, and their corresponding contribution on the response vanishes. The spectrum of the undamped natural frequencies (excluding and including shear deformation) are presented in Figures 4.77 and 4.78, respectively.

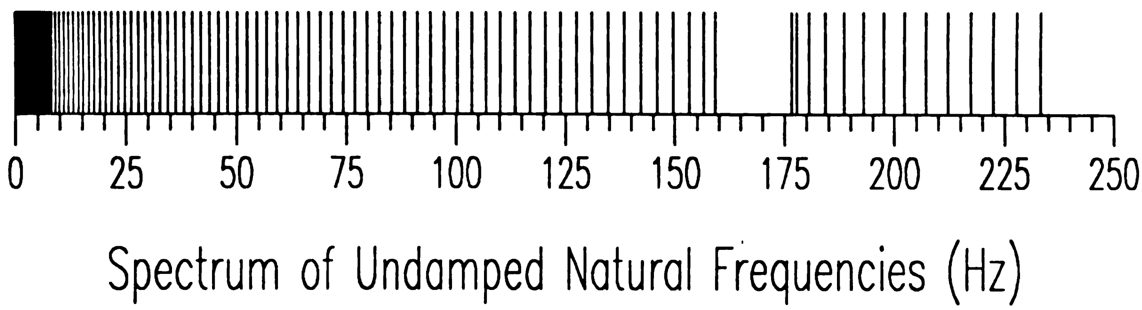

Figure 4.77 : Undamped natural frequencies of the Golden Gate bridge center span excluding shear deformation

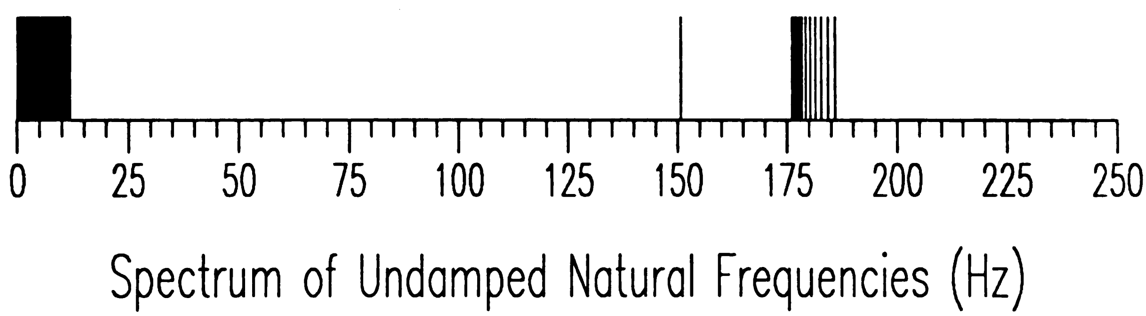

Figure 4.78 : Undamped natural frequencies of the Golden Gate bridge center span including shear deformation

The change in the natural frequencies when shear deformation is included is dramatic and somewhat unexpected. This behavior may be partly due to the use of a simple beam model to represent a stiffening truss which has a complex arrangement of members. Seismic response studies using 3-D models that have been conducted (Baron, et. al. 1976), have all used beam elements to simplify stiffening trusses and therefore no literature appears to be available to confirm the behavior seen here when shear deformation is included.

The first eighteen mode shapes of the center span are shown in two sets in Figures 4.79 and 4.80. The first five modes when shear deformation is included are similar to those when shear deformation is excluded (see Figures 4.79 and 4.2). A switching of the mode rank starts at mode 6, which switches to mode 7 when shear deformation is included.

The total lateral displacement response of the center span cables and deck are presented in Figures 4.81 and 4.82, respectively, for the analyses of including and excluding shear deformation using a general ground motion model. Figure 4.81 indicates that the displacement response when shear deformation included is 15% to 17% lower than that when shear deformation is excluded. Figure 4.82 on the other hand indicates that when shear deformation is included the lateral displacement response of the deck increases at most locations, while decreasing slightly near mid-span.

Figures 4.83 and 4.84 show the center span deck moment and shear responses for the analyses excluding and including shear deformation using a general ground motion model. Figure 4.83 show a severe drop in the deck moment response, when shear deformation is included. Figure 4.84 indicates similar drop for the shear response.

The increase in the lateral displacement response of the center span deck can be explained by studying the contributions of the modes contributing most to the response. Figure 4.54 indicates that modes 1, 2, 3, and 4 contribute 53%, 26.6%, 3.5%, and 0.6% of the total dynamic response when shear deformation is excluded. Table 4.10 shows the ratios of modal variances when shear deformation is included to corresponding modal variances when shear deformation is excluded . The modal response ratios reveal that the displacement response of modes 1 and 2 are not affected significantly when shear deformation is

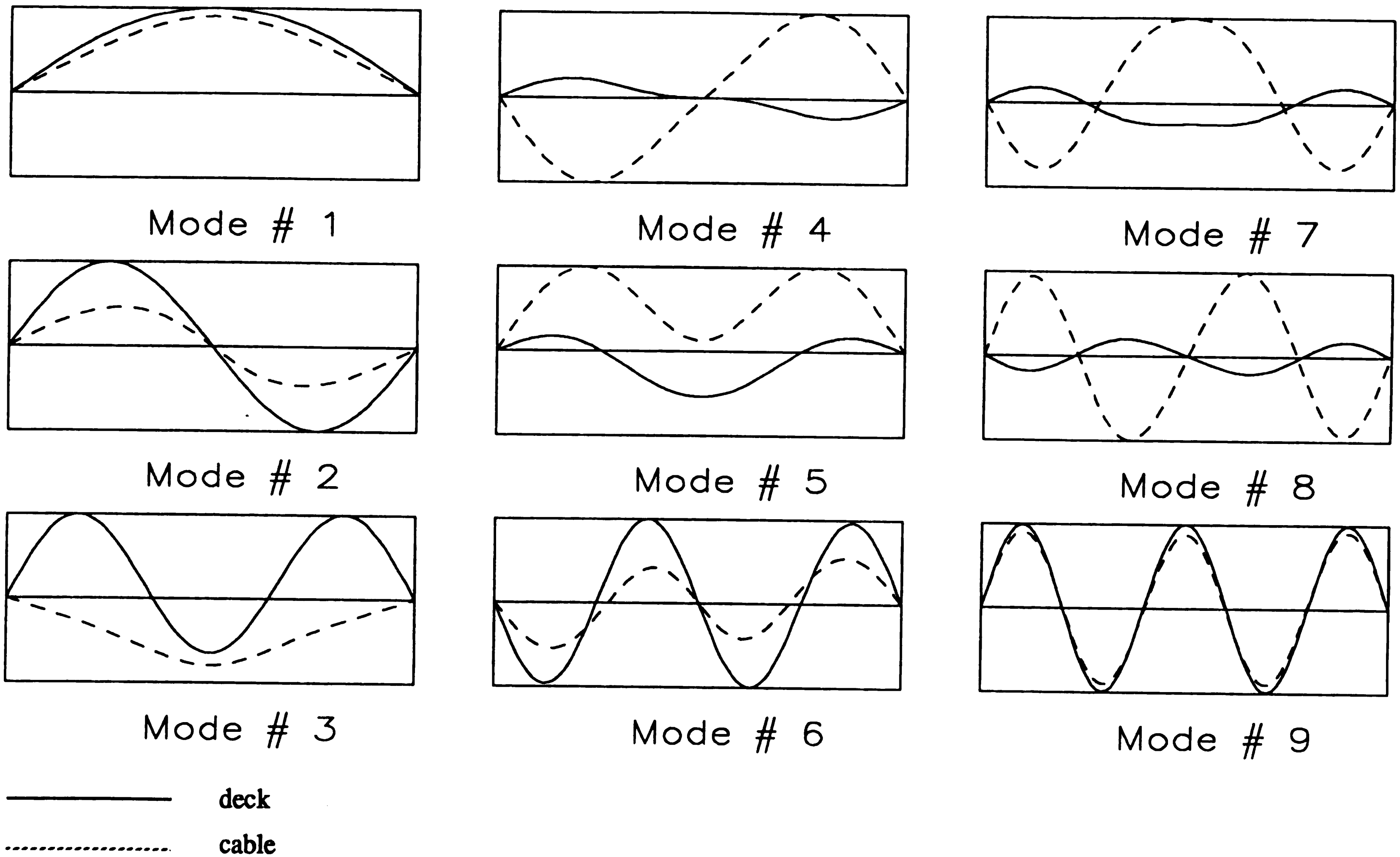

Figure 4.79 : First set of mode shapes of the center span including shear deformation

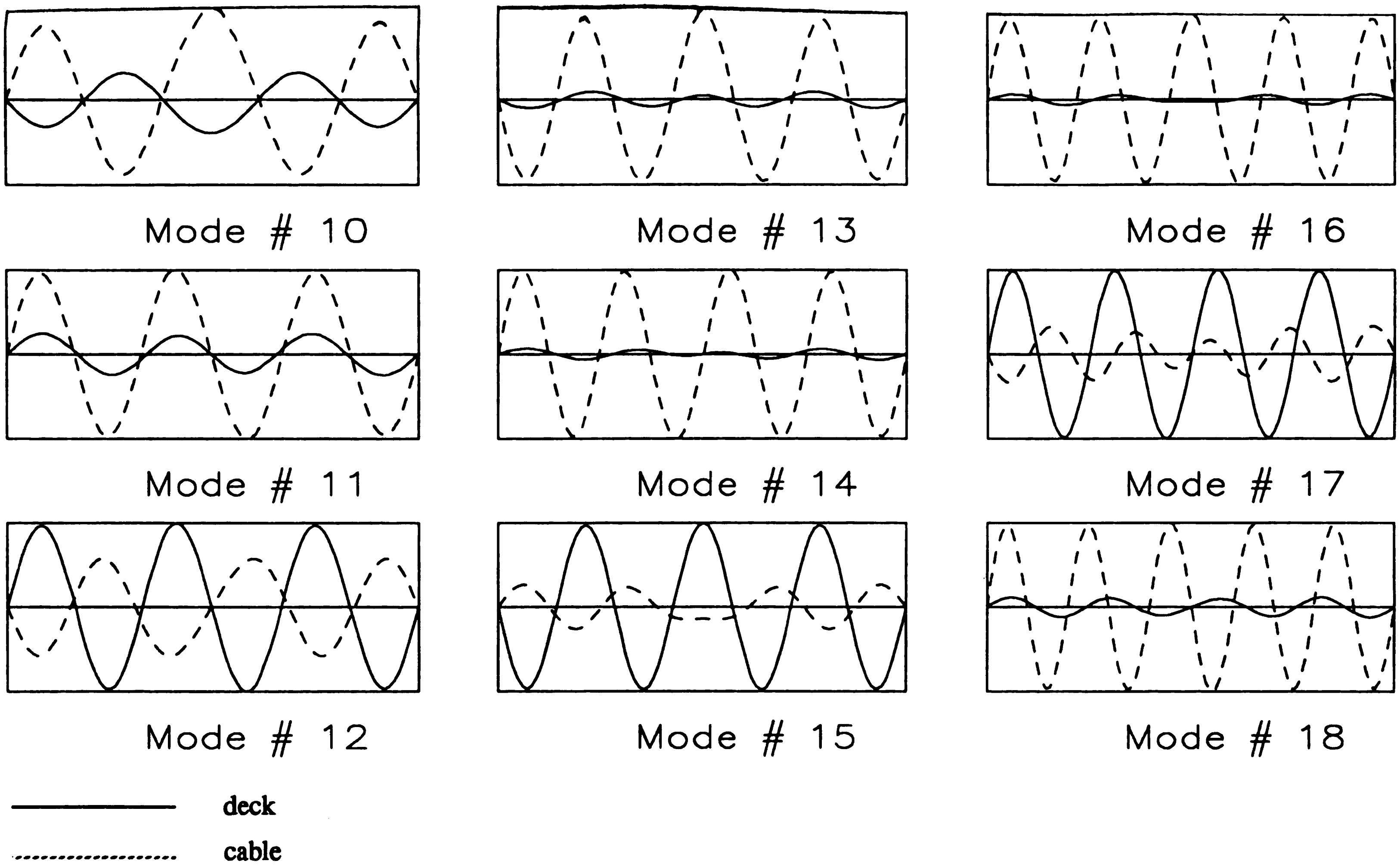

Figure 4.80 : Second set of mode shapes of the center span including shear deformation

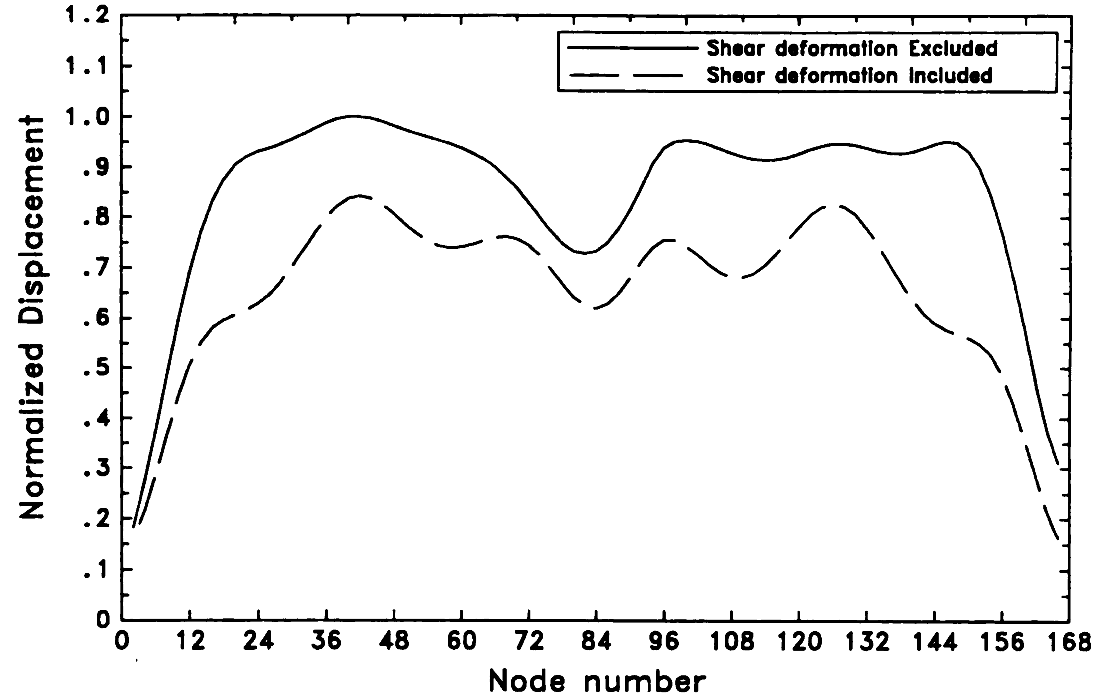

Figure 4.81 : Normalized displacement variances of the center span cables

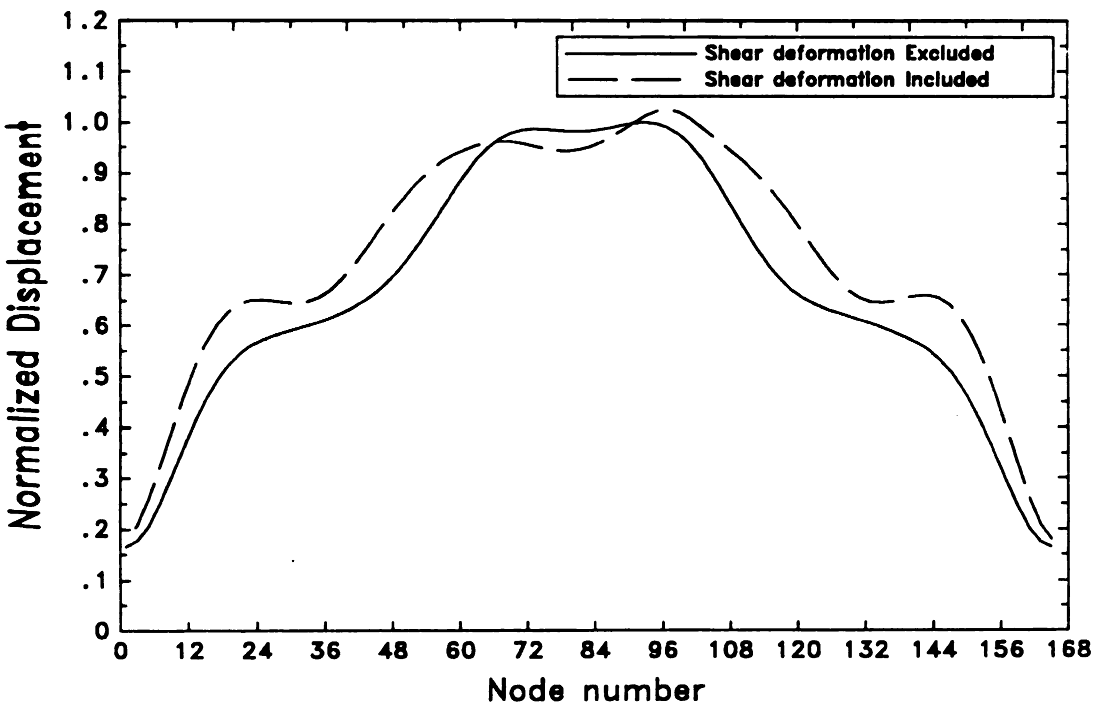

Figure 4.82 : Normalized displacement variances of the center span deck

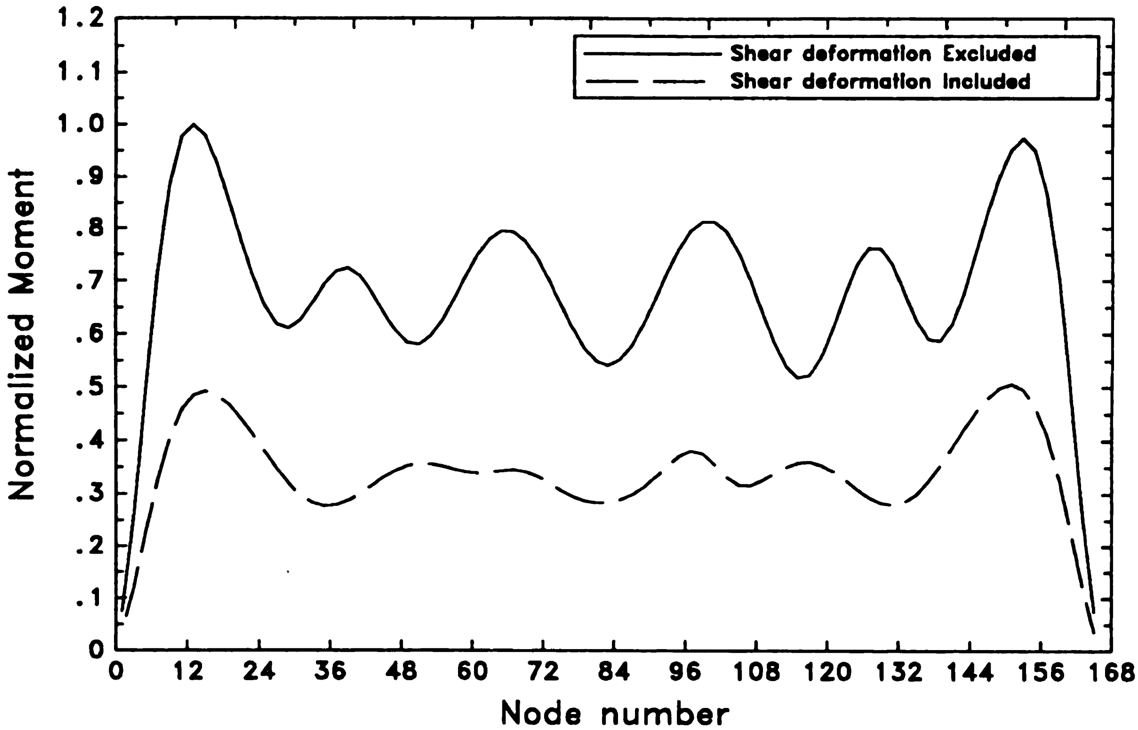

Figure 4.83 : Normalized moment variances of the center span deck

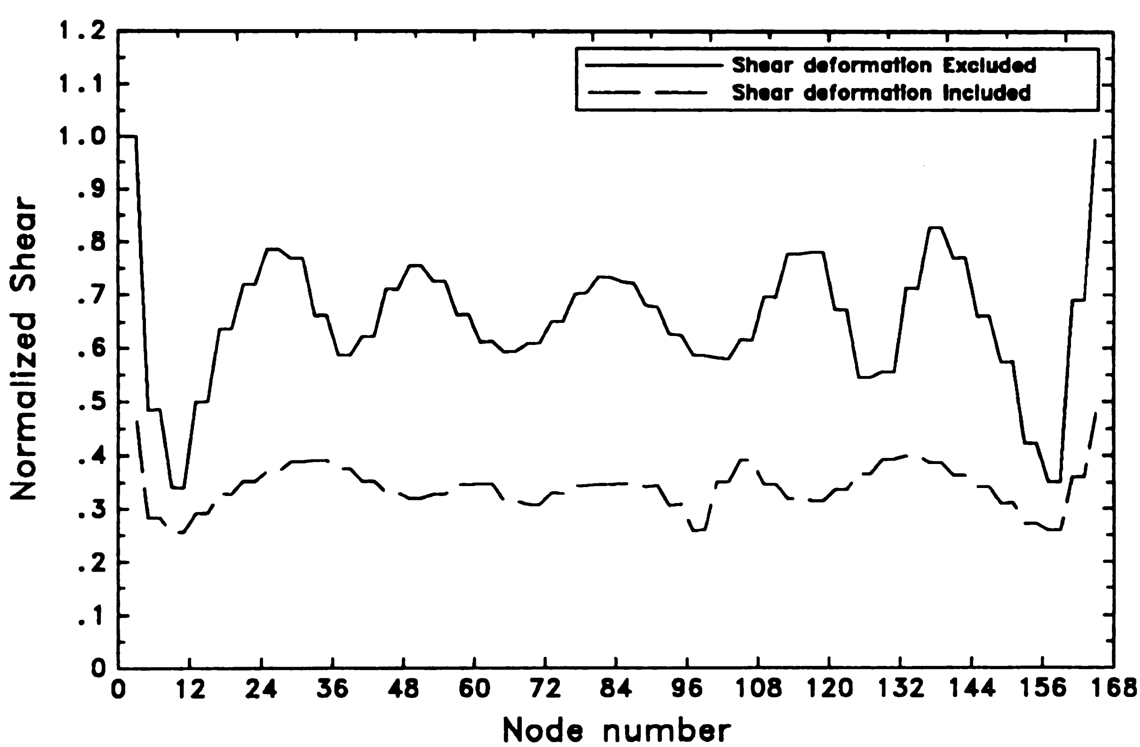

Figure 4.84 : Normalized shear variances of the center span deck

Table 4.10 : Ratios of corresponding modal responses of center span including and excluding shear deformation.

Mode Number				Quarter-span (Node 41)		Mid-span (Node 83)	
Shear deformation excluded Case # 1		Shear deformation included Case # 2		$\frac{\text{Modal variance for case \# 2}}{\text{Modal variance for case \# 1}}$		$\frac{\text{Modal variance for case \# 2}}{\text{Modal variance for case \# 1}}$	
No.	Frequency(Hz)	No.	Frequency(Hz)	Displacement	Moment	Displacement	Moment
1	0.0480	1	0.0478	1.0048	2.4816	0.9864	1.6577
2	0.1079	2	0.1039	0.9644	2.0445	0.0000	0.0000
3	0.1985	3	0.1833	2.8713	6.0502	8.1504	4.4566
4	0.2189	4	0.2180	0.6446	1.1280	0.0000	0.0000
5	0.2238	5	0.2186	0.0000	0.3259	0.4586	0.3155
6	0.3249	7	0.3226	0.0000	0.0000	0.4835	0.0000
7	0.3537	6	0.3035	0.0000	0.0000	0.0000	0.0000
8	0.3910	8	0.3780	0.0000	0.0000	0.0000	0.0000

included. The displacement response of mode 3, however, is is increased significantly when shear deformation is included.

The moment response of the center span deck at node 41 is mainly contributed to by mode 15 when shear deformation is excluded. The relative contribution of this mode is found to be 49.6% (see Figure 4.56). This mode becomes mode 12 when shear deformation is included and its response is reduced to 21.7%. Figure 4.57 indicates that the relative modal contribution of the diagonal terms of the first 23 modes contribute only 51.5% of the total dynamic response, and the relative modal contribution of the cross terms sum to only 2.5%. The remaining contributions to the moment response are therefore from higher modes. When shear deformation is included, the frequencies of most of these higher modes shift to low values (see Figure 4.78), and as a result, the transformed modes no longer contribute significantly to the moment response.

The results of this section indicate that a dramatic change in the dynamic properties and response of the center span occurs when shear deformation is included in the analysis.

5. Summary and Conclusions

5.1 Summary

This research was conducted to study the effects of spatially varying ground motion on the lateral response of the Golden Gate suspension bridge. The bridge has a center span of length 4,200 feet and side spans of length 1,125 feet. The ground motion model proposed by Harichandran and Vanmarcke (1986), which accounts for the propagation and correlation between the accelerations at two different points, was used.

Three ground motion models were used in the study. The first was the general ground motion model, which included both the travelling wave effect as well as the correlation effects between the acceleration at two different points characterized by a coherency function. The second model was for fully correlated ground motion in which all supports move identically. The third model included only wave propagation and neglected coherency loss.

5.1.1 Finite Element Model

The method adopted for analysis was a 2-D finite element based technique, which takes into account the characteristics of both the cable and deck. In this model the cable is idealized by a set of string elements, while the deck is idealized by a set of beam elements. The two types of elements, connected by rigid hangers, form the bridge element. This technique was applied to the spans of the Golden Gate bridge to assemble the overall mass and stiffness matrices.

5.1.2 Response Components

The first mode of the side span has a relatively low natural frequency (0.31 Hz). This ,however, did not strongly influence the components that comprise the total response. The most important component of the response was found to be the dynamic one and it contributes about 100% to the total response. In the displacement response the maximum static contribution was found to be 4% and the covariance contribution to be around -3%. The variances of the force responses are completely dominated by the dynamic component and contributions from the static and covariance components are negligible.

The first natural frequency of the center span is extremely low (0.048 Hz). The dynamic component dominates the cable displacement response and it is found to be about 110%, the static component contributes about 10%, and the covariance component contributes about -20%. A similar trend is found for the deck displacemens, but the dynamic component contributes about 124%, the static component contributes about 18%, and the covariance component contributes about -42%. These results indicate that the pseudo-static and covariance components contribute significantly to the total response and neglecting these terms would result in about 10% to 24% over-estimate in the displacement responses.

5.1.3 Lateral Response

Response variances due to the more common types of excitation consisting of identical or delayed support motions were computed and compared to responses due to the general spatially varying ground motion model. For the side span, the use of identical support excitations

- over-estimates the moment response by as much as 23% (at node 15) and under-estimates it by as much as 20% (at node 23); and
- over-estimates the shear response by as much as 41% (at node 5) and under-estimates it drastically at mid-span.

The use of delayed excitations gives acceptable results for the side span response, with

- a maximum over-estimation of about 11% for the displacement response of the deck and cable, respectively, (at nodes 15 and 16); and
- a maximum under-estimation of the shear response by 15% (at node 19).

For the center span, the use of identical support excitations

- over-estimates the moment response by as much as 124% (at mid-span) and under-estimates it by as much as 63% (at node 69);
- over-estimates the shear response by as much as 54% (at node 93) and drastically under-estimates it near mid-span; and
- over-estimates the displacement response by as much as 84% (at node 84) and under-estimates it by as much as 22% (at node 100).

The use of delayed excitations for the center span yields significantly different responses compared to those due to the general ground motion model, with the moment and shear responses being under-estimated by as much as 28% (at node 115).

5.1.4 Effect of Apparent Wave Velocity

For the general ground motion model the effect of increasing the apparent wave velocity from 1,700 m/sec to ∞ was examined. For the side span, the increase in the velocity produced

- at most a 5% and 4% increase in the displacement response variance at mid-span of the cable and deck, respectively;
- at most an 8% increase in the moment response at midspan and an 18% decrease near the quarter span; and
- at most a 25% increase in the shear response at quarter-span and a 70% decrease at midspan.

For the center span the increase in the velocity produced

- at most an increase of 35.7% in the cable displacement response (at node 84) and an increase of 13% in the deck displacement response at mid-span;
- at most an increase of 58.3% in the deck moment response at mid-span; and
- a decrease in the deck shear response by as much as -37% at mid-span.

5.1.5 Modal Contributions

The relative modal contributions to the dynamic responses were examined in detail to assist in understanding the contribution of modal covariances and to understand which modes are important for particuler responses. The study was performed for both the side and center spans at quarter and mid-span locations.

For the side span the dynamic deck displacement response is contributed to mainly by the first 5 modes and their corresponding covariances, while for the cable the first 8 modes are significant. The dynamic moment and shear responses require a larger number of modes, with the moment requiring about 19 modes and the shear requiring more than 20 modes.

The center span deck displacement response has a greater number of participant modes, with mode 15 being a strong contributer to the response at quarter-span. The force responses have contributions from a large number of modes, but the contributions from the first few modes is very small.

5.1.6 Transient Response

Transient response analyses show that the side span displacement response variances attain about 96% of their stationary values after 40 seconds of stationary excitation. A similar behavior was found for the moment response. The rate at which the responses grow is greatly dependent on the percentage contribution of the lower modes. The results for the side span indicate that transient response should be considered if the responses are not to be grossly over-estimated.

Transient response analyses of the center span show that due to the first natural frequency being extremely low, the displacement responses which have a strong contribution from the first mode greatly exceed their stationary values. The level of exceedance, however, is strongly dependent on the nature of the excitation spectrum at very low frequencies, and extreme care should be used in specifying the excitation spectrum if the results are to be considered seriously. The transient force responses, however, do not overshoot their stationary values, since they do not have strong contributions from the low frequency modes. The time taken for the transient responses to settle to their stationary values is much larger for the center span, and it is clear that transient effects must be considered when analyzing the center span for realistic durations of strong earthquake excitation.

5.1.7 Effect of Shear Deformation

For the general ground motion model the effect of including shear deformation was examined. For the side span, the inclusion of shear deformation produced

- a softening behavior of the side span occured with a drop of about 13% in the value of the first natural frequency;
- a shift in the band of frequency containing nine modes from 11.2 - 63 Hz to 4.6 - 7.6 Hz;
- a shifting in the mode order , with modes 4, 5, 6, and 7 (excluding shear deformation) becoming modes 5, 4, 7, and 8 (including shear deformation);
- consistently lower displacement responses of the side span cable and deck;
- a severe drop in the deck moment response (53% at mid-span) and shear response (60% at nodes close to support).

For the center span the inclusion of shear deformation produced

- a shift in the band of frequency containing 120 modes from 0 - 33 Hz to 0 - 7.25 Hz;
- a switching in mode order;
- a lower cable displacement response of at most 17%;
- an increase in the lateral displacement response of the deck at most locations, with a slight decrease near mid-span; and
- a severe drop in the deck moment and shear response.

Bibliography

Abdel-Ghaffar, A. M. and Stringfellow, R. G. (1984). "Response of suspension bridges to travelling earthquake excitations : Part II-Lateral response," *Soil Dynamics and Earthquake Engineering*, 3(2).

Abdel-Ghaffar, A. M. and Rubin, L. I. (1983). "Lateral earthquake response of suspension bridges," *Journal of Structural Engineering*, ASCE, 109(3).

Abdel-Ghaffar, A. M. and Rubin, L. I. (1982). "Suspension bridge response to multiple support excitations," *Journal of Engineering Mechanics Division*, ASCE,108(EM2).

Abdel-Ghaffar, A. M. (1978). "Free lateral vibration of suspension bridges," *Journal of Structural Mechanics*, ASCE, 104(3),503.

Abdel-Ghaffar, A. M. (1976). "Dynamic analysis of suspension bridge structures," *EERL 76-01*, California Institute of Technology, Pasadena, California.

Barnoski, R. L., and Maurer, J. R. (1969). "Mean-square response of simple mechanical systems to nonstationary random excitation," *Journal of Applied Mechanics*, June, 221-227.

Baron, F., Arikan, M., and Hamati, R. E. (1976). "The effects of seismic disturbances on the Golden Gate Bridge," *EERC Report No. 76-31*, Earthquake Engineering Research Center of California, Berkeley.

Castellani, A. and Felotti, P. (1986). "Lateral vibration of suspension bridges," *J. Struct. Eng.*, 112(9), 2169-2173.

Caughy, T. K., and Stumpf, H. J. (1961). "Transient response of a dynamic system under random excitation," *Journal of Applied Mechanics*, December, 563-566.

Clough, R. W., and Penzien, J. (1975). *Dynamics of strucuras*, McGraw-Hill Book Company, New York.

Harichandran, R. S. (1991). "Estimating the spatial variation of earthquake ground motion from dense array recordings," *Structural Safety*, 10, 219-233.

Harichandran, R. S. and Wang, W. (1988). "Response of one- and two-span beams to spatially varying seismic excitation," *Report No. MSU-ENGR-88-002*, College of Engineering, Michigan State University, East Lansing, Michigan.

Harichandran, R. S., and Vanmarcke, E. (1986). "Stochastic variation of earthquake ground motion in space and time," *Journal of Engineering Mechanics*, ASCE, 112(2), 154-174.

Hirai, A., etal. (1960). "Lateral stability of suspension bridge subjected to foundation-motion," *Proc., Second World Conference on Earthquake Engineering*, Japan, Vol. II, 931-945.

IMSL (1987). *IMSL User's Manual, International Mathematical and Statistical Libraries*, Inc., Vol. 1, Houston, Texas.

Ito, M. (1966). "Lateral rigidity of suspension bridge," *Symposium on suspension*, Lisbon, paper No. 7, 7.1-7.8.

Jennings, P. C., Housner, G. W., and Tsai, N. C. (1968). "Simulated earthquake motions," *Earthquake Engineering Research Laboratory*, California Institute of Technology, Pasadena, California.

Konishi, I. and Ymada, Y. "Earthquake resistant design of long span suspension bridges," *Proc., Third World Conference on Earthquake Engineering*, New Zealand, Vol. II, pp. IV/K/12.

Moisseif, L. S. and Leinhard, F. (1933). "Suspension bridges under the action of lateral forces," *Trans.*, ASCE, 98, 1080-1109.

Paine, C. D. (1970). "Supplement to the final report of the chief Engineer-Golden Gate Bridge," *Golden Gate Bridge, Highway and Transportation District.*

Przemieniecki, J. S. (1968). *Theory of matrix structural analysis*, Dover Publications, Inc. New York.

Rubin, L. I., Abdel-Ghaffar, A. M., and Stringfellow, R. G. (1983). "Earthquake response of long-span suspension bridge," *Report No. 83-SM-13*, Department of Civil Engineering, Princeton, N.J.

Selberg, A. (1958)., Discussion of "The lateral rigidity of suspension bridges," by Silverman, K., *Proc.*, ASCE, No. EM1, 1520-29-1520-31.

Sigbjonsson, R. and Hjorth-Hansen, E. (1981). "Along-wind Response of Suspension bridge with special reference to stiffening by horizontal cables," *Eng. Struct.*, 3, 27-37.

Silveman, I. K. (1957). "The lateral rigidity of suspension bridges," *Proc.*, ASCE, 83(3), 1292-1-1292-17.

Strauss, J. B. (1937). "The Golden Gate Bridge," *Report to the Board of Directors of the Golden Gate Bridge and Highway District*, California.

Sweidan, B. N. (1990). "Stochastic response of Deck Arch Bridges to correlated support excitations," Ph.D. Thesis, Department of Civil and Environmental Engineering, Michigan State University, East Lansing, Michigan.

Zerva, A., Ang, A. H-S., and Wen, Y. K. (1988). "Lifeline response to spatially variable ground motions," *Earthquake Engineering and Structural Dynamics*, 16,361-379.